Holographic Tools for Probing the Dynamics of Strongly Coupled Field Theories

John F. Fuini

A dissertation
submitted in partial fulfillment of the
requirements for the degree of

Doctor of Philosophy

University of Washington

2016

Reading Committee:

Laurence Yaffe, Chair

Andreas Karch

David Kaplan

Program Authorized to Offer Degree:
Physics

University of Washington

Abstract

Holographic Tools for Probing the Dynamics of Strongly Coupled Field Theories

John F. Fuini

Chair of the Supervisory Committee:
Professor Laurence Yaffe
Department of Physics

Since it was conjectured almost 20 years ago, AdS/CFT duality, or holography, has enabled steady progress in understanding certain gauge theories in the strongly coupled limit. In this thesis we examine various aspects of holography and holographic techniques, as well as particular applications to the dynamics of strongly coupled plasmas. We discuss the energy loss of general probe defects in generic holographic plasmas and the lifetime of quasinormal modes of sufficiently short-wavelength in a strongly coupled $\mathcal{N} = 4$ Super Yang-Mills (SYM) plasma. We then perform a thorough investigation of the far-from-equilibrium dynamics of the SYM plasma, focusing on how the presence of large magnetic fields or chemical potentials affect the timescale of equilibration. Finally we discuss some non-relativistic directions by finding a covariant construction of Lagrangians for spinor fields in generic Newton-Cartan backgrounds via a non-relativistic reduction, which may assist in the construction of non-relativistic versions of holography.

TABLE OF CONTENTS

LIST OF FIGURES

ACKNOWLEDGMENTS

There are some truly amazing human beings at the University of Washington. I'd like to thank the many wonderful people that have contributed positively to my life in the last six years. They are: Bridget Bertoni, Han-Chih Chang, Christoph Uhlemann, Andreas Karch[1], David McKeen, Maxwell Hansen, Rachel Ryan, Stefan Janiszewski, Shauna Story, Seyda Ipek, Brandon Robinson, Jakub Scholtz, Thomas Epelbaum, Siavash Golkar, Erik Lentz, Allison Duffy, Carolyn Auchter, Pedro Sales-de-Bruin, Devon Mortensen, Catherine Provost, Nathan Froemming, Akshay Ghalsasi, Yu-Sheng Liu, Matthias Kaminski, Laurence Yaffe, Andreas Karch, David Kaplan, Ann Nelson, Steve Sharpe and Steve Ellis.

I am extremely grateful to Laurence Yaffe and Andreas Karch for teaching me how to think about problems and for their leadership, mentorship and patience.

Finally, I want to specifically thank my good friend Bridget for her unending support and encouragement.

[1]Once as a mentor and once as a friend.

Chapter 1

INTRODUCTION

One of the most incredible, yet unintuitive, theoretical discoveries made in the last twenty years is the Anti-de Sitter/Conformal Field Theory correspondence (AdS/CFT), conjectured by Juan Maldacena in 1997 [1]. In its strongest form, the conjecture relates type IIB superstring theory in $AdS_5 \times S^5$ spacetime to $\mathcal{N} = 4$ Super Yang-Mills (SYM) theory with an $SU(N_c)$ gauge group and Yang-Mills coupling constant g_{YM}, which lives in four dimensional Minkowski space. At first inspection these two theories are wildly different. On the 'AdS' side of the conjecture, we have a quantum theory of gravity in ten dimensions, described by the interactions of open and closed oscillating strings with string length $l_s = \sqrt{\alpha'}$ denoting the scale of quantum oscillations. On the 'CFT' side, we have a supersymmetric conformal field theory in four dimensions with no gravity whatsoever. And yet, the correspondence states that all observables calculated on either side of this *duality* are precisely the same – that in fact the theories themselves are mathematically identical.

Since the original correspondence was discovered, there have been many manifestations of the duality, which are collectively referred to as *holography*. However, for our purposes, we will be interested in the original holographic example and its generalization to finite temperature.

A feature of critical importance is that the correspondence is a strong-weak coupling duality. This means that when one side of the duality is strongly coupled, the other is weakly coupled. Since calculations are easier, and often only possible pertubatively (in the weak coupling regime), the correspondence allows us to calculate quantities on one side in the weak coupling regime, and in doing so learn about the other side in the strongly coupled regime. This feature is extremely useful for studying the properties of a strongly coupled

QFT. For the interests of this thesis, we will dial the 't Hooft coupling, $\lambda = g_{YM}^2 N_c$, to be very large, so that we are considering the CFT in the strongly coupled limit. We are then assured that the AdS side will be weakly coupled and thus (possibly) calculable.

In the large N_c and large λ limit, the AdS side of the duality reduces to classical supergravity, which can basically be thought of as general relativity (GR) with extra field content. We add in the large N_c limit so that the gravitational calculations will be more manageable, but N_c is of course a parameter in the dual theory as well. Thus, at the end of the day we will make computations in supergravity to find out information about the SYM field theory, when the field theory is in the regime of large N_c and large coupling λ.

In this introductory chapter, we will give a brief introduction to AdS/CFT, focusing on the parts of the correspondence which are most relevant for the remainder of the thesis. A fully-contained treatment of holography is outside of our scope, but we refer the reader to [2, 3, 4, 5, 6, 7, 8] and references therein, from which many ideas and explanations in this introductory chapter were taken[1].

We will conclude this introductory chapter with sections that present specific topics of holographic research relevant to the thesis and the Ph.D. work of the author. These sections will serve to provide a starting point for understanding the subsequent chapters.

1.1 Holography Background

First let us familiarize ourselves with the theories and parameters involved, and try to motivate where this unintuitive correspondence comes from.

On the AdS side, we have type IIB superstring theory on the background $AdS_5 \times S^5$. The AdS_5 part of the background geometry has a radius of curvature, L, and the S^5 part shares this radius of curvature as well, and provides a dimensionless number in terms of the string length, L/l_s. The string parameter α' is related both to the string tension, as $\tau = 1/2\pi\alpha'$, as well as the string length, $l_s = \sqrt{\alpha'}$. There is also the dimensionless coupling strength of the

[1]The author is particularly fond of the presentation found in the recent textbook [6] and strongly encourages any new student of holography to purchase it.

strings, g_s. The two free dimensionless parameters on the AdS side of the correspondence are thus g_s and L/l_s. On the CFT side, we have $\mathcal{N}=4$ SYM theory with an $SU(N_\mathrm{c})$ gauge group and Yang-Mills coupling constant g_YM, and thus the theory is governed by N_c and g_YM.

The correspondence tells us that the two theories have partition functions in the presence of sources which are equivalent, and that the two free parameters in each theory are related via

$$g^2_\mathrm{YM} = 2\pi g_s\,, \quad 2g^2_\mathrm{YM}N_\mathrm{c} = \frac{L^4}{l_s^4}\,. \tag{1.1}$$

1.1.1 Motivation for Holography

We seek to motivate the correspondence by appealing to two different viewpoints of the soliton-like objects in superstring theory known as D-branes. We will follow the particularly pedagogical presentations of [2, 3, 6].

Superstring theory has fundamental string objects, as well as soliton-like solutions known as Dirichet-Branes (D-branes) upon which open strings can end. Dp-branes are D-branes that are of $p+1$ dimensionality[2] . If the brane is embedded in a spacetime of dimension $d > p$, the brane extends infinitely into p spatial dimensions[3], and is localized in the remaining $d-p-1$ spatial directions. Since open string endpoints must lie on the brane, they are fixed in the remaining coordinates to where the branes sit, and thus satisfy Dirichlet condition in these coordinates. Conversely, for the p directions into which the brane extends, the endpoints may move along the brane and thus satisfy Neumann conditions in these coordinates. For type IIB superstring theory there are only stable Dp-branes for odd p.

We will start by considering a stack of these Dp-branes placed in ten-dimensional space time (N_c branes in number), and we can inquire about the dynamics of open and closed strings along with the Dp-brane stack. There are two different ways to describe the dynamics between fundamental strings and these Dp-branes, and which description is valid depends

[2] p denotes the number of directions in the brane's spatial extent.

[3] In addition to the time direction, x^0.

the strength of $g_s N_c$.

First we consider the case of $g_s N_c \ll 1$, the so-called "open string" case. We want to work with the strings perturbatively, and thus we have that $g_s \ll 1$. The Dp-branes provide a constraint for where open string endpoints must lie. Thus, the dynamics are that of the open strings and their endpoints (fixed to the brane), closed strings propagating in empty space and the interactions between the open strings, closed strings and the brane. Considering energies less than the string scale, $1/l_s$, will allow us to focus only on the massless modes. The plan will be to then write an effective Lagrangian for these massless modes and their interactions. The low energy description of the closed string states will give us supergravity in the full ten dimensions, while the open string massless states will have a low energy description whose Lagrangian is precisely that of $\mathcal{N} = 4$ SYM theory. Open string endpoints on a single brane in the low-energy effective action are described by a U(1) gauge theory. When we make a stack of N_c Dp-branes, we get a U(N_c) gauge theory where the effective coupling is now $g_s N_c$.

On the other hand, in the so-called "closed string perspective", we may stack many Dp-branes and achieve $g_s N_c \gg 1$. We may now consider how this stack deforms the space around it, and we may replace the stack of branes with the *geometry* sourced by the Dp-brane stack itself and then consider the dynamics of strings on this new geometry. Again we will take a low energy limit so that superstring theory becomes supergravity – this means that the characteristic length scale, L, of the geometry created by the stack must be very large compared to scale set by the string length, l_s.

Specifically, when we consider a coincident stack of D3-branes in flat ten dimensional spacetime, the two pictures summarized above give us the two sides of the duality that we will be interested in. The open string perspective will give us a weakly coupled $\mathcal{N} = 4$ SYM theory on four dimensional Minkowski space, and the closed string picture will give us type IIB supergravity in a ten dimensional background space of $AdS_5 \times S^5$, but at all times we are describing the same physical object (a stack of N_c D3-branes). Let us try to outline how these two viewpoints of the duality come about in more detail.

The open string picture, $g_s N_c \ll 1$

Let us now illustrate the open string picture of N_c coincident D3-branes, with embedding in the ten dimensional space such that they extend infinitely in x^0, x^1, x^2, and x^3, and are localized at some point in the remaining coordinates $(x^4, \ldots, x^9)$. We are interested in the regime $g_s N_\mathrm{c} \ll 1$, and there are two types of perturbative ($g_s \ll 1$) string excitations. Perturbatively, the closed strings are excitations of the empty ten dimensional space, while the open strings represent excitations of the D3-branes themselves. By restricting our attention to low energies, i.e. $E \ll (l_s)^{-1}$, we can neglect all massive string excitations, which have energy of order $(l_s)^{-1}$.

We can then create a low energy effective action for each kind of excitation along with their interactions, which has the schematic from:

$$S = S_\mathrm{brane} + S_\mathrm{int} + S_\mathrm{bulk}\,. \tag{1.2}$$

This effective action is derived by integrating out all the massive modes. The plan then is to take the "Maldacena limit", which involves keeping N_c and g (and thus g_s) fixed, along with all physical lengths scales, while taking $\alpha' \to 0$ (or equivalently $l_s \to 0$). If we perform this limit on the above effective action, each piece simplifies as follows.

Performing an α' expansion of S_bulk yields the action of supergravity in ten dimensions plus higher derivative terms which are subleading in α'. Thus, in the Maldacena limit, S_bulk becomes the action of supergravity in ten dimensional flat space.

The excitations of the brane makeup the action S_brane and are defined on the 4 spacetime dimensions of the brane world volume. The action for the endpoints of the strings on a single brane comes from the Dirac-Born-Infled (DBI) action. The leading order in α' contribution becomes

$$S_{open} = -\frac{1}{2\pi g_s}\int d^4x \left(\frac{1}{4}F_{\mu\nu}F^{\mu\nu} + \frac{1}{2}\eta^{\mu\nu}\partial_\mu\phi^i\partial_\nu\phi^j + \mathcal{O}(\alpha')\right) \tag{1.3}$$

where the fermionic fields have been omitted[4]. The action above contains the massless open string degrees of freedom, which are organized into a four-dimensional $\mathcal{N}=4$ supermultiplet, consisting of one $U(1)$ gauge field A_μ, six real scalar fields, ϕ, and four fermionic supersymmetric partners, ψ. These will become the field content of our $\mathcal{N}=4$ SYM theory. We can think about these as one $\mathcal{N}=1$ vector multiplet, $(A_\mu,\, \psi_4)$, and three $\mathcal{N}=2$ chiral multiplets, $(\psi_i,\, \varphi_i)$, where $i=1,2,3$, and φ are complex scalar fields. These can be repackaged as $(A_\mu,\, \psi_A,\, \phi_i)$ where $A=1,\ldots,4$ is the index of the fundamental representation of $SU(4)$, ϕ is real, and now $i=1,\ldots,6$ is the six-dimensional antisymmetric representation index of $SU(4)$.

Generalizing the above action to N_c D3-branes gives an extra $SU(N_\mathrm{c})$ adjoint representation label to our field content, $(A^a_\mu,\, \psi^a_A,\, \phi^a_i)$, and requires the addition of a scalar potential[5] to S_brane,

$$V = \frac{1}{2\pi g_s}\sum_{i,j}\mathrm{Tr}[\phi_j,\phi_k]^2\,, \tag{1.4}$$

where the trace is over $SU(N_\mathrm{c})$ indicies. With this potential, in the $\alpha'\to 0$ limit, S_brane becomes the bosonic part of $\mathcal{N}=4$ SYM theory, where we identify $2\pi g_s = g^2_\mathrm{YM}$.

The action governing the interactions between the open strings and the closed strings, S_int, ends up being subleading in the $\alpha'\to 0$ limit, and thus the closed strings and open strings decouple, and the S_bulk becomes free supergravity in ten dimensions.

The takeaway from this discussion is that in the open string picture ($g_s N_\mathrm{c} \ll 1$), the low energy description is that the open strings and close strings completely decouple, the open strings act as degrees of freedom in $\mathcal{N}=4$ SYM theory in the 4 dimensions of the N_c D3-brane embedding location, and the closed strings act as free supergravity in the entire ten dimensions. If there is any D3-brane separated by some distance from the stack, there

[4]The fermionic fields can be included via supersymmetric constraints.

[5]It's not fully agreed the form of the the DBI action of a stack of branes, however, the low energy form of the action is know. One can just generalize to multiple branes while demanding supersymmetry. While the gauge fields have a term involving commutators, so must the scalars. This action is then verified against open string amplitude calculations on the brane. A reader interested in the DBI action for the entire stack should see [9].

will be a Higgs phase characterized by the position of the separated brane. This will give rise to a "W mass" in the field theory dynamics, and if we don't want to lose these dynamics, we must take the $\alpha' \to 0$ limit in such a way that keeps the separation distance in string units – or the mass – fixed. This is the motivation behind the Maldacena limit's demand to keep x^i/α' fixed. Thus,

$$\alpha' \to 0, \qquad x^i/\alpha' \to constant\,. \tag{1.5}$$

The Maldacena limit is sometimes also referred to as the *decoupling limit*.

The closed string picture, $g_s N_c \gg 1$

We want to now study the closed string picture, valid for $g_s N_c \gg 1$, and examine the same Maldacena limit. At strong coupling, the N_c D3-branes are massive charged objects which will deform the background geometry, i.e. which are sources for the field content of type IIB supergravity.

The supergravity solution of N_c D3-branes in ten spacetime dimensions can be found with the ansatz

$$ds^2 = f(r)^{-1/2}\eta_{\mu\nu}dx^\mu dx^\nu + f(r)^{1/2}\delta_{ij}dx^i dx^j\,, \tag{1.6a}$$

$$e^{2\phi(r)} = g_s^2\,, \tag{1.6b}$$

$$C_{(4)} = \left(1 - f(r)^{-1}\right) dx^0 \wedge dx^1 \wedge dx^2 \wedge dx^3 + \cdots\,, \tag{1.6c}$$

where $\mu, \nu = 0, \ldots, 3$ and $i, j = 4, \ldots, 9$, with the radial coordinate defined by $r^2 = \sum_{i=4}^{9} x_i^2$, and $C_{(4)}$ is the self-dual four-form (with ellipses representing terms to make $F_{(5)} = dC_{(4)}$ self-dual).

The solution from the type IIB supergravity equations of motion reads,

$$f(r) = 1 + \left(\frac{L}{r}\right)^4\,. \tag{1.7}$$

In supergravity, L is a parameter which denotes which a particular solution. String theory

can determine it in terms of other variables of our problem, as the flux of $F_{(5)}$ through the internal S^5 counts the number of D3-branes giving the relation,

$$L^4 = 4\pi g_s N_c \alpha' \,. \tag{1.8}$$

The metric has two regions of interest characterized by $r \ll L$ or $r \gg L$. In the $r \ll L$ case, we find a *near-horizon* or *throat* region, where $f(r) \approx L^4/r^4$, and the metric reads

$$ds^2 = \frac{r^2}{L^2}\eta_{\mu\nu}dx^\mu dx^\nu + \frac{L^2}{r^2}\delta_{ij}dx^i dx^j, \tag{1.9}$$

or when we switch to inverse radial coordinate $z = \frac{L^2}{r}$, we have

$$ds^2 = \frac{L^2}{z^2}\left(\eta_{\mu\nu}dx^\mu dx^\nu + dz^2\right) + L^2 d\Omega_5^2 \,. \tag{1.10}$$

Here we have separated out the radial coordinate from the 6 transverse directions, converted to spherical coordinates. We now explicitly see the metric pertaining to an S^5 coming from the second term in the metric, and the first term is that of Anti-de-Sitter space in 5 dimensions, or AdS_5.

In the other regime, $r \gg L$, we see that $f(r) \approx 1$ and thus the metric simply reduces to flat ten dimensional spacetime,

$$ds^2 = \eta_{\mu\nu}dx^\mu dx^\nu + \delta_{ij}dx^i dx^j \,. \tag{1.11}$$

The system is thus described by the dynamics of closed strings propagating on this background spacetime, in the near-horizon region, in the flat large-r region, and in between.

As we discussed in the open string case, when we consider the low energy limit of closed strings on flat ten dimensional space, we get free supergravity in ten dimensions. The story is not as simple for the low energy limit of the near-horizon throat region.

Since g_{00} is a function of r, the energy recorded by observers at different r will be different.

Consider string excitations in the near-horizon regions at radial position r. The energy observed at position r of the excitation in units of string length, l_s, is given by $l_s E_r$. Taking a low energy limit will not get rid of the high energy string fluctuations, as an observer at $r = \infty$ will see the fluctuation extremely red-shifted from climbing out of the throat region. The exact relation is given by

$$E = \sqrt{-g_{00}} E_r = f(r)^{-1/4} E_r \,. \tag{1.12}$$

In the near horizon region, $r \ll L$, $f(r) \approx L^4/r^4$ and thus,

$$\sqrt{\alpha'} E_\infty \sim \frac{r}{L} \sqrt{\alpha'} E_r \,, \tag{1.13}$$

and this observed energy goes to zero for $r \ll L$ for any large but fixed $l_s E_r$. To an observer at $r = \infty$, this means that any energetic excitation brought closer $r = 0$ would appear to have lower energy. In taking the low energy limit, there are now two distinct excitations seen from an observer at $r = \infty$: low energy supergravity modes from the ten dimensional space far away from $r = 0$, along with any excitation originating from significantly close to $r = 0$. Thus, string fluctuations surviving in the throat region are decoupled from the supergravity degrees of freedom in the ten dimensional flat spacetime for $r \gg L$.

Note that

$$\frac{L^4}{r^4} = 4\pi g_s N_{\rm c} \frac{\alpha'^4}{r^4} \frac{1}{\alpha'^2}, \tag{1.14}$$

thus, the Maldacena limit (where α'/r is fixed), $L^4/r^4 \to \infty$, and thus we are zooming in on the $r \ll L$ throat region (the $AdS_5 \times S^5$ region).

Making the Conjecture

The idea behind making the AdS/CFT conjecture is the following. We started by trying to describe the dynamics of a stack of $N_{\rm c}$ D3-branes, and we developed two viewpoints in a low energy limit. After taking the Maldacena limit, eq. (1.5), we are left with a free

parameter, $g_s N_c$. When $g_s N_c \ll 1$, the open string picture is an easy way to describe the dynamics of these N_c coincident branes embedded in ten dimensions – we found the low energy effective theory to be $\mathcal{N}=4$ SYM theory isolated to the flat four dimensions of the brane, and decoupled from this theory, we also found free type IIB supergravity on $\mathbb{R}^{9,1}$. When $g_s N_c \gg 1$, it is the closed string picture that gives us an easy way to think about the dynamics – we found that the dynamics were captured by type IIB supergravity on $AdS_5 \times S^5$, and decoupled from this theory, we again see type IIB supergravity on $\mathbb{R}^{9,1}$. It was the Maldacena limit that gave us this nice decoupling in both perspectives of the *same* system.

Since we have two different ways of describing the same system, and since they both have a decoupled piece which is free type IIB supergravity on $\mathbb{R}^{9,1}$, it is plausible that the remaining theory in each picture should be identified. Specifically, Maldacena postulated that the $\mathcal{N}=4$ SYM theory in flat 4 dimensions from the open string picture, should be identified with the type IIB supergravity[6] theory on $AdS_5 \times S^5$ from the closed string picture. The idea is that, while the variables and field content seem wildy different, the partition functions are identical. Partition functions integrate over all values of the fields in the system – meaning that, in some way, we basically are doing a complicated change of dummy variables in the path integral, and thus all observables calculated on either side are identical. This is a remarkable conjecture, and it has passed a myriad of consistency checks [3, 10, 11], for a list of many initial consistency checks see section 6.4 of [6].

1.1.2 Symmetries/Isometries

If these theories are really to be identified, it must be that the unbroken global symmetries of each theory are equal, and we will check this now.

On the AdS side, we note that the isometry group for the AdS_5 part of the metric is

[6]It is commonly believed that doing away with the low energy limit gives a duality between $\mathcal{N}=4$ SYM theory and type IIB superstring theory in $AdS_5 \times S^5$ for all values of $g^2_{\mathrm{YM}} N_c$ and N_c, and this is called the "strongest form" of the duality.

given by $SO(4,2)$, and that the isometry group for the S^5 part of the metric is immediately given by $SO(6)$.

It happens that the symmetry group of $\mathcal{N}=4$ SYM is the superconformal group $SU(2,2|4)$ whose maximal bosonic subgroup is $SU(2,2) \times SU(4)_{\mathrm{R}} \sim SO(4,2) \times SO(6)_{\mathrm{R}}$ [3]. We thus see that the bosonic subgroup of the CFT side matches the isometries of the AdS side of the duality. It can be shown that string theory on $AdS_5 \times S^5$ does indeed have this full $SU(2,2|4)$ symmetry of the CFT, for details see chapter 7 of [6] or [3].

The fact that both sides have the same global symmetry means that we can categorize representations on both sides of the duality according to how they transform under this symmetry group. This categorization provides us with a way to link quantities on both sides of the duality, thus creating a dictionary or mapping. In general the mapping will be between operators on the $\mathcal{N}=4$ SYM side to the string theory states in the same representation on the AdS side. In the limiting procedure we are interested in, this will simplify to a mapping between $\mathcal{N}=4$ SYM operators and supergravity fields on the AdS side.

1.1.3 Large N_c, Large λ (weakest form)

Since we are interested in a strongly coupled field theory, and since we want to make calculations easier, we will take two limits of the duality which will end up making the string theory side more tractable. If we want the string theory side to be weakly coupled, $g_s \ll 1$, then to leading order we are left with classical string theory. This means that we will not need to do the genus expansion in string theory, but only tree level diagrams. On the field theory side, we see from eq. (1.1), that $g_{\mathrm{YM}} \ll 1$ as well. But we can choose to take this limit in such a way as $g^2_{\mathrm{YM}} N_{\mathrm{c}} = \lambda$ is held fixed (or equivalently L^2/α' held fixed). This will mean on the field theory side that we are taking a large N_{c} limit, for fixed λ, which is known as the 't Hooft limit. In the 't Hooft limit, the Feynman diagrams organize themselves in a $1/N_{\mathrm{c}}$ expansion at fixed λ, and in fact, the diagrams are grouped by their topology, see fig. 1.1.

For instance, from [8], we see that the vacuum-to-vacuum amplitude $\log(Z)$ can be ex-

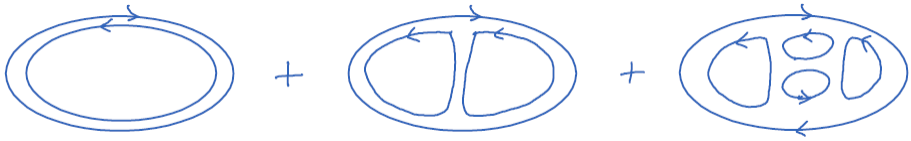

Figure 1.1: The first few planar diagrams of the 't Hooft expansion.

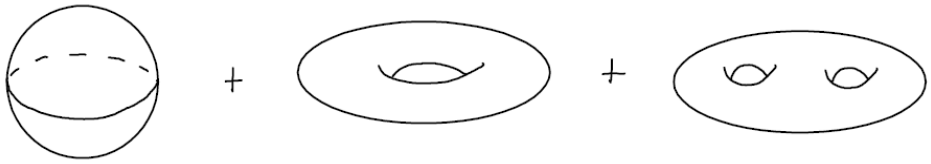

Figure 1.2: Depiction of the genus expansion for the vacuum-to-vacuum amplitude.

panded as

$$log(Z) = \sum_{n=0}^{\infty} N_c^{2-2n} f_n(\lambda) = N_c^2 f_0(\lambda) + f_1(\lambda) + \frac{1}{N_c^2} f_2(\lambda) + \cdots . \tag{1.15}$$

The leading order piece alone is made up of only planar diagrams depicted in fig. 1.1, and thus the large N_c limit is called the planar limit.

Note the similarity to the string theory genus expansion in fig. 1.2 – in closed string theory, the vacuum-to-vacuum amplitude is written as

$$\mathcal{A} = \sum_{h=0}^{2h=0} g_s^{2h-2} F_h(\alpha') = \frac{1}{g_s^2} F_0(\alpha') + F_1(\alpha') + g_s^2 F_2(\alpha') + \cdots . \tag{1.16}$$

where it appears that g_s is playing the role of $1/N_c$, as our conjectured relations (1.1) suggest.

Once this particular large N_c limit is taken, we are left with one free parameter on each side. On the field theory side, we have the 't Hooft coupling λ, and since we are interested in describing strongly coupled field theories, we will want to take $\lambda \to \infty$. Via eq. (1.1), this will mean we are taking $L^4/(\alpha')^2 \to \infty$, or equivalently $l_s/L \to 0$. This means that, on the (now classical) string theory side, our string length is much smaller than the radius

of curvature, L. In this limit of type IIB string theory, we obtain type IIB supergravity on $AdS_5 \times S^5$

Finally then, we will be interested in the dynamics of classical type IIB supergravity (the weak coupling limit of type IIB string theory), as this is precisely the dynamics of the dual field theory, $\mathcal{N} = 4$ SYM with an $SU(N_c)$ gauge group in the large N_c and strongly coupled limit.

1.1.4 Layout and Notation

It is a good idea to take a second to get familiar with the notation and layout of the geometry. In the supergravity picture, there were originally ten coordinates. These coordinates are split between the AdS_5 directions, which we will denote with index $M, N, L, \ldots$, and the coordinates on the internal space S^5 which are collectively denoted by Ω_5. The original fields of Type-IIB supergravity are decomposed on the internal space via

$$h(x^M, \Omega_5) = \sum h^I(x^\mu) Y^I(\Omega_5) \tag{1.17}$$

where the Y^I are the spherical harmonics on the internal S^5. The systems we are interested in studying in this thesis will not require the supergravity fields to have any dependence on the internal S^5 and the entire dynamics will be controlled by fields depending only on x^M, while this is not necessarily true in a more general case.

The AdS_5 part of the space is commonly analyzed in the following two sets of coordinates. The so called "Global AdS" metric:

$$ds^2_{AdS\,global} = L^2 \left(-\cosh^2 \rho \, d\tau + d\rho + \sinh^2 \rho \, d\Omega^2_{d-1} \right) \tag{1.18}$$

And the "Poincare Patch AdS" metric:

$$ds^2_{AdS\,PP} = \frac{r^2}{L^2} (\eta_{\mu\nu} dx^\mu dx^\nu) + \frac{dr^2}{r^2} \tag{1.19}$$

where L is the AdS radius of curvature. Like the name implies, Global AdS coordinates are a global covering of AdS space, whereas the Poincare coordinates are not. There are subtleties between the two coordinate choices that will not concern us – we will use solely the Poincare coordinates, and direct the interested reader to sec. 2.2 of [2] for details. Looking at the Poincare patch metric of AdS we see that at any finite value of the radial coordinate r, the space becomes Minkowski space, albeit with some overall scale factor (that depends on r). As can be seen, we are using x^μ to denote the coordinates on these Minkowski slices. The $r = \infty$ slice is the *boundary* of AdS space, and $r = 0$ is the *center* of AdS space. It is often said that the Minkowski slice *at infinity* (or at $r = \infty$) is the Minkowski space where the dual field theory *lives*. This is motivated by the fact that desired quantities in the boundary field theory are obtained via asymptotic expansions about $r = \infty$ of the gravity fields (which are defined for all r), something we will see more specifically below. The r coordinate (along with the Minkowski slices x^μ), fill out the *bulk* of the AdS space and this is where the supergravity fields live. We will also make use of an *inverted radial coordinate* z, defined via $z = L^2/r$, which sends our AdS metric to

$$\frac{L^2}{z^2}\left(\eta_{\mu\nu}dx^\mu dx^\nu + dz^2\right) \tag{1.20}$$

1.1.5 Field - Operator Map

Let us discuss the correspondence and the AdS/CFT dictionary elements we require in a more concrete fashion. The weakest form of the AdS/CFT correspondence tells us that the partition function of $\mathcal{N} = 4$ SYM at large N_c and large coupling in 4 spacetime dimensions is exactly equal to the partition function for type IIB supergravity on $AdS_5 \times S^5$. The CFT side is a conformal theory and does not have scattering matrix (S-matrix) elements. Observables composed of gauge invariant combinations of local operators are thus the natural objects to consider [2] for the duality. Symmetry groups have been established to be equal on both sides of the duality. The identification of the representations of the symmetry groups will give us a field-operator mapping, between the fields on the AdS side and the operators on

the CFT side. This field-operator mapping will dictate how we use the correspondence.

Suppose that a field[7] on the AdS side, ϕ, falls into the same representation of the shared symmetries as a gauge invariant operator $\mathcal{O}$ on the CFT side. We will denote the field and operator as "duals" and write the relation as

$$\phi \leftrightarrow \mathcal{O}\,. \tag{1.21}$$

The super conformal representations on the CFT side are realized with gauge invariant operators, the $\mathcal{O}$ in our field-operator map. However, since our fundamental fields on the CFT side all transform covariantly[8] under gauge transformations, the operators in our field-operator mapping must be composite operators. We can obtain gauge invariant operators by taking the trace of a product of our $\mathcal{N}=4$ fields at the same point x, and these are called local *single-trace operators*, i.e.

$$\mathcal{O}(x) = Tr(\phi^i \cdots \phi^j)(x)\,. \tag{1.22}$$

The single trace operators are important as they are the leading gauge invariant operators in the large N_c limit.

There are specific single trace operators, the so called *chiral primary operators*, which require special attention, and we will examine these operators more closely for the case when the operator is built out of scalars. These operators are of the form

$$\mathcal{O}(x) = Str(\phi^{\{i_1}\phi^{i_2}\cdots\phi^{i_k\}}) \tag{1.23}$$

where Str stands for the symmetrized trace of the gauge algebra. These scalars are in the

---

[7]This ϕ denotes some scalar field in the bulk, and has nothing to do with the 6 scalar fields ϕ^i that exist as fundamental fields of $\mathcal{N}=4$ SYM in the boundary theory.

[8]Except for the gauge field A_μ which clearly must transform as a connection.

adjoint representation, $\phi^i = \phi^{ia} T_a$, and so the Str is given by the sum of all permutations,

$$Str(T_{a_1} \cdots T_{a_n}) = \sum_{\sigma} Tr(T_{\sigma(a_1)} \cdots T_{\sigma(a_n)}) \,. \tag{1.24}$$

The trace is taken over the color indicies, and since the dimension of these scalar fields (in four spacetime dimensions) is 1, then the operator defined in eq. (1.23) has classical scaling dimension $\Delta = k$, and we will call it $\mathcal{O}_\Delta$. The reason that we are discussing the free scaling dimension when we plan to go to strong coupling is that the scaling dimension of a chiral primary operator is protected by supersymmetry[9], i.e. it is invariant under changes in coupling. The chiral primary operators are important because they will be dual to various fields on the gravity side, and their descendants[10] will be dual to the descendants of the fields on the gravity side.

These operators will be dual to gravity fields which transform as the same representation under the common symmetries of both theories. We will compactify all of the SUGRA fields in ten dimensions on the S^5 internal space. Thus there will be many types of fields in the AdS geometry, i.e. more scalars than just the dilaton and the axion. The precise representations of the entire symmetry group that each of these fields fall into will need to match that of the dual gauge-invariant operator on the CFT side. For example, since the chiral primary operator (1.23), $\mathcal{O}_\Delta(x)$, is a scalar under Lorentz transformations, it will need to be dual to some combination of the scalar fields after compactification on the AdS side. Performing a precise analysis of matching all of the symmetries is beyond the scope of this introduction, and we will only state a few of the elements of the field-operator map that we need for the remainder of this thesis. For further details on how matching is done in general, see [3], and for a nice reference table of the field - operator map, see table 7 therein.

Two elements of the operator field map that will play a particularly important role for

---

[9]These are the so-called 1/2 BPS operators. See chapter 3 of [6].

[10]Descendants are created by acting with P_μ on the operator/field. Essentially performing a derivative with respect to the field theory Cartesian directions (i.e. the boundary directions), x^μ .

us are the composite field theory operators $T_{\mu\nu}$ and J_μ. $T_{\mu\nu}$ is the stress-energy tensor in the boundary field theory. We will be interested in this as it will characterize the energy density of the field theory, as well as isotropy in the pressures, giving us a check on whether or not the field theory has reached equilibrium. J_μ is the conserved current for the $SU(4)_R$ global symmetry that is a part of our $\mathcal{N}=4$ boundary theory. The AdS dictionary tells us that it is the spacetime metric of AdS_5 that is dual to the stress-energy tensor (precisely what this means will be discussed shortly) and the gauge field A_μ that is dual to the conserved current J_μ. We write this as,

$$g_{\mu\nu} \leftrightarrow T_{\mu\nu}, \quad A_\mu \leftrightarrow J_\mu \tag{1.25}$$

We now define more carefully what it means for a field and operator to be "dual". We'll use some scalar field and operator for an example, $\phi \leftrightarrow \mathcal{O}$. We will begin with the scalar field, ϕ. This field originated from the supergravity fields in 10 dimensions, was then compactified on the internal space (the S^5), and is now a scalar on AdS_5. In AdS_5, the action for such a field has the following form:

$$S = -CN_c^2 \int dz d^5x \sqrt{-g} \left(g^{MN} \partial_M \phi \partial_N \phi + m^2 \phi^2 \right) . \tag{1.26}$$

The equation of motion for ϕ is then

$$(D_M D^M - m^2)\phi = 0, \qquad D_M D^M \phi = \frac{1}{\sqrt{-g}} \partial_M \left(\sqrt{-g} g^{MN} \partial_N \phi \right) . \tag{1.27}$$

With AdS_5 as our background space given in Poincare patch coordinates from (1.20), the operator above reads

$$D_M D^M = \frac{1}{L} \left(z^2 \partial_z^2 - 3z\partial_z + z^2 \eta^{\mu\nu} \partial_\mu \partial_\nu \right) \tag{1.28}$$

Translational invariance of the AdS_5 metric in the x^μ directions suggests a plane wave decomposition of the form

$$\phi(x^\mu, z) = \int d^4x \, e^{ip_\nu x^\nu} \widetilde{\phi}(p_\mu, z) . \tag{1.29}$$

Plugging this ansatz into eqns. (1.27) and (1.28) gives us the following equation for each mode,

$$\left[z^2\partial_z^2 - 3z\partial_z - (z^2 p_\mu p^\mu + m^2 L^2)\right] \widetilde{\phi}(p_\mu, z)\,. \tag{1.30}$$

Now lets concern ourselves with how the solution can behave near the boundary, $z \to 0$. We use a power series ansatz for the asymptotic behavior of $\widetilde{\phi}$ as $\widetilde{\phi} \sim z^\Delta$, and plugging in, we find two possible solutions for Δ,

$$\Delta_\pm = 2 \pm \sqrt{4 + m^2 L^2}\,. \tag{1.31}$$

The above analysis can be done for general d, in AdS_{d+1} and yields the more general relation

$$\Delta_\pm = \frac{d}{2} \pm \sqrt{\frac{d^2}{4} + m^2 L^2}\,. \tag{1.32}$$

For any d we find that $\Delta_+ + \Delta_- = d$ and $\Delta_+ > \Delta_-$.

We've now found the possible asymptotic boundary behaviors of our field, and thus we can perform a general expansion of our $\phi(x^\mu, z)$ about $z \to 0$. We have

$$\phi(x^\mu, z) \sim \phi_{(0)}(x^\mu) z^{\Delta_-} + \cdots + \phi_{(+)}(x^\mu) z^{\Delta_+} + \cdots\,, \tag{1.33}$$

where each ellipses is subleading to (and determined by) the shown preceding term. Now we want to connect quantities from this field to it's dual operator $\mathcal{O}$. First note that $\phi_{(0)}(x^\mu) = \lim_{z\to 0} \phi(x^\mu, z) z^{-\Delta_-}$. Consider a scaling transformation $x^\mu \to \lambda x^\mu, z \to \lambda z$. In the bulk, this is a diffeomorphism and thus the *scalar* bulk field simply changes as $\phi(x^\mu, z) \to \phi(\lambda^{-1}x^\mu, \lambda^{-1}z)$. Thus, no factors come from the bulk scalar field. However, $z^{-\Delta_-} = z^{\Delta_+ + d} \to \lambda^{\Delta_+ + d} z^{\Delta_+ + d}$ and thus $\phi_{(0)}(x^\mu)$ has dimension $[\text{length}]^{\Delta_+ + \mathrm{d}}$. Now, our gauge invariant chiral primary operator $\mathcal{O}$ has conformal dimension[11] Δ, which means it has

[11]The conformal dimension is traditionally given in response to energy units being scaled, as opposed to length units.

dimension of [length]$^{-\Delta}$. If we consider a deformation to the field theory of the form

$$\delta\mathcal{S} = \int d^4x\, \mathcal{O}(x)\phi_{(0)}(x)\,, \tag{1.34}$$

we see that if $\Delta = \Delta_+$ then our scalar field's asymptotic coefficient $\phi_{(0)}(x^\mu)$ has the correct dimensions to play the role of a source for the operator $\mathcal{O}$, and thus the holographic dictionary tells us that $\phi_{(0)}$ is proportional to the source for the operator $\mathcal{O}$. We call $\phi_{(0)}$ the non-normalizable mode because if the scalar field $\phi(x^\mu, z)$ has this leading z_-^Δ behavior then the total energy of the field will not be finite.

One the other hand, if the field behaves as $\phi_{(+)}z^{\Delta_+}$ then the total energy of this field configuration is finite, and thus $\phi_{(+)}$ is called the normalizable mode. Additionally, the exact same line of dimensional analysis arguments tells us that $\phi_{(+)}$ has the correct dimensions to be proportional to the expectation value $\langle\mathcal{O}\rangle$ in the state of the field theory.

In summary, when a bulk field and boundary operator are dual, $\phi \leftrightarrow \mathcal{O}$, we must asymptotically expand the bulk field towards the boundary, and note the two important coefficients. These relations between the two asymptotic coefficients of ϕ along with the field theory operator, $\mathcal{O}$, and it's expectation value, $\langle\mathcal{O}\rangle$, are what makes ϕ and $\mathcal{O}$ dual. The standard practice from the QFT point of view would be to fix the value of the source, $\phi_{(0)}$, and then extract the expectation value, $\langle\mathcal{O}\rangle$. As we have presented it, the non-normalizable mode relates to the source of the operator $\mathcal{O}$ while the normalizable mode corresponds to the expectation value of the operator in the field theory[12].

Lastly, based on the associations we've made between the asymptotic coefficients and the dual operator, we see that there is a relation between the mass of the bulk field ϕ, and the conformal dimension of the dual operator $\mathcal{O}$. For the scalar case we have

$$m^2L^2 = \Delta(\Delta - d)\,. \tag{1.35}$$

[12]There is a subtlety to this setup when the mass of the bulk scalar field is in a specific negative range, and the roles the asymptotic field coefficients may swap roles, for more information see [6]. This will not be relevant for us.

Type of field	Mass and operator dimension
scalars, massive spin two fields	$m^2L^2 = \Delta(\Delta - d)$
spin 1/2, spin 3/2	$\|m\|L^2 = \Delta - d/2$
vector	$m^2L^2 = (\Delta - 1)(\Delta + 1 - d)$
massless spin two fields	$m^2L^2 = 0, \Delta = d$
p-form fields	$m^2L^2 = (\Delta - p)(\Delta + p - d)$
rank s symmetric traceless tensor	$m^2L^2 = (\Delta + s - 2)(\Delta - s + 2 - d)$

Table 1.1: The relation between conformal operator in the CFT and the mass of the dual field on the gravitational side. Obtained from [2, 6].

Similarly, these relations can be collected for the various types of fields that exist in the AdS_{d+1} bulk, and the results from [2, 6] are reproduced in table 1.1.

For a large collection of explicit field-operator duals see table 7 of [3] as well as the description in sec. 5.6 of the same reference.

1.1.6 n-point Functions

Now that we know how the field operator map works, we can discuss how this is actually used in practice. We will first need the generating functional for n-point functions. Suppose we deform the action of our boundary theory,

$$S' = S - \int d^d x \, \phi_{(0)}(x)\mathcal{O}(x) \tag{1.36}$$

Now, the partition function for S' will depend on the source, $\phi_{(0)}(x)$. We have

$$Z_{\mathrm{CFT}}[\phi_{(0)}] = \langle \exp\left(\int \mathrm{d^d x} \, \phi_{(0)}(\mathrm{x})\mathcal{O}(\mathrm{x})\right)\rangle_{\mathrm{CFT}} \tag{1.37}$$

where the expectation is taken in the original theory. The gravitational side is governed by $S_{\mathrm{sugra}}[\phi]$ which is derived from a Kaluza-Klein reduction of ten-dimensional type IIB supergravity on $AdS_5 \times S^5$. If we have a particular source $\phi_{(0)}$ in mind, we know from the

previous section and eq. (1.33) that we can restrict the classical solution of ϕ to have an asymptotic coefficient that is precisely the $\phi_{(0)}$ seen in (1.36). Since we are in the limit where we are dealing with classical supergravity on the bulk side, this means our partition function, with the specified boundary value of the scalar field, is given simply as[13]

$$Z_{\text{sugra}}[\phi_0] = \exp\left(-S_{\text{sugra}}[\phi]\Big|_{\lim_{z\to 0}(\phi(x,z)z^{\Delta-d})=\phi_{(0)}(x)}\right). \tag{1.38}$$

The key point is that the generating functionals on both sides of the duality are *equivalent*.

Consider the calculation of an n-point correlation function of $\mathcal{O}$ in the CFT,

$$\langle \mathcal{O}_1 \dots \mathcal{O}_n \rangle = \frac{\delta^n}{\delta\phi_{(0)} \dots \delta\phi_{(0)}} Z_{\text{CFT}}[\phi_{(0)}]\Big|_{\phi_{(0)}=0} \tag{1.39}$$

In the $\lambda \gg 1$ limit, the standard techniques of perturbation theory run into trouble because we cannot expand Z_{CFT} perturbatively in a small coupling. With the AdS/CFT conjecture, we can replace the generating functional with the equivalent generating functional (1.38) from supergravity,

$$\langle \mathcal{O}_1 \dots \mathcal{O}_n \rangle = \frac{\delta^n}{\delta\phi_{(0)} \dots \delta\phi_{(0)}} Z_{\text{CFT}}[\phi_{(0)}]\Big|_{\phi_{(0)}=0} = \frac{\delta^n}{\delta\phi_{(0)} \dots \delta\phi_{(0)}} Z_{\text{sugra}}[\phi_{(0)}]\Big|_{\phi_{(0)}=0}, \tag{1.40}$$

which is given by (1.38).

This whole process is nicely summarized in [6] and we repeat their bulletpoints here:

- Determine the bulk field ϕ which is dual to the operator $\mathcal{O}$ of dimension Δ and compute S_{sugra} by reducing type IIB supergravity on the sphere S^5.

- Solve the supergravtiy equations of motion for ϕ, subject to the boundary condition $\phi(x,z) \sim z^{d-\Delta}\phi_{(0)}(x)$ for $z \to 0$.

[13] It is easiest to discuss the Euclidean case. If one wants the field theory to live in Minkowski space, we must make a Wick rotation which adds an i to the exponent in the partition function but also has some subtleties we will not discuss here, see ref. [12].

- Insert the solution $\widetilde{\phi}$ into the supergravity action, subject to the appropriate boundary behavior.

- Take variational derivatives with respect to the source $\phi_{(0)}$ to obtain connected correlation functions.

In practice, for this work, the first bulletpoint has already been completed for operators of interest, and we are only left performing the last three.

1.1.7 Holographic Renormalization

We know that Quantum Field Theories exhibit UV divergences. If this mathematical equivalence is real, we should see these divergences show up in the dual gravitational theory as well, say, when calculating n-point functions. It may seem odd to expect divergences from a classical theory, but these are merely infinite volume divergences on the bulk side. We will need analogous ways to regulate and renormalize these divergences. In attempting to calculate n-point functions given by eq. (1.40) one runs into these divergences near the boundary. "Holographic Renomalization" is a procedure of regularizing these divergences, adding counterterms and then using a renormalized action to calculate the n-point functions instead. The entire process is well explained in references [13, 14].

Without going into details, one forms a regularized action, S_{reg}, by using the original action evaluated on the classical solution, but cutting off the radial integral at some ϵ away from the boundary. The on-shell action for S_{reg} will have divergences with various powers of ϵ and sometimes $\log(\epsilon)$. We will need to remove these divergences with counter terms. We cannot just subtract the divergences seen in S_{reg}, we must instead build S_{ct} out of local functions of the sources attached to appropriate functions of ϵ such that they cancel the divergent pieces of S_{reg}. Finally, we form S_{ren} via

$$S_{\text{ren}} = \lim_{\epsilon \to 0} (S_{\text{reg}} + S_{\text{ct}}) \,. \tag{1.41}$$

The result for calculating finite n-point functions involves taking variations of S_{ren} instead of the original action. For example, for 1-point functions that we will be interested in, the prescription becomes

$$\langle \mathcal{O}(x) \rangle = \frac{1}{\sqrt{g_{(0)}(x)}} \frac{\delta S_{\text{ren}}}{\delta \phi_{(0)}(x)} \,, \tag{1.42}$$

$$\langle \mathcal{J}_\mu(x) \rangle = \frac{1}{\sqrt{g_{(0)}(x)}} \frac{\delta S_{\text{ren}}}{\delta A^\mu_{(0)}(x)} \,, \tag{1.43}$$

$$\langle \mathcal{T}_{\mu\nu}(x) \rangle = \frac{2}{\sqrt{g_{(0)}(x)}} \frac{\delta S_{\text{ren}}}{\delta g^{\mu\nu}_{(0)}(x)} \,, \tag{1.44}$$

where the subscript (0) denotes the leading coefficient in an asymptotic radial expansion of the field.

1.1.8 Generalization to Finite Temperature

Everything we have discussed so far has been for a field theory at zero temperature. What happens in the bulk geometry if we turn on a non-zero temperature in the field theory? If these two theories are really equivalent there should be some geometrical manifestation of the field theory being in equilibrium at a finite temperature. We will state the relevant results and concepts for studying the duality at a non-zero temperature, for a more detailed review see: [15] for finite temperature QFT, [16] for gravity dual and Hawking-Page/deconfinement phase transition, [17] for thermodynamics of black D3-branes, and [18] for thermodynamics of $\mathcal{N} = 4$ SYM.

It turns out that the gravitational dual of the boundary being at a finite temperature is the existence of a *black brane* in the bulk geometry[14]. A black brane is like a black hole but with planar horizon geometry. This should be visualized as a planar horizon at some radial value $r = r_h$ in the bulk. The solution that contains a black brane is not the standard AdS_5 given by eq. (1.19), but is instead the five-dimensional AdS-Schwarzschild black brane solution (discussed below), which has a Hawking temperature T_{H} associated with it, and it

[14]Rather, this is the dual setup when the entropy of the plasma is $\mathcal{O}(N_c^2)$ and the plasma is deconfined. See [16].

is this temperature that is identified with the temperature of the equilibrium field theory on the boundary.

Recall that the standard finite temperature partition function,

$$Z = tr[\exp(-\beta\mathcal{H})] \tag{1.45}$$

is a trace over an operator that looks identical to the time evolution operator if one replaces $t = -i\beta = -i/T$, as $\beta = 1/T$, meaning the time coordinate becomes imaginary.

In finite temparture quantum field theory Green's functions are defined by

$$G^C(x_1, \ldots, x_n) = \langle T_C[\hat{\phi}(x_1) \ldots \hat{\phi}(x_n)]\rangle_\beta \tag{1.46}$$

where $\hat{\phi}$ is an operator in the field theory[15], and the thermal ensemble average of any operator is defined by

$$\langle\hat{\phi}\rangle_\beta = \frac{tr[\hat{\phi}\,\exp(-\beta\mathcal{H})]}{tr[\exp(-\beta\mathcal{H})]}\,. \tag{1.47}$$

The time ordering is controlled by the complex time contour C, i.e. ordering is determined by where the time coordinates of each operator lie along this curve.

The standard derivation of the imaginary time formalism involves taking C to extend from 0 to $-i\beta$ along the imaginary time axis. One then compactifies the Euclidean time $\tau = it$ on a circle $\tau\,\varepsilon\,[0, \beta]$. Fields will then necessarily satisfy periodic or anti-periodic conditions on this time circle depending on whether they are bosonic or fermion, respectively. If the time coordinate is periodic, then the Fourier transform conjugate variable, ω, must be quantized. These quantized values are called Matsubara frequencies. Once one knows the Feynman rules for a QFT at zero temperature, the corresponding rules for calculating the thermal Green's function for a thermal field theory in equilibrium are straightforwardly obtained – see table 11.1 of [6].

On the gravitational side, the dual geometry to the boundary field theory in equilibrium

[15]Not the scalar field ϕ in the bulk discussed earlier.

at finite temperature is given by the five-dimensional AdS-Schwarzschild black brane,

$$ds^2 = -U(r)\,dt^2 + \frac{dr^2}{U(r)} + \frac{r^2}{L^2}\,(dx^i)^2 \tag{1.48}$$

$(i = 1, 2, 3)$, with

$$U(r) \equiv \frac{1}{L^2}\left(r^2 - \frac{r_{\rm h}^4}{r^2}\right), \tag{1.49}$$

where the zero of $U(r)$ determines the horizon location. Note that this geometry approaches AdS space as $r \to \infty$, and thus the space is one of many "Asymptotically AdS" spaces. The horizon temperature is proportional to the horizon radius,

$$\pi T_{\rm h} = r_{\rm h} L^{-2}. \tag{1.50}$$

We can see this by the following exercise. Taking our metric, make the following variable change $r = rh\left(1 + \frac{\rho^2}{L^2}\right)$ and $\tau = it$. The distance away from the horizon is measured by ρ, and our near horizon metric, $\frac{\rho}{L} \ll 1$, becomes

$$ds^2 \sim \frac{4\rho^2 r_{\rm h}^2}{L^4} d\tau^2 + d\rho^2 + \frac{r_h^2}{L^2} dx^2\,. \tag{1.51}$$

Now define $\theta = 2\frac{r_{\rm h}}{L^2}\tau$ and we have,

$$ds^2 \sim \rho^2 d\theta^2 + d\rho^2 + \frac{r_h^2}{L^2} dx^2\,. \tag{1.52}$$

The (ρ, θ) part of this metric looks like polar coordinates. Demanding no conical singularity at $\rho = 0$ requires that we impose periodicity of $\theta = \theta + 2\pi$. Converting back to our imaginary time coordinate τ, this implies a periodicity of $\tau = \tau + \pi L^2/r_{\rm h}$. So our periodicity is $\beta = \pi L^2/r_{\rm h}$ and thus the Hawking temperature is $T_{\rm H} = 1/\beta = r_{\rm h}/\pi L^2$. Since these coordinates extend to the boundary, the boundary coordinates have the same imaginary time periodicity and thus the same temperature. This is what the AdS/CFT dictionary tells us, that the Hawking temperature of the black brane in our Asymptotically AdS space is the

temperature of the dual boundary field theory.

1.2 Near-Equilibrium Techniques

A particularly important experimental application of holographic calculations involves the quark-gluon-plasma (QGP) created in heavy-ion collisions at the Relativistic Heavy-Ion Collider in New York and the Large Hadron Collider in Switzerland. There is evidence that the dynamics of the early-time QGP produced in heavy-ion collisions are dominated by a strongly coupled regime [19, 20]. We know of only certain gauge theories which have holographic duals, and thus can be studied via holography, and quantum chromodynamics (QCD) – the underlying theory of the QGP – is not one of them. The simplest of the theories with holographic duals is $\mathcal{N}=4$ SYM, but additionally, there are reasons to believe that $\mathcal{N}=4$ SYM is actually a good approximation for QCD in the energy regimes produced in heavy-ion collisions [21, 22]. In fact, holography has assisted us in understanding various parts of QGP phenomenology, including shear viscosity, drag, screening lengths and jet quenching [23, 5]. Regardless, we can certainly use the tools of holography to learn about the properties of a strongly-coupled $\mathcal{N}=4$ SYM plasma, and then perhaps extrapolate to the QCD plasma.

If one wants to study strongly coupled plasmas with holographic duals, we've seen from the introduction that we can use holography to recast the problem into a gravitational one. Suppose then, that we have an equilibrium gravitational background dual to an equilibrated field theory system of interest. The most straight forward and easiest of questions to ask involve teasing out features of the system in a way that does not disturb the system itself. This lack of disturbance, or 'back-reaction', is called the *probe approximation*. This is a familiar concept from electrodynamics, where one uses test charges to find out the value of the electric field or electric potential without changing the field itself (not technically possible for realistic charges). This is also done in classical Newtonian dynamics using test masses to find the gravitational field and potential. Likewise, we will want to introduce small probes into our system which do not back-react, and try to extract useful information.

1.2.1 Dragging Defects

One phenomenologically relevant issue involves the energy loss of a probe (or test) quark dragged through a strongly coupled plasma (either $\mathcal{N}=4$ SYM or QCD). Part of understanding plasma thermalization is learning how a single hard probe loses energy to the surrounding plasma. This sort of analysis had been done for the weakly-coupled case, but since there is support for QGP being strongly coupled, we can use holography to calculate these quantities for the $\mathcal{N}=4$ SYM proxy theory. This is experimentally interesting as we can think about massive quarks as being probes, particularly the 'bottom' quark (the 'top' decays too quickly to form bound states). The way these heavy quarks equilibrate, and their elliptic flow (a measure of azimuthal asymmetry) differs from the lighter quarks because of how heavy they are. Understanding the energy loss rates as a function of the mass of the probe quark gives us information in a direction of understanding elliptic flow. Energy loss of hard probes is also relevant to understanding jet quenching - a phenomenon where two or three hard probes are ejected back to back but some of the probes thermalize with the bulk of the QGP and thus are not seen by the detector. A full holographic analysis of hard probes was performed and presented in a very nice paper found here [24].

In the second chapter of this thesis, we extend and generalize these types of energy loss calculations by considering other backgrounds, and other dimensional defects. In order to stay as general as possible, we use a generic form for metrics sourced by general D_p-branes (as opposed to only D_3-branes we discussed in the introduction) as well as backgrounds coming from 'holographic superconductors' [16]. We also generalize the defect itself to include dimensions larger that zero, which can help understand vorticies (one dimensional defects) in superconductors. This work can be found in chapter 2 of this thesis.

---

[16] Holographic superconductors are a part of another facet of holography interested in answering questions pertaining to condensed matter theory, sometimes referred to as 'AdS/CMT'. We will touch on these interests in sec. 1.4.

1.2.2 Infinite Momentum Excitations

Additionally, one can move beyond the probe approximation, and in fact we must if we want to describe the dynamics of a strongly coupled plasma. The next step is linearized response which involves considering only very small perturbations to the system in equilibrium. An interesting part of linearized response are the so-called *quasi-normal modes*.

In gravitational systems, we can add small perturbations to metric components, keep only first order in these small perturbations, and solve the equations of motion for the perturbation coming from Einstein's equations. From a holographic viewpoint, these fluctuations represent small deviations from the equilibrium configuration of the field theory. These perturbations oscillate and die as a function of time as they thermalize, thus the eigenfrequncies involved are complex. One can see this from the gravitational side as well – fluctuations in the metric can be absorbed by the black brane (which we need to represent a finite temperature field theory) and thus again, we expect to find complex frequencies. A good starting point for understanding quasi-normal modes in the context of holography can be found in [25] as well as section 12.1.3 of [6].

We will be interested in a particular kind of perturbation. A small perturbation of stress-energy tensor in the limit of infinite wave vector. One might expect that a pulse with significantly high momentum will be long lived. We are interested in the propagation of such a pulse, and thus need to know how the pulse is composed of quasi-normal modes and their corresponding frequencies. Work in this area is currently being finished by JF, Christoph Uhlemann, and Laurence Yaffe, and will be on *arXiv.org* shortly following the publication date of this thesis. For now, let us discuss an introduction to the ideas and results.

The idea is to study the damping of high momentum excitations of a strongly coupled $\mathcal{N} = 4$ SYM plasma with an $SU(N)$ gauge group in the large-N limit via the holographic tools we have discussed. The timescale for relaxation of non-hydrodynamic perturbations in this plasma is set by the inverse temperature T^{-1} [26]. Holographically, this is the time it takes for metric perturbations in the bulk to be absorbed by the black brane which sets

the thermal equilibrium state. We find that even in the strong coupling limit, however, very high momentum states are weakly damped. Specifically, the quasinormal mode frequencies for a given momentum, q, in the large-q limit is given by

$$\omega_n(q) \sim |q| \left[1 + s_n \, e^{-i\pi/3} \left(\frac{\pi T}{q} \right)^{4/3} \right], \tag{1.53}$$

where s_n is a real constant. Because of the fact that $|q| \gg T$ for these excitations, they exhibit a small imaginary part when compared to their real part. The imaginary part of the frequency governs the rate of damping, and thus, these excitations may indeed, in some sense, be thought of as long-lived quasiparticles. It should be noted that these excitations are quite rare in a thermal distribution precisely because $|q| \gg T$.

The forthcoming paper derives the form of equation 1.53 by recasting the equation of motion for the modes and navigating a subtle WKB approach, and then numerically calculates s_n via pseudo-spectral methods. The coefficients are calculated for each of the various spin channels of perturbations that may be excited in the metric. Once the frequencies are accurately calculated, sufficiently weak planar shocks are built from a superposition of quasi-normal modes. At zero temperature, these modes would propagate at the speed of light, as can be seen from the $T \to 0$ limit of the dispersion relation 1.53. However, when a low temperature is turned on, these shocks will experience drag brought on by thermal excitations, slowly damping the profile of the shock and dispersing out the modes.

1.3 Far-From-Equilibrium Techniques

To study dynamics more thoroughly we can go past the probe and linearized approximation to the full non-linear and far-from-equilibrium dynamics of the strongly coupled plasma. This is necessarily much more difficult and computationally intense - and indeed, where the bulk of my thesis lies. A thorough introduction to the methodologies of numerical calculations in AdS space can be found in [27].

The idea is to perturb the spacetime as far as one likes and monitor the dual field theory's

path to equilibrium. There are many physically interesting reasons to perform such a study. Again, we motivate with an interest towards the QGP. One of the more phenomenologically interesting properties of the QGP is the fact that the plasma produced in heavy-ion collisions very quickly becomes amenable to the methods of hydrodynamics. Hydrodynamics is only applicable for small variations in the thermodynamic state variables, when there is some sense of local equilibration, and yet the production of the QGP comes about from an extremely violent process. This rapid equilibration timescale was unexpected and can be investigated with a full non-linear and holographic approach [26, 28, 29].

With a desire to a more accurately describe the dynamics of the QGP, we can consider how large magnetic fields or finite baryon density effects the timescale of equilibration. While electromagnetic fields are weaker than the strong force present in the QGP, it is thought that large but transient fields play a role in equilibration, and thus it is worthwhile to explore this effect. Additionally, experimentally realizable QGP happens at finite baryon density (or chemical potential) and we are interested in exploring the effect that this has on the equilibration timescale. Both of these effects are investigated in chapter 3.

1.4 Non-Relativistic Directions

Finally, we've included a project that is a departure from our QGP motivated work. Another experimental motivation for holography lies in condensed matter physics. These systems have interesting prospects for holography as they can be experimentally realized and probed in the laboratory and be tuned to strong coupling. There is a community developing around the study of condensed matter systems using holography, collectively refereed to as 'AdS/CMT'. For a great review on types of problems and system they address, see [30, 31]

One of the main differences between these studies and what we have been studying before, is that these systems have different symmetry groups and are sometimes non-relativistic. Specifically, one wants to develop new manifestations of holography, which have boundary QFT's that exhibit the properties and symmetries of the condensed matter system you wish to study. There has been an effort to develop non-relativitic versions of holography,

and progress in this area requires a solid understanding of the symmetry groups of interest on the field theory side. One such non-relativistic structure is called the Newton-Cartan structure and we are interested in how one could obtain the Newton-Cartan structure for fermions via a non-relativistic reduction. Put simply, we wanted to see how this particular non-relativistic structure could arise from a relativistic parent theory at high energies. This work is presented in chapter 4.

Chapter 2

ENERGY LOSS OF GENERIC DEFECTS

This chapter is based on a publication in collaboration with Andreas Karch [32]. The bulk of the calculations were performed by me (JF), the writing of the manuscript was shared, and Andreas performed the bulk of the interpretation.

2.1 Introduction

The duality between Type IIB string theory on $AdS_5 \times S^5$ and $\mathcal{N} = 4$ SU(N) supersymmetric Yang-Mills (SYM) [1, 33, 4] has been studied extensively as a means to provide insight to the inner workings of strongly coupled systems where perturbation theory is not valid, and where lattice gauge theory and Monte Carlo techniques are available but struggle with real time physics. Motivated by the QGP created at RHIC, holography has helped guide our understanding of shear viscosity, drag, screening length and jet quenching to name a few; see [23] for a recent perspective on these developments by one of us. The dual description of a classical string ending on a probe brane has given information on the characteristics of a point particle, possibly a quark, traveling through the Yang-Mills plasma, which is thought to be a good approximation for the strongly coupled QCD. Recently it has been seen that one can also study extended defects with dimensions larger than a point, living in AdS_d spaces, the idea being that one can shed new light on the dynamics of energy loss at strong coupling [34]. We extend the ideas of [35, 36, 34] to a general metric with a compact internal space. We produce general solutions for the equation of motion and the energy loss of an extended defect moving uniformly through the bulk whose geometry is described by a generic brane-like metric. We study two examples in detail, general Dp-brane metrics and holographic superfluids. After working out the energy loss for Dp-branes, we

find that the energy loss of these extended probes is given by simple power laws in velocity and temperature, revealing that the energy loss depends only on an effective temperature multiplied by the velocity squared - the moving probe being affected only by a blue-shifted energy density - despite the existence of an intrinsic scale in the underlying theory. We then apply our results to dragging string- and sheet-like defects through holographic superfluids.

We organize these ideas as follows: In section II, we will calculate a general equation of motion and solution to a uniformly moving defect in a general bulk theory. We then find a general energy loss formula for said defect. In section III, we apply these results to metrics created by general Dp-branes. In section IV, we apply our results to a holographic superfluid.

2.2 Calculations

We want to study a general holographic brane-like metric. This metric will preserve the symmetries of the dual field theory. Therefore, it should be rotationally invariant and translationally invariant in both the spatial and time dimensions. In addition it should preserve the isometries of the internal space. To these ends, we introduce the following diagonal metric

$$\begin{aligned} ds^2 &= G_{\mu\nu}dx^\mu dx^\nu \\ &= G_{tt}dt^2 + G_{xx}\sum_{i=1} dx_i^2 + G_{uu}du^2 + G_{\theta\theta}d\Omega^2, \end{aligned} \tag{2.1}$$

with $N+2$ total space-time dimensions. At this point, the $N+1$ spatial coordinates are arbitrarily separated into M Cartesian coordinates and $N-M$ spherical angles of the internal space. The additional radial coordinate is denoted by u. It is understood that $G_{\theta\theta}$ is only a function of u and since none of our results depend on the details of the internal space we will take $d\Omega^2$ be a unit sphere - i.e. $d\Omega^2$ contains the appropriate terms for the angular variables of a unit sphere of arbitrary dimension. The background will continue to solve the same equations of motion should the sphere be replaced with any other compact Einstein manifold. We are only considering metrics whose G_{ii} depend only on u, and whose G_{tt} and

G_{xx} grow with u at the same rate, both of which grow faster with u than $G_{\theta\theta}$. The rationale behind this is that the gravity theory in the bulk has a dual interpretation in terms of a field theory at the $u = \infty$ boundary which lives in $M + 1$ space-time dimensions.

In a manner similar to [34], we introduce a defect of spatial dimension $n + 1$ in the bulk. The defect has n spatial dimensions orthogonal to u which are divided into m infinitely extended Cartesian directions on the boundary, denoted $\vec{y}$, and $n - m$ angular directions, denoted $\vec{\theta}$. It will then move in an additional transverse direction, x. Since the dimensionality of the bulk puts constraints on the size of the defect we find $m + 1 \leq M$ and $n + 1 \leq N$.

In the static gauge, the world-volume map is of the form $X = (t, u, \vec{y}, \vec{\theta}, x(t, u, \vec{y}, \vec{\theta}), \vec{z} = const)$ where $\vec{z}$ are any additional unused orthogonal coordinates in the bulk. The induced metric on the world volume is defined as $g_{\alpha\beta} = G_{\mu\nu}\frac{\partial X^\mu}{\partial \sigma^\alpha}\frac{\partial X^\nu}{\partial \sigma^\beta}$. We find $g = \det(g_{\alpha\beta})$ to be

$$\begin{aligned} g = G_{xx}^m G_{\theta\theta}^{n-m}[&G_{tt}G_{uu} + G_{tt}G_{xx}(x_{,u})^2 \\ &+ G_{uu}G_{xx}(x_{,t})^2 + G_{tt}G_{uu}\sum_i^m (x_{,y_i})^2 \\ &+ \frac{G_{tt}G_{uu}G_{xx}}{G_{\theta\theta}}\sum_j^{n-m}(x_{,\theta_j})^2] \end{aligned} \tag{2.2}$$

where $(x_{,\sigma})$ denotes the partial derivative of x with respect to the coordinate σ.

Our general metric will have some intrinsic scale governed by its radii of curvature, all of which we take parametrically to be of the same order R. The bulk theory will be governed by classical gravity if R abides by $M_{pl}R \gg 1$, where $M_{pl}^N = 1/16\pi G$, (ensuring our curvature is not too large in Planck units). We want to describe the defect by the following Nambu-Goto-like action

$$S = -T_0 \int e^{-\Phi}\sqrt{-g}\prod_i d\sigma_i \tag{2.3}$$

where g is given by (2.2), T_0 is the tension and the integral is over all world-volume coordinates. Φ is a function of the background scalar fields, the dilaton field, ϕ, for example. Unlike the coupling to the background metric, the functional form of the coupling to the

background scalars is not fixed by diffeomorphism invariance and in principle $e^{-\Phi}$ can be a complicated function of the background scalars. As long as the background scalars respect the symmetries of the metric, they can only depend on the radial coordinate u and we can treat Φ as a function of u. Two important probes we are going to consider in examples for $\Phi(u)$ are a fundamental string, whose action has the form (2.3) with $\Phi = 0$, and probe D-branes, whose action is of the form (2.3) with $\Phi = \phi$. We can trust the classical treatment of this action so long as $T_0 R^{n+2} \gg 1$. Additionally, demanding that $(M_{pl}R)^N \gg T_0 R^{n+2}$ will render gravitational back-reaction negligible.

With $\mathcal{L} = -T_0 e^{-\Phi}\sqrt{-g}$ we find the following canonical momentum densities:

$$\begin{aligned}
\Pi^t_x &= \frac{\partial \mathcal{L}}{\partial(x_{,t})} = -T_0 \frac{G_{uu}G_{xx}^{m+1}G_{\theta\theta}^{n-m}}{\sqrt{-g}}(x_{,t})e^{-\Phi} \\
\Pi^u_x &= \frac{\partial \mathcal{L}}{\partial(x_{,u})} = -T_0 \frac{G_{tt}G_{xx}^{m+1}G_{\theta\theta}^{n-m}}{\sqrt{-g}}(x_{,u})e^{-\Phi} \\
\Pi^{y_i}_x &= \frac{\partial \mathcal{L}}{\partial(x_{,y_i})} = -T_0 \frac{G_{tt}G_{uu}G_{xx}^{m}G_{\theta\theta}^{n-m}}{\sqrt{-g}}(x_{,y_i})e^{-\Phi} \\
\Pi^{\theta_i}_x &= \frac{\partial \mathcal{L}}{\partial(x_{,\theta_i})} = -T_0 \frac{G_{tt}G_{uu}G_{xx}^{m+1}G_{\theta\theta}^{n-m-1}}{\sqrt{-g}}(x_{,\theta_i})e^{-\Phi}
\end{aligned} \tag{2.4}$$

Requiring a vanishing variation in our action yields

$$\sum_i^n \partial_{\sigma_i}(\Pi^{\sigma_i}_\mu) = 0 \tag{2.5}$$

Setting μ to x gives us our equation of motion.

We are interested in a solution of a uniformly moving object. The defect should move in a direction transverse to its spatial extent and travel with a constant velocity in the x direction. Thus, our ansatz is

$$x(t, u, \vec{y}) = vt + x(u).$$

With this form, g becomes independent of time and our equation of motion, $\sum_i^n \partial_{\sigma_i}\Pi^{\sigma_i}_{mu} =$

0, will then reduce to

$$\partial_u \left(\frac{G_{tt} G_{xx}^{m+1} G_{\theta\theta}^{n-m}}{\sqrt{-g}} (x_{,u}) e^{-\Phi} \right) = 0,$$

which gives us

$$(x_{,u})^2 = \frac{C^2 e^{2\Phi}(-g)}{G_{tt}^2 G_{xx}^{2(m+1)} G_{\theta\theta}^{2(n-m)}}, \tag{2.6}$$

and plugging in for g

$$(x_{,u})^2 = -(Ce^{\Phi})^2 \frac{G_{uu}}{G_{tt} G_{xx} e^{2\Phi}} \{ \frac{G_{tt} + G_{xx} v^2}{G_{tt} G_{xx}^{m+1} G_{\theta\theta}^{n-m} e^{-2\Phi} + C^2} \} \tag{2.7}$$

We expect on physical grounds, that $(x_{,u})$ should be real, and thus $(x_{,u})^2$ and $(-g)$ should be positive. From (2.7), we see that this will be true if $G_{tt}+G_{xx}v^2$ and $G_{tt}G_{xx}^{m+1}G_{\theta\theta}^{n-m}e^{-2\Phi}+C^2$ both switch sign at the same value of u. Assuming that there is at most one root, call it u_c, we can solve for it from

$$G_{tt}(u_c) + G_{xx}(u_c) v^2 = 0 \tag{2.8}$$

and if this root exists, we have

$$C = \pm e^{-\Phi} \sqrt{-G_{tt} G_{xx}^{m+1} G_{\theta\theta}^{n-m}}|_{u=u_c}.$$

The case where u_c does not exist occurs in our example of a holographic superfluid and will be discussed in section IV. The induced metric can be diagonalized and this diagonal form has a time component which vanishes when $G_{tt}(u_c) + G_{xx}(u_c)v^2 = 0$. This tells us that u_c denotes the worldvolume horizon.

Using (2.8) to plug in for G_{tt} and defining $\widetilde{C} = C/v$ we have

$$\widetilde{C} = \pm e^{-\Phi} \sqrt{G_{xx}^{m+2} G_{\theta\theta}}|_{u=u_c} \tag{2.9}$$

The momentum loss rate, due to momentum flowing along the defect and towards the

horizon, is given by -Π^u_x which is seen from (2.4) and (2.6) to be

$$-\Pi^u_x = T_0 C. \tag{2.10}$$

The momentum loss rate directly gives us the drag force density. The energy loss rate, $-\Pi^u_t$, is simply v times the momentum loss rate. Physically, we expect that we have energy flowing towards the horizon of the black brane, which requires our loss rate to be positive. We thus pick the positive sign for $\widetilde{C}$.

$$\widetilde{C} = e^{-\Phi}\sqrt{G^{m+2}_{xx} G^{n-m}_{\theta\theta}}|_{u=u_c}. \tag{2.11}$$

While we have established that this stationary solution is a consistent solution to the equations of motion, what is less obvious is that it is stable. Small fluctuations around dragging sheets in AdS_7 have recently been studied in [37] and it has been found that these fluctuations do not exhibit any instabilities, that is any modes that grow exponentially in time. A new potential instability in our case is the slipping mode on the internal space, that is fluctuations in the θ directions that take our defect off the equator of the internal sphere. As such fluctuations reduce the volume of the defect (and hence its potential energy), they clearly correspond to negative mass squared modes and are hence potentially problematic. It is well known from the case of static defects, starting with the work on flavor probe branes [38], that these negative mass squared slipping modes often are actually stable. For a background AdS space the basic physics behind this is the BF bound [39]. The potential energy gain of the fluctuation is offset by the kinetic energy cost of any fluctuation in a spacetime geometry that effectively corresponds to a finite size box. A similar effect also occurs in the more general holographic metrics. In particular, it has been shown in [40] that supersymmetric Dq-brane defects in black Dp-brane backgrounds (which will be the first example we apply our results to) have stable slipping modes. For non-supersymmetric defects stability of the slipping mode will have to be checked on a case by case basis.

2.3 p-branes

We now turn to the example of general Dp-branes which create geometries dual to SYM in $p+1$ dimensions on the boundary, at finite temperature. From [41] we see that in the limit that

$$g_{YM}^2 = (2\pi)^{p-2} g_s \alpha'^{(p-3)/2} = \mathsf{fixed},$$

as

$$\alpha' \to 0$$

where $g_s = e^{\phi_\infty}$, and g_{YM} is the Yang-Mills coupling constant, the Dp brane metric becomes,

$$\begin{aligned} ds^2 = \alpha' \{ & \frac{u^{(7-p)/2}}{g_{YM}\sqrt{d_p N'}} \left[-(1 - \frac{u_0^{7-p}}{u^{7-p}}) dt^2 + dy_\parallel^2 \right] \\ & + \frac{g_{YM}\sqrt{d_p N'}}{u^{(7-p)/2}(1 - \frac{u_0^{7-p}}{u^{7-p}})} du^2 \\ & + g_{YM}\sqrt{d_p N'} u^{(p-3)/2} d\Omega_{8-p}^2 \} \end{aligned} \tag{2.12}$$

which indeed is of the general form (2.1). Here, N' is the number of branes and $d_p = 2^{7-2p}\pi^{\frac{9-3p}{2}}\Gamma(\frac{7-p}{2})$.

The dilaton is

$$e^{\phi} = (2\pi)^{2-p} g_{YM}^2 (\frac{g_{YM}^2 d_p N'}{u^{7-p}})^{\frac{3-p}{4}}, \tag{2.13}$$

and

$$u_0^{7-p} = \frac{\Gamma(\frac{9-p}{2}) 2^{11-2p} \pi^{\frac{13-3p}{2}}}{(9-p)} g_{YM}^4 \epsilon, \tag{2.14}$$

where ϵ corresponds to the energy density of the Yang-Mills theory.

Following the outline laid out in the previous section, we first need to find u_c from (2.8). Extracting G_{tt} and G_{xx} from (2.12), and plugging into (2.8) we find

$$u_c = \frac{u_0}{(1-v^2)^{1/(7-p)}} \tag{2.15}$$

At this stage we need to commit to the nature of the probe, that is we need to chose a particular function Φ. Let us first focus on the case where the dragging object is a D$(n+1)$-brane itself, in which case it couples to the string theory dilaton ϕ with an overall prefactor of $e^{-\phi}$ in the action, that is $\Phi = \phi$. From (2.10) we find we can isolate the dependence of $\widetilde{C}$ on v and T

$$\widetilde{C} = P(1-v^2)^A T^B \tag{2.16}$$

Where the prefactor is,

$$P = \left(\frac{(\alpha')^{n+2}(2\pi)^{2(p-2)}}{g_{YM}^4 (g_{YM}\sqrt{d_p N})^{2m-n-p+5}} \right)^{\frac{1}{2}} \left(\frac{4\pi}{7-p} \right)^B, \tag{2.17}$$

$$A = -\frac{1}{4}\left(5 + m - p + \frac{(p-3)(n-m)}{(7-p)} \right) \tag{2.18}$$

and

$$B = -2\frac{(7-p)}{(5-p)}A. \tag{2.19}$$

Here we have made use of the relation

$$u_0 = \left(\frac{4\pi T}{7-p} \right)^{\frac{2}{5-p}}. \tag{2.20}$$

Various dependencies of $\widetilde{C}$ on velocity and temperature are shown in the following tables for different values of p (rows) and n (columns). Each table has a specific value of m, and the entries in the table are of the form $\{A,B\}$, where A and B are defined as in (2.16).

Table I shows the dependencies for allowing our defect to have a point on the internal sphere, $n = m$. For table II we allow one spatial dimension of the defect to go to the internal space (our defect must have a minimum dimension of $n = 1$, as we are insisting that one of our spatial dimensions lives in the internal sphere). For table III we allow two spatial dimensions of our defect to go to the internal space (now our defect must have at least 2 spatial dimensions, $n = 2$, and p must contain n, meaning $p \geq 2$).

$p\backslash n$	0	1	2	3	4
1	$\{-1, 3\}$	$\{-\frac{5}{4}, \frac{15}{4}\}$	N/A	N/A	N/A
2	$\{-\frac{3}{4}, \frac{5}{2}\}$	$\{-1, \frac{10}{3}\}$	$\{-\frac{5}{4}, \frac{25}{6}\}$	N/A	N/A
3	$\{-\frac{1}{2}, 2\}$	$\{-\frac{3}{4}, 3\}$	$\{-1, 4\}$	$\{-\frac{5}{4}, 5\}$	N/A
4	$\{-\frac{1}{4}, \frac{3}{2}\}$	$\{-\frac{1}{2}, 3\}$	$\{-\frac{3}{4}, \frac{9}{2}\}$	$\{-1, 6\}$	$\{-\frac{5}{4}, \frac{15}{2}\}$

Table 2.1: $\{A,B\}$ displayed for the case where the defect does not extend into the internal space, $m = n$.

$p\backslash n$	1	2	3	4
1	$\{-\frac{11}{12}, \frac{11}{4}\}$	N/A	N/A	N/A
2	$\{-\frac{7}{10}, \frac{7}{3}\}$	$\{-\frac{19}{20}, \frac{19}{6}\}$	N/A	N/A
3	$\{-\frac{1}{2}, 2\}$	$\{-\frac{3}{4}, 3\}$	$\{-1, 4\}$	N/A
4	$\{-\frac{1}{3}, 2\}$	$\{-\frac{7}{12}, \frac{7}{2}\}$	$\{-\frac{5}{6}, 5\}$	$\{-\frac{13}{12}, \frac{13}{2}\}$

Table 2.2: $\{A,B\}$ displayed for the case where the defect extends into one dimension in the internal space, $m = n - 1$.

$p\backslash n$	2	3	4
2	$\{-\frac{13}{20}, \frac{13}{6}\}$	N/A	N/A
3	$\{-\frac{1}{2}, 2\}$	$\{-\frac{3}{4}, 3\}$	N/A
4	$\{-\frac{5}{12}, \frac{5}{2}\}$	$\{-\frac{2}{3}, 4\}$	$\{-\frac{11}{12}, \frac{11}{2}\}$

Table 2.3: $\{A,B\}$ displayed for the case where the defect extends into two dimensions of the internal space, $m = n - 2$.

The Dp-brane energy density obeys the following relation, $\epsilon \sim T^{2\frac{(7-p)}{5-p}}$. Under a boost, we expect $\epsilon \to \gamma^2\epsilon$ and thus $T^{2\frac{(7-p)}{(5-p)}} \to \gamma^2 T^{2\frac{(7-p)}{(5-p)}}$. This motivates the definition of

$$T_{\mathsf{eff}} = \gamma^{\frac{(5-p)}{(7-p)}} T = \gamma^{-2A/B} T. \tag{2.21}$$

With this definition of the effective temperature we see that, analogous to relation (2.20), we have an identical relation between the worldvolume horizon and the effective temperature,

$$u_c = \left(\frac{4\pi T_{\mathsf{eff}}}{7-p}\right)^{\frac{2}{5-p}}. \tag{2.22}$$

Consequently we see that $T^B = (1-v^2)^{-A} T^B_{\mathsf{eff}}$ and so we can rewrite $\widetilde{C}$ as

$$\widetilde{C} = P T^B_{\mathsf{eff}}. \tag{2.23}$$

This tells us that the loss rate of the moving defect is only dependent on velocity in a trivial way - the defect only sees a blueshifted energy density - and that there are no sensitivities to the microscopic details of the plasma despite the fact that g_{YM} is a dimensionfull quantity and hence defines a microscopic scale in the system. Presumably this is a consequence of the hidden conformal invariance that is present in the Dp brane systems as first exhibited in [42].

There is an area of overlap between this work and [34], where in the latter, various dimensional defects are studied is AdS spaces of variable dimension. Our results for a Dp-brane with $p = 3$ reproduce the equation of motions and loss rates found in [34] for the case AdS_5, as it should. For the case of a pointlike defect, $m = n = 0$, our results can be compared to the formulas quoted for the dragging string in [43] following the analysis of dragging strings in general holographic metrics performed in [36]. Our $m = n = 0$ results are for a dragging D-string, as we included an overall $e^{-\phi}$ coupling in the action. To compare with the results for the dragging fundamental string we have to set $\Phi = 0$ in our analysis

(that is, the worldvolume action is independent of the dilaton). It is easy to see that in this case our general expression (2.10) indeed nicely reduces to the result of [43]. Other than the trivial velocity dependence, the energy loss rate still only depends on velocity and temperature via a power of u_c, and hence, due to (2.22), via the effective temperature.

Last but not least, it is interesting to note that for the case $m = n = 1$ and $p = 6$, our defect's energy loss rate is independent of both velocity and temperature, other than the expected velocity squared dependence. In $p = 6$ case, there is no good decoupling limit [41] and it is not clear what significance should be attached to this result.

2.4 Superfluidity

Pointlike probes have been used to study superfluids that have a gravity dual [44, 45]. This is an area in which strongly interacting extended defects exist in nature (vortices in Liquid Helium) and thus suggests a possible analysis using a gauge-string duality. Following the layout of [46], we are interested in using a superconducting black hole in AdS_5.

The bulk theory has metric, gauge field, and a complex scalar field (magnitude η and phase θ) degrees of freedom, and is governed by

$$\mathcal{L}_{bulk} = R - \frac{1}{4}F_{\mu\nu}^2 - \frac{1}{2}\left[(\partial_\mu \eta)^2 + \Sigma(\eta)(\partial_\mu \theta - qA_\mu)^2\right] - V(\eta).$$

This Lagrangian density allows a charged black brane solution to the metric of the form

$$ds^2 = e^{2A(u)}(-h(u)dt^2 + d\vec{x}^2) + \frac{du^2}{h(u)}, \tag{2.24}$$

where $A_\mu dx^\mu = A_0(u)dt$, $\eta = \eta(u)$, $\theta = 0$, $A(u)$ is the warp factor, $h(u)$ is the blackening function, and u is the "radial coordinate" that is defined between $-\infty$ and ∞. V and Σ are in principle free functions of η which in reference [46] are taken to be $V(\eta) = -\frac{3}{L^2}\cosh^2(\frac{\eta}{2})(5 - \cosh(\eta))$ and $\Sigma(\eta) = \sinh^2(\eta)$. These particular forms are required for a consistent truncation of Type II B supergravity on a Sasaki-Einstein manifold [47]. The blackening function

smoothly interpolates from 1 at large u, to its asymptotically value v_{IR}^2 as $u \to -\infty$.

We can now apply our general formulae to the gravity dual metric for this holographic superfluid. We first reproduce some results of [46]. A string in the bulk has the following action,

$$S = -\int d\sigma d\tau \frac{1}{2\pi\alpha'} Q(\eta)\sqrt{-g}, \tag{2.25}$$

where $Q = \cosh(\frac{\eta}{2})$, and α' is the square of the string length scale and goes to zero in the limit of infinite string tension. We compare their action for the string (20) to our general formula (2.3) setting $m = n$ and $n = 0$ so that we are discussing the same defect. We find that we should make the associations $T_0 \to \frac{1}{2\pi\alpha'}$, and $e^{-\Phi(u)} \to Q(\eta(u))$.

Following our prescription for finding the solution to a uniformly moving defect, we first find the root of equation (2.8) where we are now using the metric appropriate for our bulk theory in AdS_5 (2.24). We see that $G_{tt} = -e^{2A}h$, $G_{xx} = e^{2A}$ and $G_{uu} = h^{-1}$.

From (2.8), u_c should be given by $h(u_c) = v^2$. It is clear from the form of $h(u)$ that if $v^2 < v_{IR}^2$ there is no solution, and thus the value $h(u)$ approaches as $u \to -\infty$ defines a cutoff velocity, v_{IR} [46]. Defects whose velocities are below this cutoff experience zero drag force.

For velocities above the cutoff, we find the non-zero drag force density from the momentum density of our uniformly moving defect, $\Pi_x^u = -T_0\widetilde{C}v$, which comes from (2.4), with $(x_{,u})$ given by (2.6) and $\widetilde{C}$ defined in (2.11). We correctly reproduce the following,

$$\widetilde{C} = \pm e^{2A(u_c)}Q(u_c) \tag{2.26}$$

and again choosing the positive sign we have,

$$\Pi_x^u = -\frac{e^{2A(u_c)}}{2\pi\alpha'}Q(u_c)v = f_{\mathsf{drag}}. \tag{2.27}$$

We can now easily extend these arguments to a sheet-like defect. This comes down to setting $n = 1$ and continuing to demand that $m = n$. Since our general solution to (2.8) does

not depend on the dimensionality of the defect, we will again find the same cutoff velocity for the sheet. This supports the interpretation of [46] as this cutoff velocity is a property of the system and not of the defect. The drag force will be modified as it is proportional to $\widetilde{C}$, which depends on n through (2.11). We find,

$$\widetilde{C}_{\mathsf{sheet}} = \pm e^{3A(u_c)} Q(u_c) \tag{2.28}$$

and

$$\Pi^u_x = -\frac{e^{3A(u_c)}}{2\pi\alpha'} Q(u_c) v = f_{\mathsf{sheet,drag}} \tag{2.29}$$

Like in the case of a dragging string in this holographic superfluid background, our analysis has been performed entirely in the effective four dimensional language. While the background itself is a consistent truncation of a full ten dimensional solution, it is not entirely obvious what sort of object is described by the defect action eq. (2.25) with the specific form fo $Q(\eta)$ from the ten 10 dimensional point of view. For the case of dragging strings in the background of five-dimensional charged black holes that correspond to spinning black branes in ten dimension this question has been carefully addressed in [48] and indeed the use of the analog of eq. (2.25) turned out to be questionable in that case. Here we take the point of view of simply being interested in an effective four dimensional description and take the action of the form eq. (2.25) as it is the most general two derivative action consistent with symmetries.

2.5 Discussion

We gave a systematic study of dragging sheets in arbitrary holographic metrics. Our results reconfirm in this most general setting the general structure that was found for pointlike defects in general holographic metrics as well as for the study of dragging sheets in anti-de Sitter spaces: the energy loss is completely insensitive to microscopic details of the system and only depends on the velocity via an overall blueshifted energy density. This seems to be the most general characteristic of energy loss at "strong coupling", where a particle

interpretation of the medium is not possible.

An example that may have a real world counterpart is the study of string like defects (corresponding to dragging membranes) in holographic superconductors. Vortices in superfluid Helium and their energy loss can be studied experimentally. To the extent that holographic superfluids and superconductors are candidates for real world systems, the loss rate experienced by a vortex in such a medium could be a physical observable.

Chapter 3

FAR-FROM-EQUILIBRIUM DYNAMICS

This chapter is based on a publication in collaboration with Laurence Yaffe [49]. The methodology and strategy behind the work comes from pioneering work by Laurence Yaffe and his former student, Paul Chesler [27]. The entirety of the numerical programming, implementation, and visualization of the results were done by JF. The writing of the manuscript was shared for roughly equally. The bulk of the interpretation and creation of the ideas behind the simple model at the end was performed by Laurence, while the actual fitting of the model was performed by JF.

3.1 Introduction

The discovery of gauge/gravity duality (or "holography") has enabled the study of previously intractable problems involving the dynamics of strongly coupled gauge theories.[1] In the limit of large gauge group rank N_c, and large 't Hooft coupling λ, the strongly coupled quantum dynamics of certain gauge field theories may be mapped, precisely, into classical gravitational dynamics of higher dimensional asymptotically anti-de Sitter (AdS) spacetimes [1, 4, 51]. Numerical studies of the resulting gravitational dynamics can shed light on poorly understood aspects of the quantum dynamics of strongly coupled gauge theories.

Using the simplest example of gauge/gravity duality, applicable to maximally supersymmetric $SU(N_c)$ Yang-Mills theory ($\mathcal{N}=4$ SYM), this approach has been applied to a succession of problems of increasing complexity involving far from equilibrium dynamics. These include homogeneous isotropization [26, 52, 53], colliding shock waves [28, 54, 55, 56, 57, 58], and turbulence in two-dimensional fluids [59, 60]. A detailed presentation of the methods

[1] See, for examples, refs. [2, 3, 50] and references therein.

used in most of these works is available [27].

In this paper, we extend previous work on the dynamics of homogeneous but anisotropic $\mathcal{N}=4$ SYM plasma [26, 52, 53]. We examine the influence on the equilibration dynamics of a non-zero global $U(1)$ charge density, or a background magnetic field. Inclusion of these effects is motivated by the physics of relativistic heavy ion collisions [61, 20, 5]. Hydrodynamic modeling of near-central events clearly indicates that the baryon chemical potential μ_B in the mid-rapidity region is significantly smaller than the temperature, but not by an enormously large factor at RHIC energies.[2] Hence, it is desirable to understand the sensitivity of the plasma equilibration dynamics to the presence of a baryon chemical potential and associated non-zero baryon charge density. Similarly, it is clear that large, but transient, electromagnetic fields are generated in heavy ion collisions. A growing body of work [64, 65, 66, 67, 68] suggests that electromagnetic effects may play a significant role despite the small value of the fine structure constant. Electromagnetic effects on equilibrium QCD properties are also under study using lattice gauge theory [69, 70, 71, 72].

The large N_c, strongly coupled $\mathcal{N}=4$ SYM plasma we study is, of course, only a caricature of a real quark-gluon plasma. But it is a highly instructive caricature which correctly reproduces many qualitative features of QCD plasma (such as Debye screening, finite static correlation lengths, and long distance, low frequency dynamics described by neutral fluid hydrodynamics). Moreover, in the temperature range relevant for heavy ion collisions, quantitative comparisons of bulk thermodynamics, screening lengths, shear viscosity, and other observables show greater similarity between $\mathcal{N}=4$ SYM and QCD than one might reasonably have expected [21, 22]. Since the composition of a plasma depends on the chemical potentials, or associated charge densities, of its constituents, studying the dependence of the equilibration dynamics on a conserved charge density provides a simple means to probe the sensitivity of the dynamics to the precise composition of the non-Abelian plasma. This, in small measure, may help one gauge the degree to which $\mathcal{N}=4$ SYM plasma properties can

[2] Inferred values of μ_B/T at chemical freeze-out are about 0.15 for RHIC collisions at $\sqrt{s_{NN}} = 200$ GeV, and roughly 0.005 for LHC heavy ion collisions with $\sqrt{s_{NN}} = 2.8$ TeV [62, 63].

be extrapolated to real QCD plasma. At the very least, strongly coupled $\mathcal{N}=4$ SYM theory provides a highly instructive toy model in which one may explore, quantitatively, non-trivial aspects of non-equilibrium gauge field dynamics.[3]

The remainder of the paper is organized as follows. Section 3.2 summarizes necessary background material. This includes the coupling of an Abelian background gauge field to a $U(1)$ subgroup of the $SU(4)_R$ global symmetry group of $\mathcal{N}=4$ SYM. This $U(1)$ symmetry may be regarded as analogous to either the baryon number $U(1)_B$ or electromagnetic $U(1)_{\rm EM}$ flavor symmetries of QCD. Turning on a background magnetic field implies an enlargement of the theory under consideration from $\mathcal{N}=4$ SYM to $\mathcal{N}=4$ SYM coupled to electromagnetism (which we abbreviate as SYM+EM). The combined theory is no longer scale invariant; this has important implications which we discuss. This section describes the 5D Einstein-Maxwell theory which provides the holographic description of the states of interest, presents our coordinate ansatz (based on a null slicing of the geometry), and summarizes relevant portions of the holographic dictionary relating gravitational and dual field theory quantities. This section also records the reduced field equations which emerge from our symmetry specializations, describes the relevant near-boundary asymptotic behavior, and summarizes properties of the static equilibrium geometries to which our time dependent solutions asymptote at late times.

The following section 3.3 briefly describes our numerical methods, which are based on the strategy presented in ref. [27]. When studying states with a non-zero charge density (but no background magnetic field) appropriate numerical methods for asymptotically AdS Einstein-Maxwell theory are immediate generalizations of methods which have previously been found to work well for pure gravity. However, the inclusion of a background magnetic field induces a trace anomaly in the dual quantum field theory which, in the gravitational description, manifests in the appearance of logarithmic terms in the near-boundary behavior of fields. Such non-analytic terms degrade the performance of spectral methods, on which

[3]Previous work examining thermalization in plasmas with non-zero chemical potential (not involving numerical solutions of far from equilibrium geometries) includes refs. [73, 74, 75, 76].

we rely, and necessitate careful attention to numerical issues. Section 3.3 also describes the specifics of our chosen initial data.

Results are presented in section 3.4. We focus on the evolution of the expectation value of the stress-energy tensor. We first discuss the sensitivity of the equilibration dynamics to features in the initial data and, in particular, examine the extent to which the evolution shows nonlinear dependence on the initial departure from equilibrium. We find that only disturbances in the geometry originating deep in the bulk, very close to the horizon, generate significant nonlinearities. This is broadly consistent with earlier work [52, 53]. However, for a very wide variety of initial disturbances, including ones which generate extremely large pressure anisotropies, we find remarkably little nonlinearity in the equilibration dynamics, often below the part-per-mille level.

We then present comparisons of the equilibration dynamics as a function of the charge density or background magnetic field. We focus on comparisons in which the form of the initial departure form equilibrium and the energy density, or the equilibrium temperature, is held fixed while either the charge density or magnetic field is varied. These comparisons reveal surprisingly little sensitivity to the charge density, or magnetic field, even at early times when the departure from equilibrium is large.

We verify the late time approach to the expected equilibrium states, and extract the leading quasinormal mode (QNM) frequency from the late time relaxation. Quasi-normal mode frequencies extracted from our full nonlinear dynamics are compared, where possible, with independent calculations of QNM frequencies based on a linearized analysis around the equilibrium geometry. This provides a useful check on our numerical accuracy.

We define an approximate equilibration time based on the relative deviation of the pressure anisotropy from its equilibrium value, and examine the dependence of this time on charge density or external magnetic field. Once again, changes in this quantity are largest for initial disturbances which originate very close to the horizon, but the overall sensitivity of the equilibration time to the charge density or magnetic field is remarkably modest.

The final section 4.7 discusses and attempts to synthesize the implications of our results.

We present a simple model of equilibration times, for initial disturbances which are well localized in scale, which agrees rather well with our numerical results (but becomes less accurate for disturbances localized extremely close to the horizon). We end with a few concluding remarks.[4]

3.2 Ingredients

3.2.1 $\mathcal{N}=4$ SYM in an external field

We study maximally supersymmetric $SU(N_c)$ Yang-Mills theory ($\mathcal{N}=4$ SYM) on four dimensional Minkowski space when the conserved current for a $U(1)$ subgroup of the $SU(4)_R$ global symmetry group either (a) has a non-vanishing charge density, or (b) is coupled to a background Abelian gauge field describing a uniform magnetic field. The embedding of the $U(1)$ symmetry is chosen such that the $U(1)$ commutes with an $SU(3)$ subgroup of the $SU(4)_R$ global symmetry.

The coupling to the external field has the usual form[5]

$$S = S_{\rm SYM} + \int d^4x\, j^\alpha(x) A^{\rm ext}_\alpha(x)\,, \tag{3.1}$$

where $j^\alpha(x)$ is the conserved $U(1)$ current normalized such that the four Weyl fermions of $\mathcal{N}=4$ SYM have charges $\{+3,-1,-1,-1\}/\sqrt{3}$ and the three complex scalars have charge $+2/\sqrt{3}$. The overall factor of $1/\sqrt{3}$ in these charge assignments has no physical significance, but is chosen so that the trace anomaly and electromagnetic beta function (induced when this current is gauged) have convenient coefficients, as will be seen below.[6] The background

---

[4] As this paper neared completion, we learned of the somewhat related work by A. Buchel, M. Heller, and R. Myers [77]. These authors examine quasinormal mode frequencies in $\mathcal{N}=2^*$ SYM and argue that, in this non-conformal deformation of $\mathcal{N}=4$ SYM, the longest equilibration times are largely set by the temperature with little sensitivity to other scales.

[5] We use a mostly-plus Minkowski space metric, $\eta_{\mu\nu} \equiv {\rm diag}(-1,+1,+1,+1)$.

[6] These charge assignments are $1/\sqrt{3}$ times those used in ref. [78]. Overall rescaling of these charge assignments has implications for the holographic description which are noted below in footnote 11.

$U(1)$ gauge field $A^{\rm ext}_\alpha(x)$ we take to have the form

$$A^{\rm ext}_\alpha(x) \equiv \mu\,\delta^0_\alpha + \tfrac{1}{2}\mathcal{B}\,(x^1\delta^2_\alpha - x^2\delta^1_\alpha)\,, \tag{3.2}$$

with μ the chemical potential which, in equilibrium, will be conjugate to the charge density j^0, and $\mathcal{B}$ the amplitude of a constant magnetic field pointing in the x^3 direction. Although it should be straightforward to study dynamics when both the charge density j^0 and magnetic field $\mathcal{B}$ are non-zero, in this paper we focus for simplicity on the cases of either a non-zero charge density with vanishing magnetic field, $j^0 \neq 0$ and $\mathcal{B} = 0$, or non-zero magnetic field with vanishing charge density, $j^0 = 0$ and $\mathcal{B} \neq 0$.

With a non-zero magnetic field $\mathcal{B}$ in the x^3 direction, changes in the background gauge field under a translation in the x^1 or x^2 directions, or a rotation in the x^1-x^2 plane, can be compensated by a suitable $U(1)$ gauge transformation. Hence, the theory retains full spatial translation invariance as well as rotation invariance in the x^1-x^2 plane.

We will be interested in initial states which: (*i*) have non-trivial expectation values $\langle T^{\alpha\beta}(x)\rangle$ and $\langle j^\alpha(x)\rangle$ for the stress-energy tensor and $U(1)$ current density, respectively; (*ii*) are invariant under spatial translations as well as $O(2)$ rotations in the $x^1{-}x^2$ plane; and (*iii*) are invariant under the $SU(3)_R$ subgroup of the $SU(4)_R$ global symmetry which commutes with our chosen $U(1)$.

Since all $\mathcal{N}=4$ SYM fields transform in the adjoint representation of the $SU(N_{\rm c})$ gauge group, the stress-energy and $U(1)$ current expectation values both scale as $O(N_{\rm c}^2)$ in the large $N_{\rm c}$ limit. For later convenience, we define a rescaled energy density ε and charge density ρ, via

$$\langle T^{00}\rangle \equiv \kappa\,\varepsilon\,, \qquad \langle j^0\rangle \equiv \kappa\,\rho\,, \tag{3.3}$$

with

$$\kappa \equiv (N_{\rm c}^2{-}1)/(2\pi^2)\,. \tag{3.4}$$

$\mathcal{N}=4$ SYM is a conformal field theory with a traceless stress-energy tensor. Adding

a chemical potential μ introduces a physical scale, but does not modify the microscopic dynamics of the theory and hence does not affect the tracelessness of the stress-energy tensor. In contrast, introducing an external magnetic field does affect the microscopic dynamics and, in particular, generates a non-zero trace anomaly,[7]

$$T^{\alpha}{}_{\alpha} = -\tfrac{1}{4}\,\kappa\,\left(F^{\rm ext}_{\mu\nu}\right)^2 = -\tfrac{1}{2}\,\kappa\,\mathcal{B}^2\,. \tag{3.5}$$

The trace anomaly generated by the external magnetic field implies that the theory is no longer scale invariant. For example, the ground state energy density, as a function of magnetic field, need not have the simple form of some pure number times $\mathcal{B}^2$. This will be seen explicitly below. The trace anomaly implies that there must be logarithmic dependence on a renormalization point. To interpret this dependence, it is appropriate to adopt the perspective that adding an external magnetic field means that the theory under consideration has been enlarged — it is now $\mathcal{N}=4$ SYM coupled to $U(1)$ electromagnetism (SYM+EM). The complete action of the theory is the SYM action, minimally coupled to the $U(1)$ gauge field, plus the Maxwell action for $U(1)$ gauge field,

$$S_{\rm SYM+EM} = S_{\rm SYM,\,min.\ coupled} + S_{\rm EM}\,, \tag{3.6}$$

with

$$S_{\rm EM} \equiv -\int d^4x\ \tfrac{1}{4e^2}\,F^2_{\mu\nu}\,. \tag{3.7}$$

The electromagnetic coupling e^2 (having been scaled out of covariant derivatives) appears as an inverse prefactor of the Maxwell action. We regard the electromagnetic coupling e^2 as arbitrarily weak. Hence, quantum fluctuations in the $U(1)$ gauge field are negligibly small,

---

[7] We define the external gauge field such that no factor of an electromagnetic gauge coupling appears in the interaction (3.1), in our $U(1)$ covariant derivatives, or in the trace anomaly (3.5). The coefficient of $-\frac{1}{4}F^2_{\mu\nu}$ in the trace anomaly (3.5) equals the EM beta function coefficient b_0, given below in eq. (3.9). (Note that the sign of the trace anomaly depends on the metric convention in use.)

allowing us to view the EM gauge field as a classical background field.[8]

However, just as in QED, fluctuations in the SYM fields which are electromagnetically charged will cause the electromagnetic coupling e^2 to run with scale. The associated renormalization group (RG) equation for the inverse coupling has the usual form,

$$\mu \frac{d}{d\mu}\, e^{-2} \equiv \beta_{1/e^2}(e^{-2}) = -b_0 + O(e^2)\,, \tag{3.8}$$

with the one-loop beta function coefficient[9]

$$b_0 \equiv \kappa \Big[\tfrac{1}{6} \sum_\alpha (q_{\rm f}^\alpha)^2 + \tfrac{1}{12} \sum_a (q_{\rm s}^a)^2 \Big] = \kappa\,. \tag{3.9}$$

Here, $q_{\rm f}^\alpha = (3,-1,-1,-1)/\sqrt{3}$ and $q_{\rm s}^a = (2,2,2)/\sqrt{3}$ are the charge assignments of the four Weyl fermions and three complex scalars, respectively. Integrating this renormalization group equation leads, as usual, to

$$1/e^2(\mu) = b_0 \ln(\Lambda_{\rm EM}/\mu) + O[\ln(\ln \Lambda_{\rm EM}/\mu)]\,, \tag{3.10}$$

with the RG invariant scale $\Lambda_{\rm EM}$ denoting the Landau pole scale where the (one loop approximation to the) electromagnetic coupling diverges.

The total stress-energy tensor derived from the combined action (3.6) will equal the $\mathcal{N}=4$ SYM stress-energy tensor, augmented with minimal coupling terms to the EM gauge

---

[8] In an arbitrary background $SU(4)$ gauge field, the divergence of the $SU(4)_R$ current acquires an anomalous contribution, $\partial^\mu J^a_\mu \propto d^{abc} F^b_{\mu\nu} F^{\mu\nu c}$. This anomaly, when specialized to our chosen $U(1)$ subgroup, is proportional to the sum of the cubes of our fermion charges and is non-zero, $\sum_\alpha (q_{\rm f}^\alpha)^3 = 8/\sqrt{3}$. To make the combined SYM+EM theory well defined, one could add to the theory additional fermions, charged under the $U(1)$ but with no SYM interactions, which would cancel this $U(1)$ anomaly. As we are not concerned with quantum fluctuations in the $U(1)$ gauge field, the presence of this $U(1)$ anomaly (in the absence of compensating spectators) is irrelevant for our purposes.

[9] A non-renormalization theorem in supersymmetric $\mathcal{N}=4$ SYM implies that the short distance behavior of the current-current correlation cannot depend on the 't Hooft coupling λ [11]. This implies that the leading EM beta function coefficient b_0 does not depend on λ, and hence may easily be evaluated in the $\lambda \to 0$ limit.

field, plus the classical Maxwell stress-energy. An essential point, however, is that while the total stress-energy tensor is well-defined, partitioning the stress-energy tensor into separate SYM and EM contributions is inherently ambiguous, as the individual pieces depend on the renormalization point. We define

$$T^{\alpha\beta}_{\rm tot} \equiv T^{\alpha\beta}_{\rm EM}(\mu) + \Delta T^{\alpha\beta}_{\rm SYM}(\mu)\,, \tag{3.11}$$

with[10]

$$T^{\alpha\beta}_{\rm EM}(\mu) \equiv \frac{1}{e^2(\mu)}\left[F^{\alpha\nu}F^{\beta}{}_{\nu} - \tfrac{1}{4}\eta^{\alpha\beta}F^{\mu\nu}F_{\mu\nu}\right], \tag{3.12}$$

and

$$\Delta T^{\alpha\beta}_{\rm SYM}(\mu) \equiv T^{\alpha\beta}_{\rm SYM,\,min.\ coupled}(\mu)\,. \tag{3.13}$$

The partitioning (3.11) of the stress-energy tensor puts all quantum corrections other than the running of the EM coupling into the SYM contribution $\Delta T^{\alpha\beta}_{\rm SYM}(\mu)$. The scale dependence must, of course, cancel between the two terms because the total stress-energy tensor is a physical quantity. Therefore, the scale dependence in the SYM contribution to the stress-energy must simply compensate the known running of the inverse electromagnetic coupling (3.8) in the Maxwell stress-energy tensor (3.12),

$$\mu\frac{d}{d\mu}\,\Delta T^{\alpha\beta}_{\rm SYM}(\mu) = -\mu\frac{d}{d\mu}\,T^{\alpha\beta}_{\rm EM}(\mu) = b_0\left[F^{\alpha\nu}F^{\beta}{}_{\nu} - \tfrac{1}{4}\eta^{\alpha\beta}F^{\mu\nu}F_{\mu\nu}\right]. \tag{3.14}$$

Specializing to zero temperature states in a constant static magnetic field $\mathcal{B}$, the scale dependence (3.14) plus dimensional analysis implies that the SYM contribution to the ground state energy density is a non-analytic function of magnetic field,

$$\varepsilon(\mu) = c_0\,\mathcal{B}^2 - \tfrac{1}{4}\mathcal{B}^2\ln(|\mathcal{B}|/\mu^2) = \tfrac{1}{4}\mathcal{B}^2\ln\big[\mathcal{B}^*(\mu)/|\mathcal{B}|\big], \tag{3.15}$$

[10]Note that $T^{\alpha\beta}_{\rm EM}(\mu)$ is not the metric variation of some renormalized EM action (whose separation from the total action would not be well-defined). Rather, eq. (3.12) is simply defining $T^{\alpha\beta}_{\rm EM}(\mu)$ as the classical EM stress-energy tensor multiplied by the scale-dependent inverse EM coupling.

with c_0 some pure number. (Here and henceforth, when considering physics in a non-zero magnetic field $\varepsilon(\mu) \equiv \Delta T^{00}_{\rm SYM}(\mu)/\kappa$ denotes the SYM portion of the rescaled energy density.) In the second form of eq. (3.15), the analytic term has been absorbed by defining a scale dependent "fiducial" magnetic field amplitude,

$$\mathcal{B}^*(\mu) \equiv \mu^2 e^{4c_0} \,. \tag{3.16}$$

Note that the ground state energy acquires a simple quadratic form when the renormalization point is chosen to scale with the magnetic field, $\varepsilon(|\mathcal{B}|^{1/2}) = c_0\, \mathcal{B}^2$. Our numerically determined value for the coefficient c_0 is given below in eq. (3.68).

When considering low temperature physics in a background magnetic field, $T^2 \ll |\mathcal{B}|$, it is natural to choose a renormalization point $\mu = O(|\mathcal{B}|^{1/2})$, as this is the relevant scale which cuts off long range fluctuations in the charged SYM fields. We will employ two choices for the renormalization point. One choice is $\mu = 1/L$, with L the AdS curvature scale (discussed below); this choice is computationally convenient but not physically significant. We will also report and discuss results with $\mu = |\mathcal{B}|^{1/2}$. For later convenience, we define abbreviations for the (rescaled) energy density evaluated at these two renormalization points,

$$\varepsilon_L \equiv \varepsilon(1/L)\,, \qquad \varepsilon_{\mathcal{B}} \equiv \varepsilon(|\mathcal{B}|^{1/2})\,. \tag{3.17}$$

3.2.2 Holographic description

The holographic description of SYM states, within our sector of interest, in the limit of large $N_{\rm c}$ and large 't Hooft coupling λ, is given by classical Einstein-Maxwell theory on 5-dimensional spacetimes which are asymptotically AdS_5 [79]. The 5D bulk action is

$$S_5 \equiv \frac{1}{16\pi G_5} \int d^5x\, \sqrt{-G}\, \left(R - 2\Lambda - L^2\, F_{MN}F^{MN}\right), \tag{3.18}$$

with $G_5 \equiv \frac{\pi}{2} L^3/N_c^2$ the 5D Newton gravitational constant, $\Lambda \equiv -6/L^2$ the cosmological constant, and L the AdS curvature scale.[11] Setting to zero the variation of the action with respect to the metric gives the Einstein equation,

$$R_{KL} + (\Lambda - \tfrac{1}{2}R)\, G_{KL} = 2L^2 \left(F_{KM} F_L{}^M - \tfrac{1}{4} G_{KL}\, F_{MN} F^{MN} \right), \tag{3.19}$$

while varying the bulk gauge field (with $F_{MN} \equiv \nabla_M A_N - \nabla_N A_M$) gives the usual sourceless Maxwell equation, $\nabla_K F^{KL} = 0$.

A 5D Chern-Simons term, $A \wedge F \wedge F$, could be added to the action (3.18) and would appear with a known coefficient in a consistent truncation of 10D supergravity. (See, for example, refs. [79, 78].) However, as stated above, in this paper we consider solutions with non-zero chemical potential μ or non-zero magnetic field $\mathcal{B}$, but not both μ and $\mathcal{B}$ non-zero. For such solutions, the Chern-Simons term makes no contribution to the dynamics and hence may be neglected.

As usual in holography, the expectation value $\langle T^{\alpha\beta}(x) \rangle$ of the stress-energy tensor is determined by the subleading near-boundary behavior of the 5D metric G_{MN}. The leading near-boundary behavior of the bulk gauge field A_M will be fixed by our chosen external $U(1)$ gauge field (3.2), while the expectation value $\langle j^\alpha(x) \rangle$ of the $U(1)$ current density is determined by the subleading near-boundary behavior of the bulk gauge field. The precise relations will be shown below.

Following ref. [27], we choose a coordinate ansatz, based on generalized Eddington-Finklestein (EF) coordinates, which is natural for gravitational infall problems. The metric

---

[11] The coefficient of the Maxwell action may, of course, be set to an arbitrary value by suitably rescaling the bulk gauge field A_M. However, as the on-shell variation of the gravitational action with respect to the boundary value of the gauge field defines the associated current, such rescaling changes the normalization of the $U(1)$ current in the holographic description. It will be seen below that the coefficient of the Maxwell term in our action (3.18) is correctly chosen so that the $U(1)$ current normalization is consistent with our previous charge assignments. If charge assignments are chosen, for example, to be larger by a factor of $\sqrt{3}$, then either the Maxwell term in the action (3.18) must be multiplied by a factor of 3, or else one must regard the boundary value of the bulk gauge field as equaling $\sqrt{3}$ times the QFT gauge field (and the charge density in the bulk theory as equal to the QFT charge density divided by $\sqrt{3}$), as was done in ref. [78].

has the general form

$$ds^2 = \frac{r^2}{L^2}\, g_{\alpha\beta}(x,r)\, dx^\alpha dx^\beta - 2\, w_\alpha(x)\, dx^\alpha dr, \tag{3.20}$$

where r is the bulk radial coordinate and $x \equiv \{x^\alpha\}$, $\alpha = 0, \cdots, 3$, denotes the four remaining spacetime coordinates. The spacetime boundary lies at $r = \infty$; the $\{x^\alpha\}$ may be regarded as coordinates on the spacetime boundary where the dual field theory "lives". Curves of varying r, with x held fixed, are radially infalling null geodesics, affinely parameterized by r. The one-form $\widetilde{w} \equiv w_\alpha\, dx^\alpha$ (which is assumed to be timelike) depends only on x, not on r. These infalling coordinates remain regular across future null horizons.

The form of the ansatz (3.20) remains invariant under r-independent diffeomorphisms,

$$x^\alpha \to \bar{x}^\alpha \equiv f^\alpha(x)\,, \tag{3.21}$$

as well as radial shifts (with arbitrary x dependence),

$$r \to \bar{r} \equiv r + \lambda(x)\,. \tag{3.22}$$

We use the diffeomorphism freedom (3.21) to transform the timelike one-form $\widetilde{w}$ to the standard form $-dx^0$ (or $w_\alpha = -\delta^0_\alpha$). Our procedure for dealing with the radial shift invariance (3.22) is discussed below in subsection 3.2.6.

We are interested in geometries which, at large r, asymptotically approach (the Poincaré patch of) AdS_5. This will be the case if $g_{\alpha\beta}(x,r)$ approaches $\eta_{\alpha\beta}$ as $r \to \infty$, with $\eta_{\alpha\beta} \equiv \mathrm{diag}(-1,1,1,1)$ the usual Minkowski metric tensor. Demanding that the metric and bulk gauge field satisfy the Einstein-Maxwell equations, one may derive the near-boundary asymptotic behavior of the fields. Using radial gauge, $A_r = 0$, for the bulk gauge field, and a suitable choice of the radial shift (3.22) (which eliminates $O(1/r)$ terms in $g_{\alpha\beta}$), one finds that for

solutions of interest, the metric and gauge field have asymptotic expansions of the form

$$g_{\alpha\beta}(x,r) \sim \eta_{\alpha\beta} + \left[g^{(4)}_{\alpha\beta}(x) + h^{(4)}_{\alpha\beta}(x)\, \ln \tfrac{r}{L}\right] (L^2/r)^4 + O\big[(L^2/r)^5\big]\,, \tag{3.23a}$$

$$A_\alpha(x,r) \sim A^{\rm ext}_\alpha(x) + A^{(2)}_\alpha(x)\,(L^2/r)^2 + O\big[(L^2/r)^3\big]. \tag{3.23b}$$

The coefficient $h^{(4)}_{\alpha\beta}$ of the logarithmic term in the metric is only non-zero when there is an external EM field,

$$h^{(4)}_{\alpha\beta} = F_{\alpha\nu}F_\beta{}^\nu - \tfrac{1}{3}\,\eta_{\alpha\beta}\,(F_{\mu\nu}F^{\mu\nu} + F_{0\nu}F_0{}^\nu)\,. \tag{3.24}$$

For a constant magnetic field in the x^3 direction, $\|h^{(4)}_{\alpha\beta}\| = \frac{1}{3}\,\mathcal{B}^2\,\mathrm{diag}(+2,\,+1,\,+1,\,-2)$. The subleading asymptotic coefficients $g^{(4)}_{\alpha\beta}(x)$ and $A^{(2)}_\alpha(x)$ cannot be determined solely from a near-boundary analysis of the field equations, and depend on the form of the solution throughout the bulk. However, asymptotic analysis does show that $\sum_{i=1}^3\, g^{(4)}_{ii} = -\frac{1}{3}\,F_{0\nu}F_0{}^\nu$. The subleading metric coefficients $g^{(4)}_{\alpha\beta}(x)$ and $h^{(4)}_{\alpha\beta}(x)$ encode the expectation value of the SYM stress-energy tensor [80, 13]. The appropriate holographic relation is

$$\langle T_{\mu\nu}\rangle = \kappa\left\{\widetilde{g}^{(4)}_{\mu\nu} - \eta_{\mu\nu}\,\mathrm{tr}\,(\widetilde{g}^{(4)}) + [\ln(\mu L) + \mathcal{C}]\,\widetilde{h}^{(4)}_{\mu\nu}\right\}, \tag{3.25}$$

where[12]

$$\widetilde{g}^{(4)}_{\mu\nu} \equiv g^{(4)}_{\mu\nu} + \tfrac{1}{4}\,\eta_{\mu\nu}\left(g^{(4)}_{00} + \tfrac{1}{4}\,h^{(4)}_{00}\right), \qquad \widetilde{h}^{(4)}_{\mu\nu} \equiv h^{(4)}_{\mu\nu} + \tfrac{1}{4}\,\eta_{\mu\nu}\,h^{(4)}_{00}\,, \tag{3.26}$$

$\kappa \equiv L^3/(4\pi G_N) = (N_{\rm c}^2-1)/(2\pi^2)$, and $\mathcal{C}$ is an arbitrary renormalization-scheme dependent

[12] In Fefferman-Graham (FG) coordinates, for which $ds^2 \equiv (L^2/\rho^2)\big[\widetilde{g}_{\alpha\beta}(\widetilde{x},\rho)\,d\widetilde{x}^\alpha\,d\widetilde{x}^\beta + d\rho^2\big]$, one has $\widetilde{g}_{\alpha\beta}(\widetilde{x},\rho) \sim \eta_{\alpha\beta} + \big[\widetilde{g}^{(4)}_{\alpha\beta}(\widetilde{x}) + \widetilde{h}^{(4)}_{\alpha\beta}\,\ln\frac{L}{\rho}\big]\,\rho^4 + O(\rho^6\ln\rho)$ as $\rho\to 0$. Eq. (3.26) gives the relation between the subleading asymptotic metric coefficients in our infalling EF coordinates and FG coordinates.

constant.[13] We adopt a specific value,

$$\mathcal{C} \equiv -\tfrac{1}{4}\,, \tag{3.27}$$

which will make the subsequent explicit expression (3.42a) for the energy density as simple as possible.

Inserting expression (3.24) into relation (3.26) shows that $\widetilde{h}^{(4)}_{\alpha\beta}$, the coefficient of the renormalization point dependent part of the holographic SYM stress-energy, is proportional to the classical EM stress-energy tensor,

$$\widetilde{h}^{(4)}_{\alpha\beta} = F_{\alpha\nu}F_{\beta}{}^{\nu} - \tfrac{1}{4}\,\eta_{\alpha\beta}\,F_{\mu\nu}F^{\mu\nu}\,, \tag{3.28}$$

or $\|\widetilde{h}^{(4)}_{\alpha\beta}\| = \frac{1}{2}\,\mathcal{B}^2\,\mathrm{diag}(+1,\,+1,\,+1,\,-1)$ for a constant magnetic field in the x^3 direction. Using the above relations, one also finds that $\mathrm{tr}\,(\widetilde{g}^{(4)}) = \frac{1}{12}\,F_{\mu\nu}F^{\mu\nu}$. Since $\widetilde{h}^{(4)}$ is traceless, the holographic relation (3.25) yields the stress-energy trace

$$\langle T^{\alpha}{}_{\alpha}\rangle = -3\kappa\,\mathrm{tr}\,(\widetilde{g}^{(4)}) = -\tfrac{1}{4}\,\kappa\,F_{\mu\nu}F^{\mu\nu}\,, \tag{3.29}$$

or $\langle T^{\alpha}{}_{\alpha}\rangle = -\frac{1}{2}\,\kappa\,\mathcal{B}^2$ in a constant magnetic field, in agreement with the earlier field theory result (3.5). Similarly, the renormalization point dependence of the stress-energy (3.25) coincides with the QFT result (3.14).[14]

Finally, the subleading asymptotic coefficient $A^{(2)}_{\alpha}(x)$ for the bulk gauge field encodes the $U(1)$ current density. One finds

$$\langle j_{\nu}\rangle = 2\,\kappa\,A^{(2)}_{\nu}\,. \tag{3.30}$$

---

[13] To perform the required holographic renormalization one must add a counterterm depending logarithmically on the UV cutoff. (See, for example, refs. [13, 81, 82].) As always, such a logarithmic counterterm comes with an inevitable finite ambiguity.

[14] As in ref. [78], one can also use a comparison of holographic and QFT evaluations of the $U(1)$ anomaly to confirm that the $U(1)$ current normalizations are consistent.

3.2.3 Symmetry specialization

As noted earlier, we are interested in studying solutions of Einstein-Maxwell theory which are spatially homogeneous. This implies that all metric functions depend only on x^0 and r. The arbitrary function λ in the residual radial shift diffeomorphism (3.22) will depend only on x^0. Henceforth, for convenience, we will use v as a synonym for x^0; v is a null time coordinate. (In other words, v = const. surfaces are null slices of the geometry.) At the boundary, v coincides with the time t of the dual field theory.

We also impose invariance under $O(2)$ rotations in the x^1-x^2 plane. This implies that only the g_{00}, g_{03}, g_{33}, and $g_{11} = g_{22}$ components of $g_{\alpha\beta}$ are non-zero. Our Einstein-Maxwell theory (without a Chern-Simons term) is also invariant under spatial parity, or $x^3 \to -x^3$ reflections, and for simplicity we will also impose parity invariance. This requires the vanishing of g_{03}.

For the bulk gauge field, the choice of radial gauge, $A_r = 0$, plus our imposed symmetries imply that

$$A_\alpha(x, r) = A^{\rm ext}_\alpha(x) - \phi(v, r)\, \delta^0_\alpha \,. \tag{3.31}$$

The corresponding bulk field strength, which is what appears in the field equations, can have a constant (x and r independent) magnetic field plus a radial electric field,

$$F_{12}(x, r) = \mathcal{B} \,, \quad F_{0r}(x, r) = \partial_r \phi(v, r) \equiv -\mathcal{E}(v, r) \,, \tag{3.32}$$

with all other components vanishing.

As in ref. [27], it is convenient to rename the non-vanishing metric components as

$$\frac{r^2}{L^2}\, g_{00} \equiv -2A \,, \quad \frac{r^2}{L^2}\, g_{11} = \frac{r^2}{L^2}\, g_{22} \equiv \Sigma^2\, e^B, \quad \frac{r^2}{L^2}\, g_{33} \equiv \Sigma^2\, e^{-2B}, \tag{3.33}$$

where A, B, and Σ are functions of v and r. The resulting line element is

$$ds^2 = 2dv\, [dr - A(v, r)\, dv] + \Sigma(v, r)^2 \left[e^{B(v,r)} (dx^2 + dy^2) + e^{-2B(v,r)} dz^2 \right] . \tag{3.34}$$

Henceforth, A will always denote the metric function multiplying dv^2 (times $-1/2$), not the bulk gauge field. The function Σ is the spatial scale factor (with $\Sigma^3\, dx\, dy\, dz$ the spatial volume element), while B characterizes the spatial anisotropy (which should not be confused with the magnetic field amplitude $\mathcal{B}$).

The radial derivative ∂_r is a directional derivative along infalling radial null geodesics. It proves convenient to define a corresponding directional derivative along outward radial null geodesics,

$$d_+ \equiv \partial_v + A(v,r)\,\partial_r\,. \tag{3.35}$$

The field equations which result from varying the action (3.18), inserting the above symmetry specializations, and re-expressing v-derivatives in terms of the d_+ modified time derivative (3.35), take a remarkably compact form. The Einstein equations are:

$$\Sigma'' + \tfrac{1}{2}(B')^2\,\Sigma = 0\,, \tag{3.36a}$$

$$A'' - 6(\Sigma'/\Sigma^2)\,d_+\Sigma + \tfrac{3}{2}\,B' d_+ B = +\tfrac{5}{3}\mathcal{B}^2 L^2\, e^{-2B}\,\Sigma^{-4} + \tfrac{7}{3}\,\mathcal{E}^2 L^2 - 2/L^2\,, \tag{3.36b}$$

$$(d_+B)' + \tfrac{3}{2}(\Sigma'/\Sigma)\,d_+B + \tfrac{3}{2}B'\,(d_+\Sigma)/\Sigma = -\tfrac{2}{3}\mathcal{B}^2 L^2\, e^{-2B}\,\Sigma^{-4}\,, \tag{3.36c}$$

$$(d_+\Sigma)'/\Sigma + 2(\Sigma'/\Sigma^2)\,d_+\Sigma = -\tfrac{1}{3}\mathcal{B}^2 L^2\, e^{-2B}\,\Sigma^{-4} - \tfrac{1}{3}\mathcal{E}^2 L^2 + 2/L^2\,, \tag{3.36d}$$

$$d_+(d_+\Sigma) - A'\,(d_+\Sigma) + \tfrac{1}{2}\Sigma\,(d_+B)^2 = 0\,, \tag{3.36e}$$

where primes denote radial derivatives, $h' \equiv \partial_r h$. As discussed in ref. [27], the anisotropy function B encodes the essential propagating degrees of freedom. The functions Σ and A may be regarded as auxiliary fields, determined by solving eqns. (3.36a) and (3.36b) using data on a single time slice. Information about the time evolution of B is contained in equation (3.36c). Equations (3.36d) and (3.36e) may be viewed as boundary value constraints — if they hold at one value of r, then the other equations ensure that these equations hold at all values of r.

Maxwell's equations reduce to the statements that neither the magnetic field $\mathcal{B}$, nor the radial electric flux density $\mathcal{E}\,\Sigma^3$, have any radial or temporal variation. In other words,

$\mathcal{B} = \text{const.}$, as already indicated in (3.32), and

$$\mathcal{E}(v,r) = \rho\, L\, \Sigma^{-3}(v,r)\,, \tag{3.37}$$

for some constant ρ which, from eqs. (3.30)–(3.32) plus (3.40) below, one sees is precisely the $U(1)$ charge density (rescaled by κ),

$$\langle j^0 \rangle = \kappa\, \rho\,. \tag{3.38}$$

The form (3.37) of the radial electric field simply reflects Gauss' law in 4+1 dimensions, combined with charge conservation and spatial translation invariance, which imply that ρ cannot have any temporal or spatial variation.

The bulk gauge field A_M does not appear in the field equations (except via the field strength), but one may choose to regard A_M as satisfying the radial gauge condition, $A_r = 0$, plus the condition that the time component A_v vanish at the horizon. This fixes the residual r-independent gauge freedom which remains after imposing radial gauge. With these choices, the chemical potential μ is the boundary value of A_v in the late time ($v \to \infty$) equilibrium limit. Equivalently (in radial gauge), the chemical potential μ equals the difference between the boundary and horizon values of A_v, in the equilibrium geometry. This coincides with the line integral of the radial electric field from horizon to boundary,

$$\mu = \lim_{v\to\infty} A_v\big|_{r_{\rm h}}^{\infty} = \int_{r_{\rm h}}^{\infty} dr\, \mathcal{E}(\infty, r)\,, \tag{3.39}$$

which gives the work needed to move a unit charge from the boundary to the horizon. As usual, the charge density and the chemical potential are thermodynamically conjugate. One may consider the chemical potential μ to be a function of the (rescaled) charge density ρ, or vice-versa. The choice of perspective ("canonical" vs. "grand canonical") has no bearing on the dynamics.

3.2.4 Asymptotic analysis

Asymptotic analysis of these equations is straightforward. We impose a flat boundary geometry with the requirement that $\lim_{r\to\infty} g_{\alpha\beta}(x,r) = \eta_{\alpha\beta}$, implying

$$\lim_{r\to\infty} (L/r)^2\, A(v,r) = \tfrac{1}{2}\,, \quad \lim_{r\to\infty} (L/r)\, \Sigma(v,r) = 1\,, \quad \lim_{r\to\infty} B(v,r) = 0\,, \tag{3.40}$$

for our renamed metric functions. Solutions to Einstein's equations (3.36) with this leading behavior may be systematically expanded in integer powers of $1/r$ and (for non-zero magnetic field) logarithms of r. One finds:

$$\Sigma(v,r) \sim L^{-1}[r + \lambda(v)] + \mathcal{O}[(L/r)^7 \ln^2 \tfrac{r}{L}], \tag{3.41a}$$

$$\begin{aligned} A(v,r) \sim{}& \tfrac{1}{2} L^{-2}[r+\lambda(v)]^2 - \partial_v \lambda(v) \\ &+ L^4 \left[a_4 - \tfrac{1}{3}\mathcal{B}^2 \ln \tfrac{r}{L}\right] (L/r)^2 \\ &- L^3 \left[2a_4\, \lambda(v) + \tfrac{1}{3}\mathcal{B}^2\, \lambda(v)\,(1 - 2\ln \tfrac{r}{L})\right] (L/r)^3 + \mathcal{O}[(L/r)^4 \ln \tfrac{r}{L}], \end{aligned} \tag{3.41b}$$

$$\begin{aligned} B(v,r) \sim{}& L^4 \left[b_4(v) + \tfrac{1}{3}\mathcal{B}^2 \ln \tfrac{r}{L}\right] (L/r)^4 \\ &+ L^3 \left[L^2\, \partial_v b_4(v) - 4 b_4(v)\, \lambda(v) + \tfrac{1}{3}\mathcal{B}^2\, \lambda(v)\,(1 - 4\ln \tfrac{r}{L})\right] (L/r)^5 \\ &+ \mathcal{O}[(L/r)^6 \ln \tfrac{r}{L}], \end{aligned} \tag{3.41c}$$

The constant a_4 and the function $b_4(v)$ cannot be determined just using asymptotic analysis, and the radial shift $\lambda(v)$ is completely arbitrary. The coefficient a_4 encodes the energy density which, due to homogeneity, cannot vary in time, while $b_4(v)$ encodes the anisotropy in the spatial stress. Using the holographic relation (3.25) and our convention (3.27) for defining

the stress-energy tensor, one finds

$$\langle T^{00}\rangle = \kappa\left(-\tfrac{3}{2}a_4 + \tfrac{1}{2}\,\mathcal{B}^2\,\ln\mu L\right), \tag{3.42a}$$

$$\langle T^{11}\rangle = \langle T^{22}\rangle = \kappa\left(-\tfrac{1}{2}a_4 + b_4 - \tfrac{1}{4}\mathcal{B}^2 + \tfrac{1}{2}\,\mathcal{B}^2\,\ln\mu L\right), \tag{3.42b}$$

$$\langle T^{33}\rangle = \kappa\left(-\tfrac{1}{2}a_4 - 2b_4 - \tfrac{1}{2}\,\mathcal{B}^2\,\ln\mu L\right). \tag{3.42c}$$

3.2.5 Scaling relations

Consider independent rescaling of the boundary and radial coordinates,

$$x \equiv \alpha\,\widetilde{x}\,, \qquad r \equiv \alpha^{-1}\gamma^2\,\widetilde{r}\,, \tag{3.43}$$

with α and γ arbitrary positive numbers. If the metric functions $\{A, \Sigma, B\}$ satisfy the Einstein equations (3.36), with asymptotic behavior (3.40), then the rescaled metric functions

$$\widetilde{B}(\widetilde{x},\widetilde{r}) \equiv B(x(\widetilde{x}), r(\widetilde{r}))\,, \tag{3.44a}$$

$$\widetilde{\Sigma}(\widetilde{x},\widetilde{r}) \equiv (\alpha/\gamma)\,\Sigma(x(\widetilde{x}), r(\widetilde{r}))\,, \tag{3.44b}$$

$$\widetilde{A}(\widetilde{x},\widetilde{r}) \equiv (\alpha/\gamma)^2 A(x(\widetilde{x}), r(\widetilde{r}))\,, \tag{3.44c}$$

also satisfy the Einstein equations (and our asymptotic conditions) with rescaled parameters

$$\widetilde{L} \equiv \gamma^{-1}\,L\,, \qquad \widetilde{\mathcal{B}} \equiv \alpha^2\,\mathcal{B}\,, \qquad \widetilde{\rho} \equiv \alpha^3\,\rho\,. \tag{3.45}$$

The subleading asymptotic coefficients a_4 and b_4 become

$$\widetilde{a}_4 \equiv \alpha^4\left[a_4 - \tfrac{1}{3}\,\mathcal{B}^2\ln(\gamma/\alpha)\right], \quad \widetilde{b}_4 \equiv \alpha^4\left[b_4 + \tfrac{1}{3}\,\mathcal{B}^2\ln(\gamma/\alpha)\right]. \tag{3.46}$$

Using the holographic relation (3.42) for the stress-energy expectation, one finds that

$$\widetilde{T}^{\mu\nu}(\widetilde{\mu}) = \alpha^4\, T^{\mu\nu}(\mu)\,, \tag{3.47}$$

with a rescaled renormalization point $\widetilde{\mu} \equiv \alpha\,\mu$.

If $\alpha = \gamma$, then these transformations are just a trivial rescaling of all quantities according to their dimension. But transformations with $\alpha \neq \gamma$ are non-trivial and scale bulk and boundary quantities by different amounts. In particular, transformations with $\alpha = 1$ but $\gamma \neq 1$ rescale the AdS curvature scale L without affecting the boundary coordinates or boundary parameters ($\mathcal{B}$, ρ, or μ), showing that the value of L has no physical significance (in the large $N_{\rm c}$, large λ limit for which classical gravity provides the dual description). This illustrates, explicitly, the independence of the boundary field theory on the AdS curvature scale L.

3.2.6 Apparent horizon

With a non-zero homogeneous energy density, the dual geometries of interest will have an apparent horizon at some radial position, $r = r_{\rm h}(v)$ [27]. Since we are investigating non-equilibrium dynamics, one might expect the horizon position to change significantly before ultimately settling down as the system equilibrates. However, as illustrated in fig. 3.1 it is possible, and very convenient, to use the residual radial shift diffeomorphism freedom (3.22) to place the apparent horizon at a fixed radial position,

$$r_{\rm h}(v) \equiv \bar{r}_{\rm h}\,. \tag{3.48}$$

A short exercise [27] shows that the condition for an apparent horizon to be present at $r = \bar{r}_{\rm h}$ is that this location be a zero of the modified time derivative of the spatial scale factor,

$$d_+\Sigma\big|_{r=\bar{r}_{\rm h}} = 0\,. \tag{3.49}$$

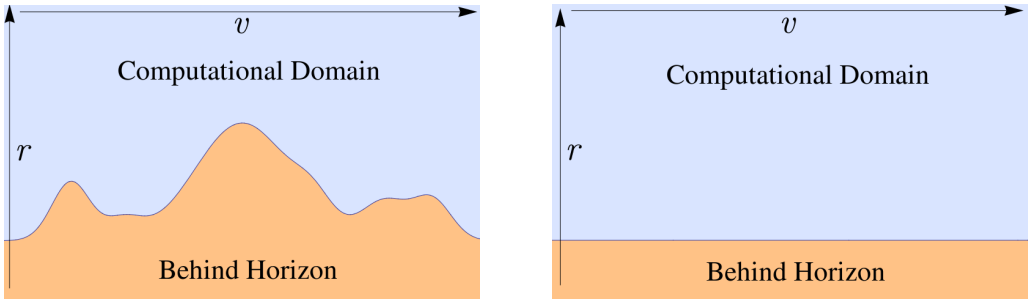

Figure 3.1: With a generic choice of the radial shift $\lambda(v)$ (left panel), the radial position of the horizon will change with time. It may be kept fixed (right panel) with a suitable choice of $\lambda(v)$.

This condition serves to fix the radial shift $\lambda(v)$. It is convenient to regard this condition as a combination of a constraint on initial data (implemented by finding the radial shift $\lambda(v_0)$ which is needed to satisfy (3.49) at some initial time v_0) together with the requirement that the horizon be time-independent, $\partial r_{\rm h}/\partial v = 0$, which requires that the time derivative of $d_+\Sigma$ vanish at the apparent horizon. Evaluating this condition, and using the Einstein equations (3.36d, 3.36e) to simplify the result, determines the value of the metric function A at the horizon,

$$A\big|_{r=\bar{r}_{\rm h}} = -\tfrac{1}{4}\, L^2\, (d_+ B)^2\,. \tag{3.50}$$

For the metric to be non-singular on and outside the apparent horizon, the spatial scale factor Σ must be non-vanishing for $r \geq \bar{r}_{\rm h}$.

3.2.7 Equilibrium solutions

Given some initial non-equilibrium state of the system, the dynamical evolution should asymptotically approach a thermal equilibrium state. In the gravitational description, this implies that the geometry should, at late times, approach some static black brane solution. The specific black brane solution will depend on the values of the conserved energy and charge densities in the chosen initial state, and on the value of the background magnetic field.

Schwarzschild

For initial states with vanishing charge density and magnetic field, the bulk geometry will equilibrate to the 5D AdS-Schwarzschild black brane solution. A standard form of this metric is

$$ds^2 = -U(\widetilde{r})\,dt^2 + \frac{d\widetilde{r}^2}{U(\widetilde{r})} + \frac{\widetilde{r}^2}{L^2}\,(dx^i)^2 \tag{3.51}$$

$(i = 1, 2, 3)$, with

$$U(\widetilde{r}) \equiv \frac{\widetilde{r}^2}{L^2} - \frac{m\,L^2}{\widetilde{r}^2}\,. \tag{3.52}$$

The radial coordinate $\widetilde{r}$ should not be confused with our Eddington-Finklestein coordinate r. The zero of $U(\widetilde{r})$ determines the horizon location,

$$\widetilde{r}_{\rm h} = m^{1/4} L\,, \tag{3.53}$$

and the horizon temperature [given by $(2\pi)^{-1}$ times the surface gravity at the horizon] is proportional to the horizon radius,

$$\pi T_{\rm h} = \widetilde{r}_{\rm h} L^{-2} = m^{1/4}/L\,. \tag{3.54}$$

In our infalling EF coordinates (3.34), this AdS-Schwarzschild solution is described by

$$\Sigma(r) = (r+\lambda)/L\,, \qquad A(r) = \tfrac{1}{2}\Sigma(r)^2 - \tfrac{1}{2} m\,\Sigma(r)^{-2}\,, \qquad B(r) = 0\,. \tag{3.55}$$

Using the holographic relation (3.42), one sees that the parameter m is related to the (rescaled) equilibrium energy density $\varepsilon \equiv \langle T^{00}\rangle/\kappa$ via

$$\varepsilon = \tfrac{3}{4}\, m\, L^{-4}\,. \tag{3.56}$$

Reissner-Nordstrom

If the initial state has a non-zero charge density but vanishing magnetic field, then the bulk geometry will equilibrate to a 5D Reissner-Nordstrom (RN) black brane [79]. This metric may be written in the form (3.51), with

$$U(\widetilde{r}) \equiv \frac{\widetilde{r}^2}{L^2} - m\,\frac{L^2}{\widetilde{r}^2} + \tfrac{1}{3}\,(\rho L^3)^2\,\frac{L^4}{\widetilde{r}^4}\,. \tag{3.57}$$

The charge density ρ of the Reissner-Nordstrom brane is bounded from above by the extremal charge density $\rho_{\max}$, given by

$$(\rho_{\max} L^3)^4 = \tfrac{4}{3}\,m^3\,. \tag{3.58}$$

The relation (3.56) between the energy density and the mass parameter m is unchanged. Hence, the extremal charge density $\rho_{\max} = \frac{4}{3}\,\varepsilon^{3/4}$.

It is convenient to express ρ in terms of the fraction x of the extremal charge density,

$$x \equiv \rho/\rho_{\max}\,. \tag{3.59}$$

The horizon radius $\widetilde{r}_{\rm h}$ is given by the outermost positive root of $U(\widetilde{r})$; explicitly,

$$\widetilde{r}_{\rm h}/L = (\tfrac{1}{3}m)^{1/4}\left[(-x^2 + i\sqrt{1-x^4})^{1/3} + (-x^2 - i\sqrt{1-x^4})^{1/3}\right]^{1/2}. \tag{3.60}$$

The horizon radius (divided by L) varies from $m^{1/4}$ down to $(\frac{1}{3}m)^{1/4}$ as x varies from 0 to 1. The horizon temperature $T_{\rm h}$ is given by

$$\pi T_{\rm h} L = (\widetilde{r}_{\rm h}/L)\left[1 - (\tfrac{1}{3}m)^{3/2}\,x^2\,(L/\widetilde{r}_{\rm h})^6\right]. \tag{3.61}$$

The horizon temperature decreases with increasing charge density, and vanishes as the charge density approaches the extremal value (or $x \to 1$).

From the perspective of the dual field theory, for any given value of the charge density

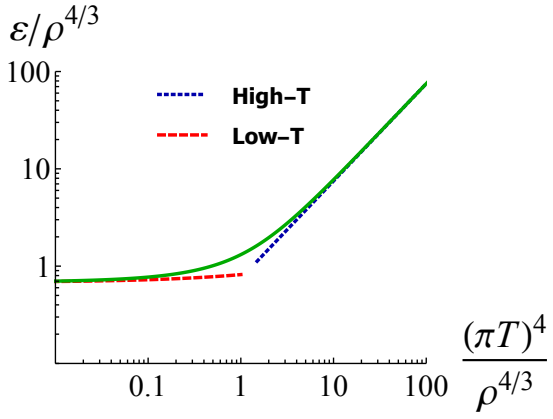

Figure 3.2: The one parameter family of non-extremal equilibrium Reissner-Nordstrom charged black brane solutions (solid line) in the plane of $\varepsilon/|\rho|^{4/3}$ vs. $(\pi T)^4/|\rho|^{4/3}$. Also shown are the high and low temperature asymptotic forms (dashed lines). In the high temperature regime, $\pi T \gg \rho^{1/3}$, the curve approaches the Schwarzschild result, $\varepsilon = \frac{3}{4}(\pi T)^4$. In the low temperature (or near extremal) regime, $\pi T \ll \rho^{1/3}$, the charge density $\rho \sim \rho_{\rm max}\big[1 - \frac{1}{8}(\frac{3}{4})^{-2/3}(\pi T)^2\rho_{\rm max}^{-2/3}\big]$ and $\varepsilon/\rho^{4/3} \sim (\frac{3}{4})^{4/3} + \frac{1}{8}\,(\frac{3}{4})^{-1/3}\,(\pi T)^2\rho^{-2/3}$.

there is a lower bound on the energy density, $\varepsilon_{\rm min}(\rho)$, which must be a monotonically increasing (and convex) function of ρ. This implies that for any given value of the energy density, there will be a maximum charge density, corresponding to a ground state with vanishing temperature. The equilibrium chemical potential μ, thermodynamically conjugate to the charge density ρ, is given by

$$\mu = \tfrac{1}{2}\,\rho\,(L^2/\widetilde{r}_{\rm h})^2\,. \tag{3.62}$$

Physically distinct non-extremal solutions may be labeled by the value of one dimensionless ratio such as $\varepsilon/|\rho|^{4/3}$ [or $(\pi T)^4/|\rho|^{4/3}$ or $\varepsilon/(\pi T)^4$, etc.]. Figure 3.2 shows a log-log plot of the curve representing these solutions in the plane of $\varepsilon/|\rho|^{4/3}$ and $(\pi T)^4/|\rho|^{4/3}$.

In our infalling EF coordinates, the RN black-brane solution is described by

$$\Sigma(r) = (r+\lambda)/L\,, \qquad A(r) = \tfrac{1}{2}\Sigma(r)^2 - \tfrac{1}{2}m\,\Sigma(r)^{-2} + \tfrac{1}{6}\rho^2 L^6\,\Sigma(r)^{-4}\,, \tag{3.63}$$

and $B(r) = 0$.

Magnetic branes

When the magnetic field is non-zero, the bulk geometry will equilibrate to a stationary magnetic black brane solution. These solutions are not known analytically, but have been studied numerically [78, 80]. In our infalling coordinates, the solutions satisfy the static specialization of eqs. (3.36).[15] The near-boundary behavior of asymptotically AdS_5 solutions is given by the expansions (3.41) (but with no time dependence).

The extremal, zero-temperature magnetic brane solution interpolates smoothly between $AdS_3 \times \mathbb{R}^2$ near the horizon and AdS_5 near the boundary. In our infalling coordinates, a series in fractional powers of $\delta r \equiv r - r_h$ describes deviations from the $AdS_3 \times \mathbb{R}^2$ geometry near the horizon,

$$A(r) = \tfrac{3}{2}(\delta r/L)^2 \left[1 + \eta\, \delta r^{\gamma} + O\big(\eta^2\, \delta r^{2\gamma}\big)\right], \tag{3.65a}$$

$$\Sigma(r) = (\mathcal{B} L\, \delta r)^{1/3} \left[1 - \tfrac{1}{7}(3+\gamma)\, \eta\, \delta r^{\gamma} + O\big(\eta^2\, \delta r^{2\gamma}\big)\right], \tag{3.65b}$$

$$B(r) = -\tfrac{1}{6} \ln[27\, \delta r^4/(\mathcal{B}^2 L^8)] - \tfrac{1}{14}(13+2\gamma)\, \eta\, \delta r^{\gamma} + O\big(\eta^2\, \delta r^{2\gamma}\big), \tag{3.65c}$$

with $\gamma \equiv -1 + \frac{1}{3}\sqrt{57}$. The constant η cannot be determined from a near-horizon analysis and must be suitably adjusted after integrating eqs. (3.64) to obtain the desired boundary geometry. There is a single extremal magnetic brane solution, modulo the rescaling transformations (3.43)-(3.45) (which relate solutions with any non-zero values of the magnetic field $\mathcal{B}$ and curvature scale L), and radial shift diffeomorphisms (3.22).

For non-extremal solutions (with non-zero $\mathcal{B}$ but vanishing ρ), metric functions near the

---

[15] The resulting equations may be written explicitly as:

$$\big(A'\Sigma^3\big)'\,\Sigma^{-3} = +\tfrac{2}{3}\mathcal{B}^2 L^2 e^{-2B}\,\Sigma^{-4} + \tfrac{4}{3}\mathcal{E}^2 L^2 + 4/L^2\,, \tag{3.64a}$$

$$\big(A\Sigma'\Sigma^2\big)'\,\Sigma^{-3} = -\tfrac{1}{3}\mathcal{B}^2 L^2 e^{-2B}\,\Sigma^{-4} - \tfrac{1}{3}\mathcal{E}^2 L^2 + 2/L^2\,, \tag{3.64b}$$

$$\big(AB'\Sigma^3\big)'\,\Sigma^{-3} = -\tfrac{2}{3}\mathcal{B}^2 L^2 e^{-2B}\,\Sigma^{-4}\,. \tag{3.64c}$$

horizon have power series expansions in $\delta r \equiv r - r_{\rm h}$ of the form

$$A(r) = a_0\,\delta r\,L^{-2}\left[1 - (1 - \tfrac{5}{6}\,\mathcal{B}^2 L^4 s_0^{-4})\,a_0^{-1}\delta r + O(\delta r^2)\right], \tag{3.66a}$$

$$\Sigma(r) = s_0/\beta\left[1 + (2 - \tfrac{1}{3}\,\mathcal{B}^2 L^4 s_0^{-4})\,a_0^{-1}\,\delta r + O(\delta r^2)\right], \tag{3.66b}$$

$$B(r) = 2\ln\beta - \tfrac{2}{3}\,\mathcal{B}^2 L^4 s_0^{-4}\,a_0^{-1}\,\delta r + O(\delta r^2)\,. \tag{3.66c}$$

The coefficient a_0 is proportional to the horizon temperature,

$$T = a_0/(2\pi L^2)\,. \tag{3.67}$$

The other two undetermined constants, s_0 and β, which control the horizon values of the spatial scale factor and the anisotropy function, must be suitably adjusted after integrating eqs. (3.64) to select solutions which have the desired near-boundary behavior (with an isotropic boundary metric). If $\mathcal{B}^2 \ll T^4$, then the resulting magnetic brane geometry is a small perturbation away from the Schwarzschild black brane (3.55), while if $\mathcal{B}^2 \gg T^4$ then the geometry may be regarded as interpolating between the BTZ black brane ($\times\,\mathbb{R}^2$) near the horizon and AdS_5 near the boundary [78].

There is a one parameter family of non-extremal solutions, modulo the rescaling transformations (3.43)-(3.45) (and radial shift diffeomorphisms). Physically distinct solutions may be labeled by the value of the dimensionless ratio $\varepsilon_{\mathcal{B}}/\mathcal{B}^2$ [or $(\pi T)^4/\mathcal{B}^2$ or $\varepsilon_{\mathcal{B}}/(\pi T)^4$, etc.]. The left panel of figure 3.3 shows a log-log plot of our numerically determined curve representing these solutions in the plane of $\varepsilon_{\mathcal{B}}/\mathcal{B}^2$ and $(\pi T)^4/\mathcal{B}^2$. Extrapolating our lowest temperature numerical results to zero temperature, we find estimates of

$$c_0 \approx 0.18\,, \qquad \mathcal{B}^*(\mu) \approx 2.0\,\mu^2\,, \tag{3.68}$$

for the coefficient c_0 or the equivalent fiducial scale $\mathcal{B}^*$ defined by eqs. (3.15) and (3.16).

If one chooses to measure energy density and magnetic field in units set by the curvature

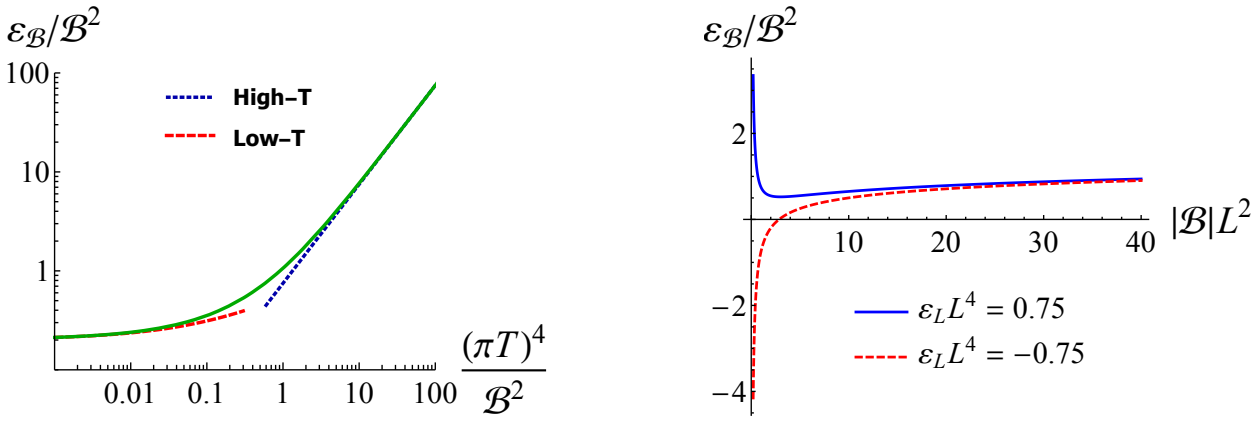

Figure 3.3: Left: The one parameter family of non-extremal equilibrium magnetic brane solutions in the plane of $\varepsilon_{\mathcal{B}}/\mathcal{B}^2$ vs. $(\pi T)^4/\mathcal{B}^2$. Also shown are the high and low temperature asymptotic forms (dashed lines). For high temperatures, $\pi T \gg |\mathcal{B}|^{1/2}$, the curve approaches the Schwarzschild result $\varepsilon = \frac{3}{4}(\pi T)^4$. For low temperatures, $\pi T \ll |\mathcal{B}|^{1/2}$, the form $\varepsilon_{\mathcal{B}}/\mathcal{B}^2 \sim c_1 + c_2\,(\pi T)^2/|\mathcal{B}|$ provides a good fit to our data for $c_1 = 0.35$ and $c_2 = 0.20$. Right: The relation between the intrinsic parameter $\varepsilon_{\mathcal{B}}/\mathcal{B}^2$ labeling magnetic brane solutions and the value of the magnetic field in curvature scale units, $|\mathcal{B}|L^2$, for two different fixed values of the curvature scale energy density, $\varepsilon_L L^4 = \pm 0.75$.

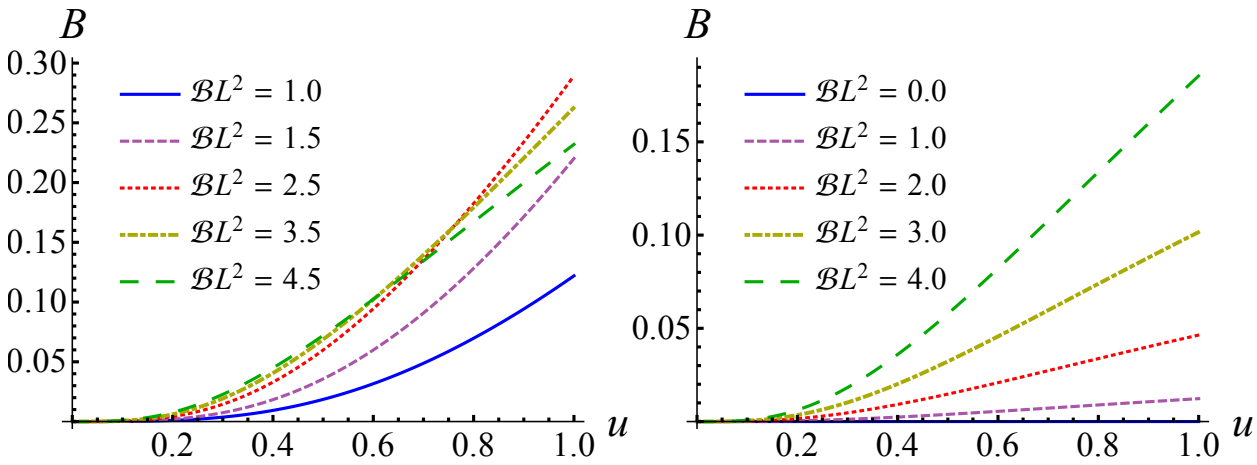

Figure 3.4: The anisotropy function $B(r)$ as a function of inverse radius $u \equiv 1/r$ for equilibrium magnetic brane solutions with different values of the magnetic field. Left panel: Solutions at fixed energy density $\varepsilon_L = 0.75\, L^{-4}$ with $\mathcal{B}L^2 = 1.0$, 1.5, 2.5, 3.5, and 4.5. Right panel: Solutions at fixed energy density $\varepsilon_{\mathcal{B}} = 8.0\, L^{-4}$ with $\mathcal{B}L^2 = 0.0$, 1.0, 2.0, 3.0, and 4.0. In all cases, the radial shift λ has been suitably adjusted to fix the horizon radius at $u = 1$. Note that the horizon value of the anisotropy function is not a monotonic function of magnetic field at fixed ε_L, but is monotonic when $\varepsilon_{\mathcal{B}}$ is held fixed.

scale L, then one may traverse the one-parameter family of magnetic brane solutions by varying $|\mathcal{B}|L^2$ for a fixed value of $\varepsilon_L L^4$ (or vice versa). The holographic relation (3.42) shows that these curvature scale dependent quantities are related to the intrinsic dimensionless parameter $\varepsilon_{\mathcal{B}}/\mathcal{B}^2$ via

$$\frac{\varepsilon_{\mathcal{B}}}{\mathcal{B}^2} = \frac{\varepsilon_L\, L^4}{(|\mathcal{B}|L^2)^2} + \tfrac{1}{4}\ln(|\mathcal{B}|L^2)\,. \tag{3.69}$$

This relation between $\varepsilon_{\mathcal{B}}/\mathcal{B}^2$ and $|\mathcal{B}|L^2$, for two different fixed values of the curvature scale energy density $\varepsilon_L L^4 = \pm 0.75$, is plotted in the right panel of fig. 3.3. Note that two different values of $|\mathcal{B}|L^2$ yield the same value of $\varepsilon_{\mathcal{B}}/\mathcal{B}^2$ (and hence describe the same physical solution) when $\varepsilon_L > 0$.

For these non-extremal magnetic brane solutions, the anisotropy function $B(r)$ increases (and the scale factor Σ decreases) smoothly as one moves inward from the boundary toward the horizon. Figure 3.4 (left) plots the resulting anisotropy function $B(r)$ for several values

of the magnetic field when the energy density at the scale $1/L$ is held fixed, $\varepsilon_L L^4 = \frac{3}{4}$. (From eq. (3.42a), this is the same as fixing the asymptotic coefficient $a_4 L^4 = -\frac{1}{2}$.) The horizon temperatures for this series of solutions, in order of increasing magnetic field, are given by $\pi T L = 0.873$, 0.806, 0.879, 1.103, and 1.347. From the figure, one may see that the horizon value of the anisotropy function is not a monotonic function of magnetic field (for fixed $a_4 L^4$).

The right panel of fig. 3.4 shows a similar set of solutions with increasing magnetic field, but now with the energy density at the scale $|\mathcal{B}|^{1/2}$ held fixed, $\varepsilon_{\mathcal{B}} = 8\, L^{-4}$. With the physical parameter $\varepsilon_{\mathcal{B}}$ held fixed, the horizon value of the anisotropy function is now monotonically increasing with magnetic field. The temperatures of these solutions (in order of increasing $\mathcal{B}$) are given by $\pi T L = 1.807$, 1.797, 1.738, 1.620, and 1.433.

3.3 Techniques

3.3.1 Computational strategy

We apply the computational strategy presented in ref. [27] to our case of homogeneous isotropization in Einstein-Maxwell theory. For convenience, we choose units in which the AdS curvature scale $L = 1$.

Required initial data, on some $v = v_0$ time slice, consists of an initial choice for the anisotropy function $B(v_0, r)$ and the radial shift $\lambda(v_0)$, along with chosen (time independent) values of the energy density ε, charge density ρ, and magnetic field $\mathcal{B}$. As noted above, the holographic relation (3.42a) shows that fixing the energy density ε at the scale $\mu = 1/L$ is equivalent to fixing the asymptotic coefficient a_4. Our choices for the initial anisotropy function will be detailed below in subsection 3.3.3.

Given a set of initial data, the linear second order radial ordinary differential equation (ODE) (3.36a) may be integrated to find the spatial scale factor $\Sigma(v_0, r)$. The two leading terms in the asymptotic behavior (3.41a) provide the integration constants needed to specify uniquely the desired solution. Next, one solves eq. (3.36d), a linear first order radial ODE for

$d_+\Sigma$. The near-boundary asymptotic behavior of this function is $d_+\Sigma \sim \frac{1}{2}(r+\lambda)^2 + a_4\, r^{-2} + \mathcal{O}(r^{-3})$ and homogeneous solutions to eq. (3.36d) behave as r^{-2} near the boundary. Hence, the chosen value of the energy density ε uniquely specifies the desired solution. With B, Σ, and $d_+\Sigma$ determined on the v_0 time slice, one next solves eq. (3.36c), a linear first order radial ODE for d_+B. The desired asymptotic behavior of this function is $d_+B \sim -2b_4\, r^{-4} + \mathcal{O}(r^{-5})$ while homogeneous solutions to eq. (3.36c) behave as $r^{-3/2}$ near the boundary. So the needed integration constant corresponds to requiring the absence of any such homogeneous solution. Finally, one solves the second order linear ODE (3.36b) to determine $A(v_0, r)$. Homogeneous solutions are linear or constant functions of r. From the asymptotic behavior (3.41b), one sees that the value of the radial shift $\lambda(v_0)$ fixes the coefficient of the homogeneous solution linear in r and provides one of the two needed boundary conditions. The second boundary condition, needed to fix the constant homogeneous solution, is provided by the horizon stationarity condition (3.50), which determines the value of A on the apparent horizon.

Having solved for the modified time derivative $d_+B(v_0, r)$, and $A(v_0, r)$, one reconstructs the ordinary time derivative of the anisotropy function via

$$\partial_v B(v_0, r) = d_+B(v_0, r) - A(v_0, r)\, \partial_r B(v_0, r)\,. \tag{3.70}$$

The time derivative of the radial shift, $\partial_v\lambda(v_0)$, is extracted from the asymptotic behavior (3.41b) of A by evaluating the $r \to \infty$ limit of $A - \frac{1}{2}(r+\lambda)^2$. These time derivatives of B and λ provide the information needed to advance in time. Using a standard numerical integration scheme, one takes a small step forward in time, advancing v to $v_0 + \Delta v$ for some timestep Δv. Repeating this process, one progressively determines the metric functions on a sequence of equally spaced time slices, $v = v_k \equiv v_0 + k\,\Delta v$. On each time slice, the asymptotic coefficient $b_4(v)$, needed to determined the stress tensor (3.42), is extracted from the large r behavior of the anisotropy function B. (In the presence of a non-zero magnetic field, one extracts b_4 from the large r limit of a subtracted, rescaled version of the anisotropy function which removes the leading logarithmic piece in eq. (3.41c). This is detailed in the next subsection.)

3.3.2 Numerical methods

We use an inverted radial coordinate $u = 1/r$, and arbitrarily choose

$$\bar{r}_{\rm h} = 1\,, \tag{3.71}$$

as our apparent horizon location. This makes our computational domain a fixed radial interval, $0 \le u \le u_{\rm h} \equiv 1$. We use a 4th order Runge-Kutta method (described in ref. [27]) for time integration. This requires four integrations of our radial ODEs per time step, but yields much better accuracy, for a given timestep Δv, than a lower order method.

To integrate the radial ODEs (3.36a–3.36d), we have used both traditional short-range finite difference approximations, and spectral methods [83]. In the latter approach, one implicitly represents the radial dependence of functions as a (truncated) series of Chebyshev polynomials. Explicitly, functions are represented by the list of their values on a discrete, finite collocation grid consisting of the points

$$u_k = \tfrac{1}{2}\Big[1 + \cos\frac{\pi\,k}{M-1}\Big]\,, \quad k = 0, \cdots, M-1\,, \tag{3.72}$$

and derivatives are represented by (dense) $M \times M$ matrices acting on the finite list of function values. The (truncated) spectral expansion converts each ODE into a straightforward linear algebra problem. Boundary conditions are simply encoded into the first or last rows of the resulting matrix [83].

Although there are subtleties (described momentarily) in applying spectral methods to our problem, we have found the use of spectral methods to be clearly superior to finite difference approximations, yielding both faster computation and more accurate results. Using an M point discretization of the computation domain, short-range finite difference methods have errors which scale as an inverse power of M while spectral methods, in favorable cases, produce errors which fall exponentially with increasing M.

Spectral methods presume that one is approximating functions which are regular and

well-behaved on the computational domain. However, our radial ODEs have regular singular points at $u = 0$ or $r = \infty$ (due to the r^2 growth of the scale factor near the boundary), and our functions Σ, $d_+\Sigma$, and A all diverge at the $u = 0$ endpoint. Therefore, we define subtracted functions in which the known singular near-boundary behavior is removed. To minimize loss of numerical precision in spectral approximations of derivatives, it is also helpful to rescale the subtracted functions so that they do not vanish faster than linearly as $u \to 0$. If the magnetic field is zero, so no logarithmic terms are present in the near-boundary behavior (3.41), then our subtracted functions are analytic in a neighborhood of the $u \in [0, 1]$ radial interval and spectral methods converge exponentially. With a non-zero magnetic field, logarithmic terms are unavoidably present, showing that $u = 0$ is a branch point of the metric functions. This degrades convergence of the spectral series, leading to power-law convergence at a rate which depends on the behavior of the leading non-analyticity. Consequently, it is desirable to subtract logarithmic terms to as high an order as is practicable. We chose to introduce subtracted/rescaled functions (denoted with a subscript 's') via:

$$\Sigma(r) = (r+\lambda) + r^{-5}\,\Sigma_s(r)\,, \tag{3.73a}$$

$$A(r) = \tfrac{1}{2}(r+\lambda)^2 - \tfrac{1}{3}\mathcal{B}^2\,\ln r\left[r^{-2} - 2\lambda\,r^{-3} + 3\lambda^2\,r^{-4} - 4\lambda^3\,r^{-5}\right] + A_s(r)\,. \tag{3.73b}$$

$$d_+\Sigma(r) = \tfrac{1}{2}\Sigma(r)^2 - \tfrac{1}{3}\mathcal{B}^2\,\ln r\left[r^{-2} - 2\lambda\,r^{-3} + 3\lambda^2\,r^{-4} - 4\lambda^3\,r^{-5}\right] + (d_+\Sigma)_s(r)\,, \tag{3.73c}$$

$$d_+B(r) = -\tfrac{2}{3}\mathcal{B}^2\,\ln r\left[r^{-3} - 3\lambda\,r^{-4} + 6\lambda^2\,r^{-5} - 10\lambda^3\,r^{-6}\right] + r^{-2}\,(d_+B)_s(r)\,. \tag{3.73d}$$

All our numerical work is performed using these subtracted/rescaled functions; we directly solve for Σ_s, $(d_+\Sigma)_s$, $(d_+B)_s$, and A_s.[16] The expressions (3.73) are used to reconstruct the original functions when needed. We also use a subtracted/rescaled anisotropy function $B_s(r)$,

[16]Note that $(d_+\Sigma)_s \neq d_+(\Sigma_s)$, and likewise for $(d_+B)_s$; these are just names for the subtracted/rescaled functions for $d_+\Sigma$ and d_+B, respectively.

introduced via

$$B(r) = \tfrac{1}{3}\mathcal{B}^2 \ln r \left[r^{-4} - 4\lambda\, r^{-5} + 10\lambda^2\, r^{-6}\right] + r^{-3} B_s(r)\,. \tag{3.74}$$

This removes leading logarithmic terms and introduces a convenient rescaling. Henceforth, B_s will be referred to as the subtracted anisotropy function.

In the above subtractions, the series in $1/r$ multiplying each logarithm are just truncated expansions of $(r+\lambda)^{-k}$ for $k = 2$, 3 or 4. The choice to truncate these binomial series was arbitrary, but we found that our numerics were sufficiently well-behaved with the above subtractions. At higher orders in $1/r$, additional terms appear which involve the asymptotic coefficient b_4 and its (a-priori unknown) time derivatives, as well as higher powers of logarithms.

3.3.3 Initial data

As indicated above, one must select the value of the energy density (or asymptotic coefficient a_4) and the initial value of the radial profile of the anisotropy function, $B(v_0, r)$. And one must choose the value of the magnetic field $\mathcal{B}$ or charge density ρ. For the charged case, with vanishing magnetic field, physics can only depend on the dimensionless combination of charge and energy densities $\rho/\varepsilon^{3/4}$, so a (positive) value of ε may be chosen arbitrarily without loss of generality. Given a choice of ε, possible values of the charge density ρ are limited by the extremality bound $|\rho| \leq \rho_{\max} = \frac{4}{3}\,\varepsilon^{3/4}$.

For the initial anisotropy function, we chose to focus on Gaussian profiles. In the $\lambda = 0$ frame,

$$B(v_0, r) = \mathcal{A}\, e^{-\frac{1}{2}(r-r_0)^2/\sigma^2}. \tag{3.75}$$

We investigate the dependence of results on the parameters of the Gaussian (amplitude $\mathcal{A}$, width σ, and mean position r_0) in the first part of section 3.4.[17] Motivated by the fact that

[17]For results from an exploration of a broader range of initial anisotropy profiles, in the case of vanishing charge density and magnetic field, see ref. [53].

in our coordinates lines of varying r, at fixed v, are radially infalling geodesics, we will refer to this initial Gaussian as a "pulse" of initial anisotropy.

For the magnetic case, as discussed above, the breaking of scale invariance implies the presence of logarithmic terms in the asymptotic behavior of the anisotropy function. We simply add the log terms shown in eq. (3.74) to the Gaussian (3.75). With vanishing radial shift, $\lambda = 0$, our chosen initial anisotropy function takes the form

$$B(v_0, r) = \mathcal{A}\, e^{-\frac{1}{2}(r-r_0)^2/\sigma^2} + \tfrac{1}{3}\mathcal{B}^2\, r^{-4} \ln r\,. \tag{3.76}$$

Arguably, a more natural choice for the magnetic case initial data might be to add a Gaussian to the full equilibrium solution for the anisotropy function in the chosen magnetic field. This could be seen as nicely paralleling the charged case (in which the equilibrium solution has vanishing anisotropy). Nevertheless, we will stick with our somewhat arbitrary choice (3.76), which is an adjustable initial pulse added to the correct asymptotics. As will be seen, the Gaussian pulse will nearly always be the dominant portion of the deviation from equilibrium and the driving force of the resulting anisotropy in the boundary stress. We doubt that differing choices in the precise form of the slowly varying function to which the Gaussian pulse is added would impact, in any significant way, the characteristic equilibration times or other significant features of the results presented below.

After choosing the initial anisotropy function (in the $\lambda = 0$ frame) the initial value of the radial shift, $\lambda(v_0)$, is adjusted to fix the location of the apparent horizon, as discussed in section 3.2.6.

It should be noted that, in all cases (charged, uncharged, magnetized) it is quite possible to select physically inconsistent initial data. This happens when the initial anisotropy, for a given energy density, is so large that no apparent horizon shields a coordinate singularity produced by a vanishing scale factor Σ. This sets a natural limit on the amplitude of the initial pulse which is meaningful to study.

3.4 Results

3.4.1 Neutral plasma

Before presenting results for equilibration in charged or magnetized plasmas, we first discuss general features of the time evolution in the uncharged, unmagnetized case and examine the sensitivity of results to specific features in the initial data. As noted above, we choose a Gaussian profile (3.75) for the initial anisotropy function, with an adjustable amplitude, width, and mean position. Typical evolution of our subtracted/rescaled anisotropy function, $B_s(v,u) \equiv u^{-3}B(v,u)$, is shown on the left in figure 3.5. One sees the initial pulse profile on the back side of the plot at $v = 0$. The figure clearly shows the influence of the pulse propagating outward and reflecting off the boundary at $u = 0$. The outgoing portion of the pulse essentially propagates along an outgoing radial null geodesic which, in our coordinates, near the boundary are 45° lines at constant values of $u + v$. The influence of the anisotropy pulse, after the reflection, largely falls through the horizon along an ingoing radial null geodesic which is instantaneous in our null time coordinate v. The asymptotic coefficient b_4, which equals the slope of B_s at $u = 0$, controls the anisotropy in the stress tensor,

$$\Delta\mathcal{P} \equiv \tfrac{1}{2}\langle T^{11}\rangle + \tfrac{1}{2}\langle T^{11}\rangle - \langle T^{33}\rangle\,, \tag{3.77}$$

with $\Delta\mathcal{P}/\kappa = 3\,b_4$. Hence, the reflection of the pulse off the boundary directly produces the pressure anisotropy $\Delta\mathcal{P}$ in the boundary theory. The time dependence of the relative pressure anisotropy,[18] defined as $\Delta\mathcal{P}/(\kappa\epsilon)$, is plotted on the right in figure 3.5.

As shown in the figure, at late times the anisotropy function approaches zero, as required for equilibration to the isotropic Schwarzschild black brane solution. At sufficiently late times, when the departure from equilibrium is small, the evolution should be well described by a linearized approximation to the full nonlinear dynamics. The linearized dynamics of

[18]Note that, for unmagnetized plasma, the energy density is three times the average pressure, $\varepsilon = \langle T^{ii}\rangle \equiv 3\overline{\mathcal{P}}$.

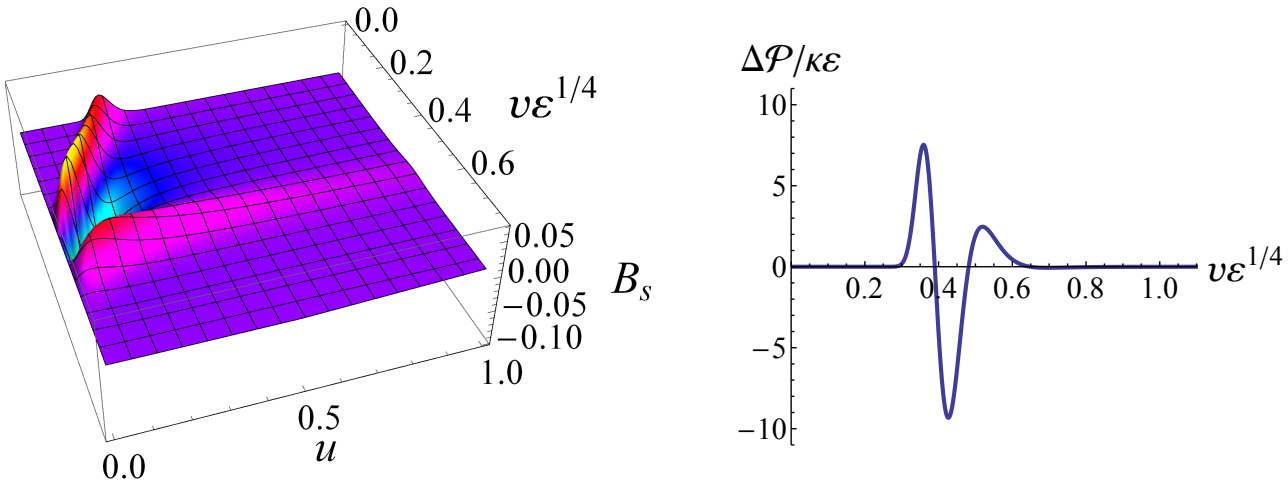

Figure 3.5: Left: Rescaled anisotropy function $B_s = u^{-3}B$, for a typical case of equilibration to the Schwarzschild black brane, as a function of inverse bulk radius u and time v. Initial pulse parameters are $\mathcal{A} = 5 \times 10^{-4}$, $r_0 = 4$ and $\sigma = \frac{1}{2}$, with $\varepsilon = \frac{3}{4}L^{-4}$. The (rescaled) energy density ε is used to the set the scale for time. One sees that the effect of the initial Gaussian pulse propagates outward, essentially along an outgoing radial null geodesic, reflects off the boundary, and then largely falls through the horizon (along an ingoing radial null geodesic which is instantaneous in v). After one "bounce", the anisotropy rapidly approaches zero. Right: The corresponding relative pressure anisotropy, $\Delta\mathcal{P}/\kappa\varepsilon \equiv \frac{1}{2}(T^{11} + T^{11} - 2T^{33})/\kappa\varepsilon$, induced in the boundary field theory, as a function of time. Note how the peaks of the pressure anisotropy correspond directly to the reflection of the anisotropy pulse off the boundary.

infinitesimal perturbations away from equilibrium may be represented as a sum of quasinormal modes (QNM), which are eigenfunctions of the linearized dynamics with complex frequencies, $\phi(t) = \mathrm{Re}(A\, e^{-i\omega t})$ with $\mathrm{Im}\,\omega < 0$. The lowest quasinormal mode (for which $-\mathrm{Im}\,\omega$ is minimal) dominates the late time approach to equilibrium. For the Schwarzschild black brane, quasinormal mode frequencies have been previously evaluated by Starinets [25]. From the late time behavior of our full nonlinear evolution, it is straightforward to extract an estimate of the lowest quasinormal mode frequency. Comparing with the independent results of ref. [25] provides a useful test of the accuracy of our numerics. Fitting the late time ($4 \lesssim v\,\varepsilon^{1/4} \lesssim 25$) portion of our calculated pressure anisotropy to a decaying, oscillating exponential, $|A|e^{(\mathrm{Im}\,\omega)v}\cos[(\mathrm{Re}\,\omega)v + \phi]$, yields an estimate of the lowest QNM frequency ω which agrees with ref. [25] to five digits, $\omega/(\pi T) \approx 3.11946 - 2.74663\,i$.

We will see the same vanishing of the anisotropy function at late times for the case of charged plasmas, whose gravitational duals equilibrate to an isotropic Reissner-Nordstrom black brane solution. For the magnetic case, however, at late times there is a non-zero profile for the anisotropy function, reflecting the spatial anisotropy of equilibrium magnetic brane solutions.

We now turn to an examination of the dependence of the pressure anisotropy on the parameters of the initial Gaussian (3.75). Of particular interest will be the dependence of the response on the amplitude and position of the initial pulse. Less interesting is the dependence on the width of the pulse, which affects the duration of the reflection off the boundary (and also produces changes more naturally associated with the position of the pulse).

In figure 3.6, we compare the pressure anisotropies created by the pulse shown in fig. 3.5, and an otherwise identical pulse with half the amplitude. Visually, one sees that the smaller amplitude pulse produces roughly half the pressure anisotropy as does the larger pulse, but with a virtually identical time course. The peak pressure anisotropy (divided by energy density), for both pulses is over 4, significantly larger than unity. Hence both initial pulses represent large departures from equilibrium. Given the highly nonlinear nature of the Ein-

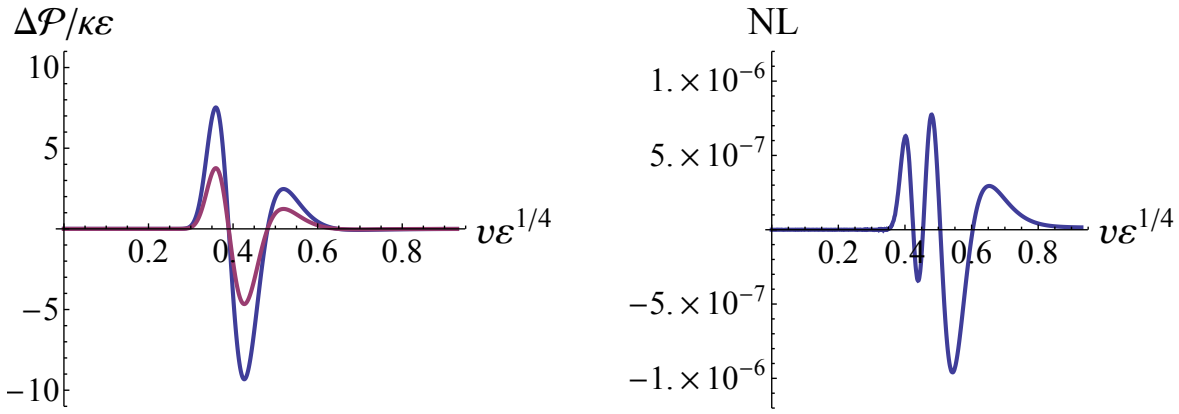

Figure 3.6: Left: The pressure anisotropy $\Delta P/\kappa\varepsilon$ produced by the same initial pulse shown in fig. 3.5 (blue curve), overlaid with the pressure anisotropy produced by an initial pulse with half the amplitude (purple curve). Halving the initial amplitude roughly halves the induced pressure anisotropy. Right: The "nonlinearity" (NL), defined as the difference between the pressure anisotropy produced by the larger pulse and twice the pressure anisotropy produced by the half amplitude pulse.

stein equations, one might have expected to see clear signs of nonlinearity in the dependence of the pressure anisotropy on the initial pulses. However, even for these pulses producing large departures from equilibrium, the amplitude of the peaks in the induced pressure anisotropy are nearly linear in the amplitude of the initial Gaussian pulse.

The right hand panel of figure 3.6 makes this comparison quantitative. This shows the nonlinearity (NL) defined as the difference between the pressure anisotropy $\Delta\mathcal{P}/\kappa\varepsilon$ of the larger initial pulse and twice the pressure anisotropy produced by the halved initial pulse. Compared to the pressure anisotropies themselves, the relative size of the nonlinearity is roughly one part in 10^7. This suggests that the dynamics, as probed by these initial pulses, are surprisingly close to a linear dynamical system.

In asymptotically AdS gravitational solutions, deviations of the geometry from that of pure AdS space necessarily vanish as one approaches the boundary. Hence, one might expect nearly linear dynamics to be evident for initial pulses which are localized sufficiently close to the boundary, while anticipating much larger nonlinearities for initial pulses localized closer

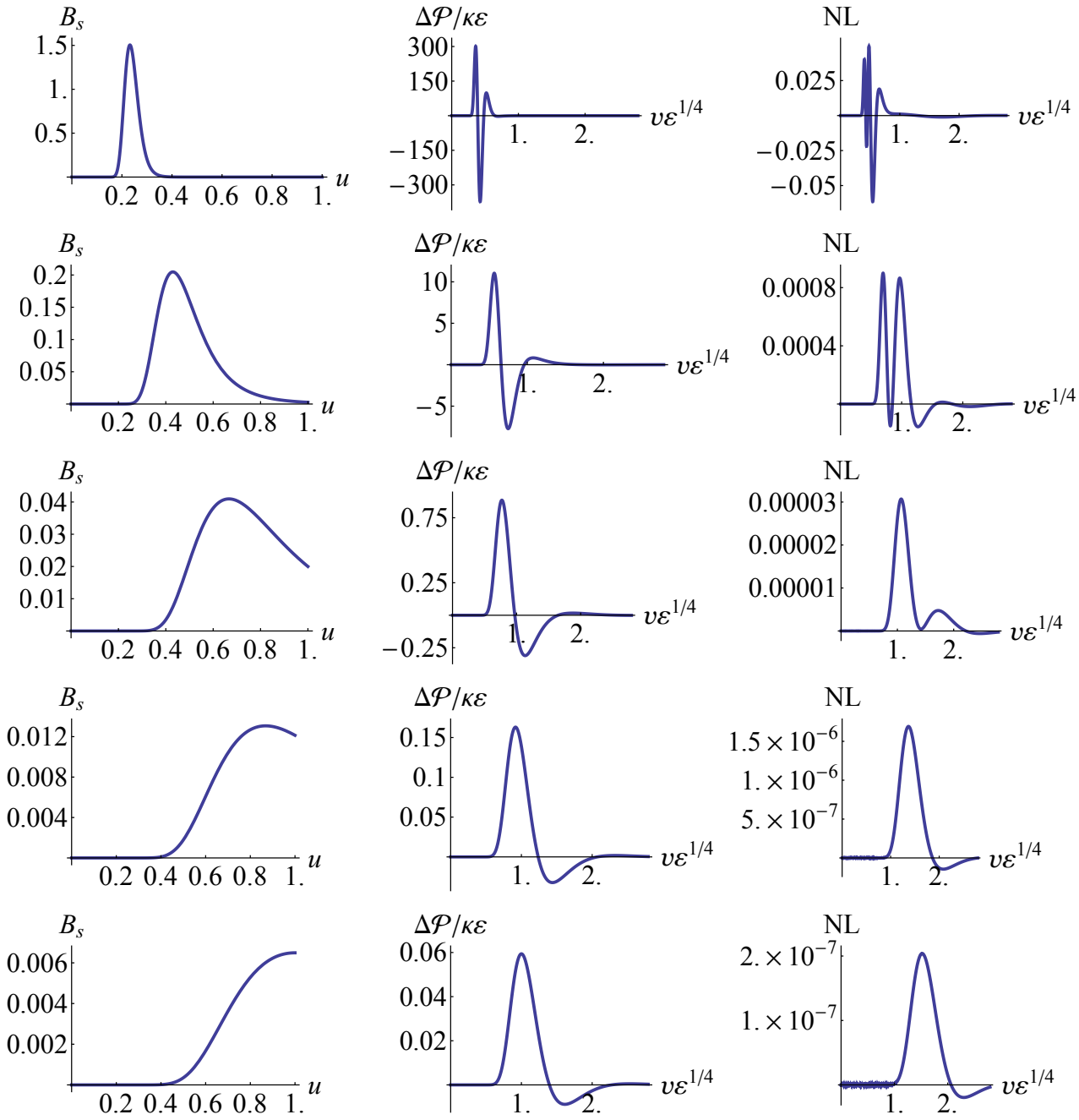

Figure 3.7: Comparisons of initial anisotropy functions (left column), induced pressure anisotropy (middle column), and nonlinearity (right column) defined as in fig. 3.6, for a series of five Gaussian initial anisotropy functions differing only in their depth in the bulk. From top to bottom, the mean position of the initial pulse, in the $\lambda = 0$ frame, is $r_0 = \{4, 2, 1, \frac{1}{2}, \frac{1}{4}\}$. In all cases the energy density is $\varepsilon = \frac{3}{4}L^{-4}$. The plots in the first row come from the same initial data as in fig. 3.5, but with the amplitude increased by a factor of 40 ($\mathcal{A} = 0.02$, $r_0 = 4$, $\sigma = \frac{1}{2}$). The left column shows the initial anisotropy function scaled by u^{-3} and plotted as a function of the inverse radial coordinate u, after adjusting the radial shift λ to fix the apparent horizon at $u = 1$.

to the horizon. To test this expectation, we used a very large Gaussian — the same initial Gaussian profile which generated fig. 3.5 but with the amplitude increased[19] by a factor of 40 — and then examined the resulting evolution when the mean position of the initial Gaussian was progressively shifted deeper into the bulk. Figure 3.7 compares the evolution for mean positions $r_0 = \{4, 2, 1, \frac{1}{2}, \frac{1}{4}\}$, in the frame with radial shift $\lambda = 0$. In all cases, the energy density was held fixed at a value ($\varepsilon = \frac{3}{4}L^{-4}$) which puts the equilibrium horizon position at $r = 1$. In other words, the only change in the five cases shown in fig. 3.7 is the radial position of the initial Gaussian anisotropy function (3.75), viewed as a function of r.

Each row of fig. 3.7 displays results for one of these five cases. In each row, the left hand panel shows the initial anisotropy function, but plotted as a function of the inverse radial coordinate u, after adjusting the radial shift λ to fix the apparent horizon at $u = 1$, as discussed in sec. 3.2.6. The middle panels show the resulting pressure anisotropy as a function of time, and the rightmost panels display the nonlinearity (NL), again defined as the difference between the pressure anisotropy of the given initial pulse and twice the pressure anisotropy after halving the initial amplitude.

From the middle column of plots, one sees that the magnitude of the pressure anisotropy decreases significantly as the initial pulse is moved deeper into the bulk. Moreover, both the time it takes for the effect of the pulse to reach the boundary, and the width of the resulting peaks in the pressure anisotropy, grow with increasing depth of the initial pulse. This reflects the usual holographic mapping between bulk and boundary: phenomena deeper in the bulk correspond to lower energy or longer time scales in the boundary field theory.

Turning to the nonlinearity plots in the right hand column, one sees that the magnitude of the nonlinearity also decreases as the pulse moves deeper into the bulk. Dividing the peak nonlinearity by the peak pressure anisotropy gives a relative measure of nonlinearity. This is about 1×10^{-4} for the top row, 3×10^{-5} for the middle row, and 3×10^{-6} for the bottom row. So in this comparison, as the initial pulse is pushed deeper into the bulk, the relative

[19]For the chosen values of position and width of the Gaussian, plus energy density $\varepsilon = \frac{3}{4}L^{-4}$, this amplitude is close to the upper limit set by demanding the existence of an apparent horizon.

nonlinearity *decreases* systematically.

This comparison does not, however, imply that nonlinearities are never significant. The amplitude of the Gaussian pulse in the initial anisotropy function was kept fixed in fig. 3.7, resulting in a decreasing size of the induced pressure anisotropy as the pulse moves deeper into the bulk. While the first two rows of the figure show pressure anisotropies which are large departures from equilibrium, $\Delta\mathcal{P}/\kappa\varepsilon \gg 1$, the final rows with $\Delta\mathcal{P}/\kappa\varepsilon \ll 1$ represent small departures from equilibrium. It is natural to ask what happens if one instead increases the amplitude as the pulse is moved into the bulk, so as to keep fixed the size of the induced pressure anisotropy.

Such a comparison is shown in fig. 3.8. The upper row of the figure shows the time dependence of the pressure anisotropy and the nonlinearity for the same pulse which generated figs. 3.5 and 3.6 ($\mathcal{A} = 5 \times 10^{-4}$, $r_0 = 4$, $\sigma = \frac{1}{2}$), while the lower row shows the pressure anisotropy and nonlinearity of a pulse with the same shape as the last row of fig. 3.7, but with larger amplitude ($\mathcal{A} = 2.5$, $r_0 = \frac{1}{4}$, $\sigma = \frac{1}{2}$). The energy density remains fixed, $\varepsilon = \frac{3}{4}L^{-4}$. The peak pressure anisotropy is similar in the two cases, and corresponds to a large departure from equilibrium. For the latter case of a pulse deep in the bulk, large enough to induce a far from equilibrium pressure anisotropy, the nonlinearity is significant, much larger than the previous examples. However, even for this case, the size of the nonlinearity relative to the peak pressure anisotropy is only about 5%, $\mathrm{NL}/(\Delta\mathcal{P}/\kappa\varepsilon) \approx 0.05$.[20]

The data shown in fig. 3.7 inspire several further questions. Looking down the middle column of the figure, one sees that the onset of the response (i.e., the time of the first peak in the pressure anisotropy) increases as the initial pulse moves deeper into the bulk but seems, perhaps, to be approaching a maximum value. Is this really true, or can one craft initial data for which the onset of the response is much greater? As shown on the left panels of the lower rows of the figure, when the average position r_0 of the Gaussian pulse is moved into the bulk,

[20]We have also examined the level of nonlinearity by comparing the pressure anisotropy resulting from a sum of two different Gaussians to the sum of anisotropies induced by the individual Gaussians. The results were comparable to those discussed above and do not warrant separate discussion.

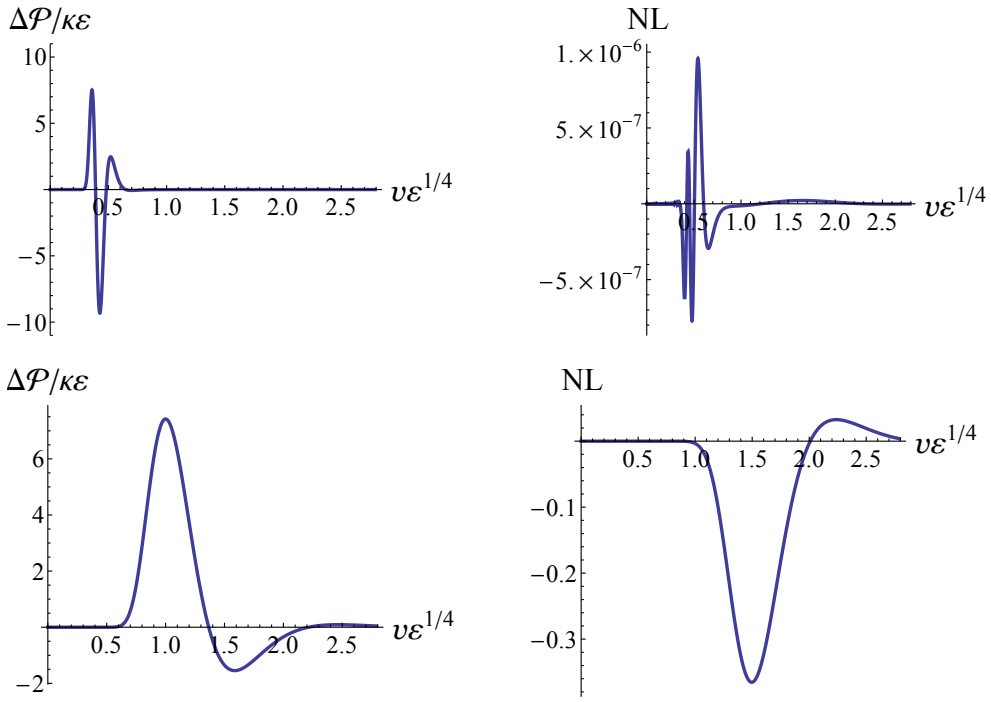

Figure 3.8: Top row: pressure anisotropy (left) and nonlinearity (right), defined as in fig. 3.6, as a function of time for the initial the pulse which created fig. 3.5. ($\mathcal{A} = 5 \times 10^{-4}$, $r_0 = 4$, $\sigma = \frac{1}{2}$). Bottom row: corresponding plots of pressure anisotropy and nonlinearity for a pulse located deeper in the bulk ($\mathcal{A} = 2.5$, $r_0 = \frac{1}{4}$, $\sigma = \frac{1}{2}$) with amplitude adjusted to produce a similar peak pressure anisotropy. In both cases the energy density is $\varepsilon = \frac{3}{4}L^{-4}$. Substantial nonlinearity is present for this case, where an initial pulse deep in the bulk has sufficient amplitude to produce a large departure from equilibrium.

an increasingly large portion of the Gaussian ends up lying behind the apparent horizon. And when plotted as a function of our computational coordinate $u = (\bar{r}-\lambda)^{-1}$ (with $\bar{r}$ the $\lambda = 0$ frame radial coordinate), initial pulses with small values of r_0 are only moderately localized near the horizon — even though these pulses had constant widths when viewed as functions of r. As may be seen by comparing the left and middle columns of fig. 3.7, it is the leading edge of the anisotropy pulse (the region of near-maximal slope) which produces the first large response in the boundary anisotropy. Looking at the last two rows of the figure, one may question whether we are doing an adequate job exploring the response from initial disturbances which are localized close to the horizon. Will initial pulses which are more strongly localized near the horizon show significantly greater nonlinearity?

Figures 3.9 and 3.10 show results of an effort to explore these questions. Fig. 3.9 shows the initial anisotropy function, along with the resulting pressure anisotropy and nonlinearity, for a significantly narrower "deep pulse" ($\mathcal{A} = \frac{1}{10}$, $r_0 = \frac{10}{11}$, $\sigma = \frac{1}{20}$). And fig. 3.10 shows a 3D plot of the time dependent anisotropy function, plus the induced pressure anisotropy, for an extremely narrow deep pulse ($\mathcal{A} = \frac{1}{10}$, $r_0 = 1$, $\sigma = \frac{1}{200}$).[21] The energy density in both cases remains fixed, $\varepsilon = \frac{3}{4}L^{-4}$. For the narrowest pulse, the amplitude $\mathcal{A} = \frac{1}{10}$ is near the upper limit which can be studied without destabilizing the horizon. In both figures 3.9 and 3.10, the peak pressure anisotropy $\Delta\mathcal{P}/\kappa\varepsilon$ is large compared to unity, showing that these pulses are producing far from equilibrium initial states.

As seen in these figures, pulses which are more sharply localized very near the horizon do lead to a delayed onset in the resulting pressure anisotropy, occurring at $v\varepsilon^{1/4} \approx 1.75$ for the case of fig. 3.9 and $v\varepsilon^{1/4} \approx 3$ for our narrowest pulse in fig. 3.10. But, within the range of pulse widths we have studied, the onset of the pressure anisotropy response is only delayed by a factor of 2–3 compared to the case of fig. 3.8. From the left panel of fig. 3.10, showing the time dependence of the (rescaled) anisotropy function B_s, one sees that the outward movement of the pulse toward the boundary resembles the behavior of

[21] This width is at the limit of what our numerics could do using a 240 point spectral grid.

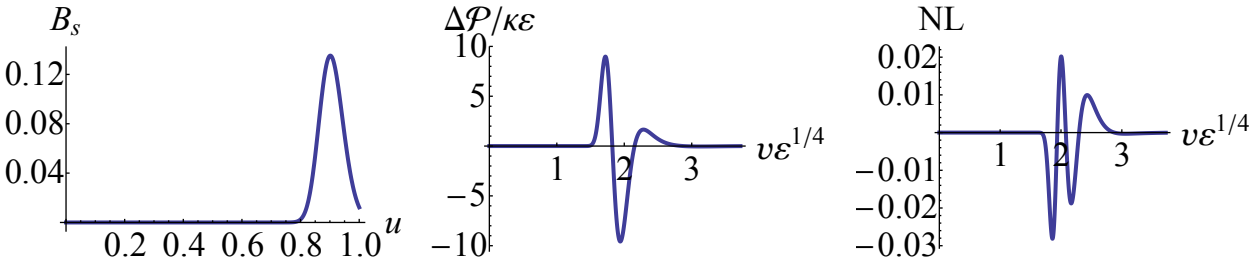

Figure 3.9: Initial anisotropy function (left), induced pressure anisotropy (middle), and nonlinearity (right) for a narrow "deep pulse" ($\mathcal{A} = \frac{1}{10}$, $r_0 = \frac{10}{11}$, $\sigma = \frac{1}{20}$) localized closer to the horizon than the deepest pulses of fig. 3.7. The energy density remains fixed at the same value, $\varepsilon = \frac{3}{4}L^{-4}$. Relative to the previous case of fig.3.8, the induced pressure response has a delayed onset, but is otherwise very similar.

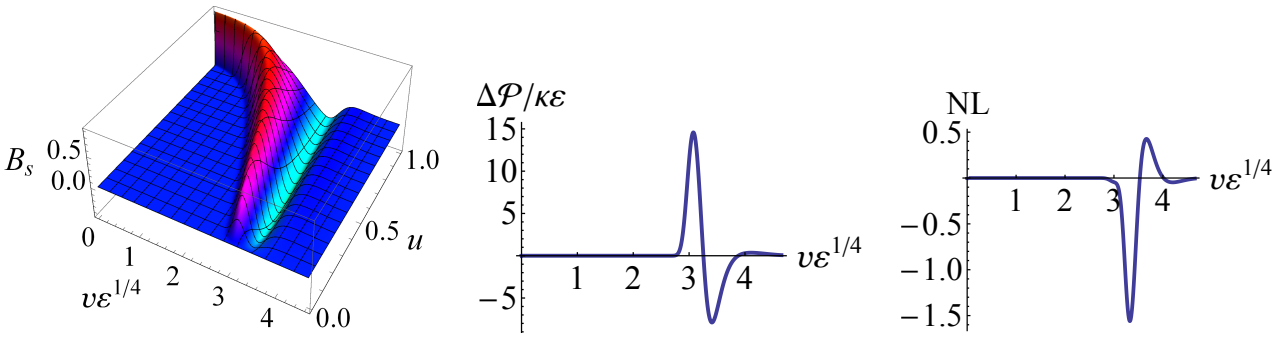

Figure 3.10: Rescaled anisotropy function B_s (left) as a function of inverted radius u and time v, for an extremely narrow pulse sitting at the horizon ($\mathcal{A} = \frac{1}{10}$, $r_0 = 1$, $\sigma = \frac{1}{200}$). Resulting pressure anisotropy (middle) and nonlinearity (right) as a function of time. Energy density $\varepsilon = \frac{3}{4}L^{-4}$. The outward movement of the pulse toward the boundary clearly resembles the behavior of outgoing null geodesics originating very close to an event horizon, which can "hug" the horizon for extended periods before eventually escaping.

outgoing null geodesics originating very close to an event horizon, which "hug" the horizon for extended periods before eventually escaping. One may wonder if the onset of the response in the pressure anisotropy could be delayed indefinitely by going to narrower and narrower initial pulses localized at the apparent horizon. We do not have a firm analytic argument, but doubt that this is possible if one simultaneously demands that the amplitude of the response remain bounded away from zero.[22]

The relative nonlinearity for the case of a narrow deep pulse shown in fig. 3.9 is quite small, about half a percent. But for the extremely narrow pulse with near maximal amplitude of fig. 3.10, the nonlinearity, relative to the pressure anisotropy, reaches the 10% level. Linearization of the dynamics about equilibrium must provide an accurate approximation to the full nonlinear dynamics when the deviation of the geometry from the equilibrium Schwarzschild black brane solution is sufficiently small, as will be true at sufficiently late times. For asymptotically anti-de Sitter geometries, where metric functions have the asymptotic forms (3.41), this will also be the case for initial data involving perturbations localized sufficiently close to the boundary. (See refs. [52, 53, 84] for related discussion.) It should be noted that reasonably good agreement between linearized dynamics and full nonlinear evolution was previously reported in ref. [52] and further explored in ref. [53]. In these works, the authors found agreement at a 20% level between the linearized and full dynamics for a variety of initial anisotropy profiles. Our results examining, more systematically, the dependence of the relative nonlinearity on the parameters of our initial Gaussian anisotropy function complement and extend this earlier work. Overall, despite prior knowledge of refs. [52, 53], we are still surprised by the small, often extremely small, levels of nonlinearity which we find even at early times when the induced pressure anisotropy is maximal, for initial perturbations localized deep in the bulk and producing large departures from equilibrium.

[22]This expectation reflects the diverging redshift of late emerging outgoing geodesics in the geometric optics picture, and is consistent with the gapped spectrum of quasinormal mode frequencies for translationally invariant perturbations.

3.4.2 Charged plasma

We now turn to the equilibration of charged plasmas (by which we mean SYM plasmas with a non-zero density of the global $U(1)$ conserved charge — not a plasma in which electromagnetic forces are included in the dynamics and Coulomb repulsion plays a significant role). As noted earlier in section 3.2.7, the bulk geometry should equilibrate to a non-singular Reissner-Nordstrom black brane solution provided the charge and energy densities satisfy the extremality bound (3.58), $\rho < \rho_{\rm max} = \frac{4}{3}\,\varepsilon^{3/4}$. However, for values of the charge density near $\rho_{\rm max}$, we find that sufficiently large initial metric perturbations can destroy the apparent horizon. We expect that such initial data are unphysical, not representing SYM initial states which could be produced by an operational procedure such as turning on time dependent external fields (which correspond to time dependent boundary data in the holographic description). In any case, we limit our attention to initial perturbations for which an apparent horizon is present at all times. We find that if one suitably decreases the amplitude of the initial departure from equilibrium while increasing the charge density, one can approach $\rho_{\rm max}$ from below while maintaining the existence of an apparent horizon.

Figure 3.11 (left) compares the time dependence of the pressure anisotropy which results from initial data consisting of precisely the same Gaussian initial anisotropy function $B(v_0, r)$ (in the $\lambda = 0$ frame) and energy density as in fig. 3.5, and a charge density ρ equal to 0, 20, 40, 60, or 80% of the extremal density $\rho_{\rm max}$. The immediately obvious qualitative result is that the five different curves are so close together than they cannot be visually distinguished! Varying the charge density (at fixed energy density and fixed initial anisotropy function) has stunningly little impact on the subsequent time evolution. This is quantified in the right panel of fig. 3.11 which plots the difference in the pressure anisotropy $\Delta\mathcal{P}/\kappa\varepsilon$ between the cases of $\rho = 0.8\,\rho_{\rm max}$ and $\rho = 0$. Comparing the scales on the right and left hand plots, one sees that for this initial anisotropy function the sensitivity to the charge density is less than one part in 10^4.

In the plots of fig. 3.11, we used the fourth root of the (rescaled) energy density, $\varepsilon^{1/4}$,

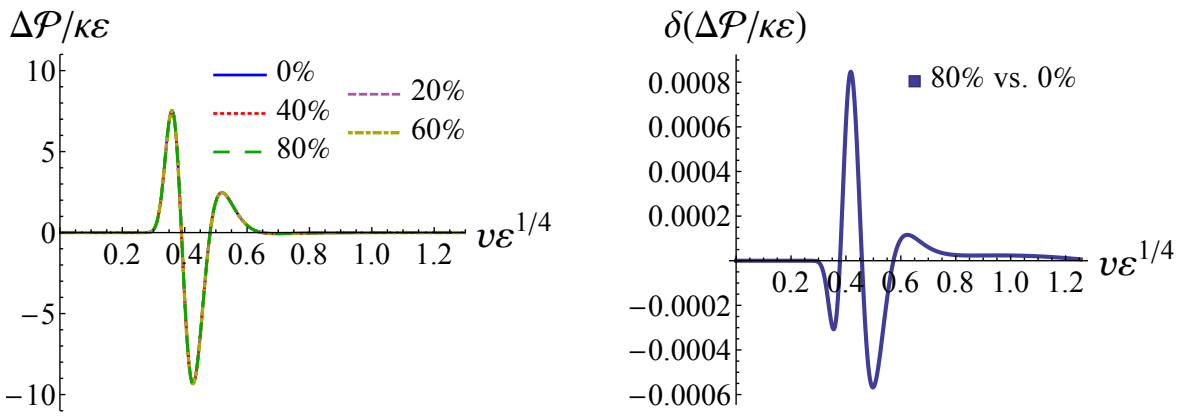

Figure 3.11: Left: time dependence of the pressure anisotropy (relative to $\kappa\varepsilon$) for values of the charge density ρ which are 0, 20, 40, 60, or 80% of the extremal density $\rho_{\max}$. The different curves are virtually indistinguishable. The initial anisotropy function $B(v_0, r)$ and energy density ε are the same as in fig. 3.5. Right: difference in $\Delta\mathcal{P}/\kappa\varepsilon$ between $\rho = 0.8\,\rho_{\max}$ and $\rho = 0$.

to set the scale for time. Since the energy density was held constant in the comparisons of fig. 3.11, this was a simple and convenient choice. For the five cases shown in the figure, $\varepsilon/(\pi T)^4 = 0.75$, 0.76 , 0.79, 0.86, and 1.03 for $\rho = 0$, 20, 40, 60 and 80% of $\rho_{\max}$, respectively. And, for comparison, the values of the equilibrium chemical potentials corresponding to these charge densities are given by $\mu/T = 0$, 0.34, 0.73, 1.26, and 2.21, respectively.

If the initial anisotropy pulse begins deeper in the bulk, then the sensitivity to the charge density is larger. Figure 3.12 shows a comparison of pressure anisotropies for differing charge densities, now using the deep pulse initial anisotropy function whose radial profile has the shape shown in fig. 3.9.[23] As seen on the left panel, the amplitude of the response increases significantly as the charge density varies from 0 to 80% of $\rho_{\max}$. However, the time course of the equilibration (e.g., the times of the first or second peaks in the response, or the zero-crossing between these peaks) is only modestly affected, with changes of 3% percent or

[23]One might guess that the pulse used in the bottom row of fig. 3.8 would exhibit greater sensitivity to charge since it had a larger nonlinearity than the deep pulse of fig. 3.9. However, the latter pulse exhibits much greater sensitivity to charge.

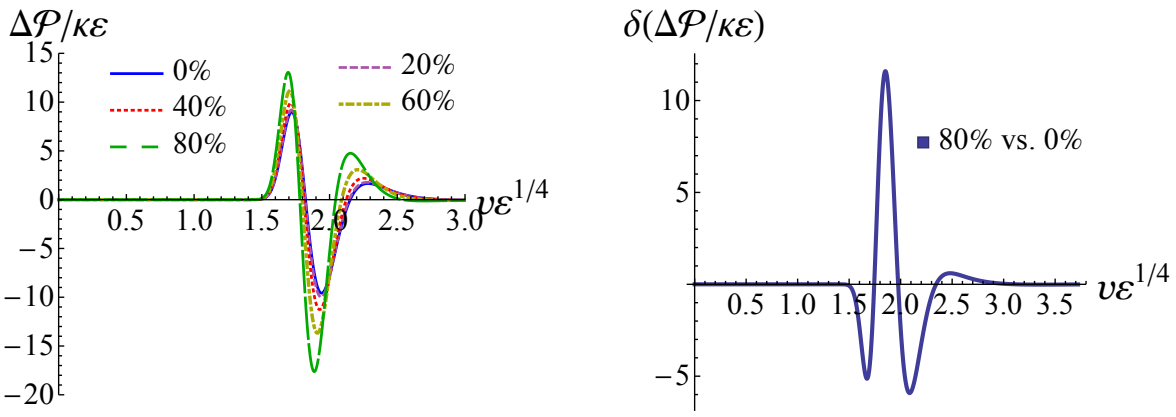

Figure 3.12: Left: comparison of pressure anisotropies produced by different charge densities, up to 80% of extremality, when the initial anisotropy function is a "deep pulse" ($\mathcal{A} = \frac{1}{10}$, $r_0 = \frac{10}{11}$, $\sigma = \frac{1}{20}$) with $\varepsilon = \frac{3}{4}\, L^{-4}$. Although the amplitude of the response grows, as shown, with increasing charge density, it is striking how little the time course of the response varies. Right: difference in pressure anisotropy $\Delta\mathcal{P}/\kappa\varepsilon$ between $\rho = 0.8\,\rho_{\rm max}$ and $\rho = 0$.

less.

The fact that the sensitivity to the charge density is greatest for pulses close to the horizon is to be expected. In the equilibrium geometry (3.57), one sees that as the radius $\widetilde{r}$ increases from the horizon, the influence of the charge density decreases rapidly relative to the other terms in the metric. Only near the horizon, and close to extremality, does the charge density produce an $O(1)$ effect on the equilibrium geometry.

At the beginning of this work, we expected that one interesting outcome would be information on the change in equilibration time produced by varying the plasma charge density. By "equilibration time", we mean some rough but useful measure of when the departure from equilibrium is no longer substantial. To make this a bit more quantitative we adopt, somewhat arbitrarily, the criterion

$$\Delta\mathcal{P}(t)/\kappa\varepsilon \leq 0.1\,, \tag{3.78}$$

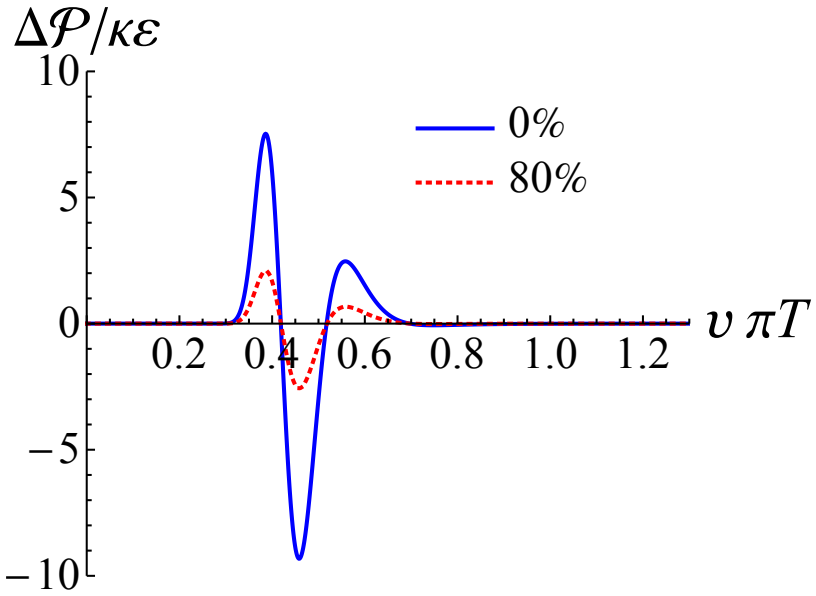

Figure 3.13: Comparison of the pressure anisotropies produced by two different charge densities, 0% and 80% of extremality, when holding fixed the equilibrium temperature, $\pi T = 1/L$. The energy densities are 0.75 and 2.68, respectively. The initial anisotropy function is same as in fig. 3.5 ($\mathcal{A} = 5 \times 10^{-4}$, $r_0 = 4$, $\sigma = \frac{1}{2}$). With time is plotted in units of inverse temperature, the relaxation time course shows negligible sensitivity to the charge density (although the amplitude of the response varies significantly).

for all times $t > t_{\rm eq}$, as indicating that the system is near equilibrium at time $t_{\rm eq}$.

Looking at the left panels of figures 3.11 and 3.12, it is clear that the effect of the charge density on any reasonable measure of equilibration time can be summarized easily: there is very little effect! Even in fig. 3.12, where the sensitivity to charge density is the largest we have found with horizon-preserving initial data,[24] the time $t_{\rm peak}$ of the initial response peak and the approximate equilibration time $t_{\rm eq}$ both vary by less than 5%.

Since figures 3.11 and 3.12 plot time in units set by the energy density, the high degree of insensitivity of the relaxation time course to the charge density seen in these figures might

[24]Achieving good numerical accuracy becomes increasingly difficult as one pushes toward extremality, where the equilibrium solution bifurcates. Investigating very near extremal behavior more carefully is an interesting topic we leave to future work.

lead one to think that the total energy density is playing a special role in setting the time scale of relaxation. But it should be borne in mind that these figures show comparisons in which, by design, both the initial anisotropy function (in the $\lambda = 0$ frame) *and* the total energy density have been held fixed. Because the ratio of energy density to temperature (to the fourth power) varies significantly with increasing charge density, it is natural to ask whether the degree of (in)sensitivity of the relaxation dynamics to the charge density is substantially different if one holds fixed the equilibrium temperature instead of the energy density. Figure 3.13 shows such a comparison. Plotted are the pressure anisotropies resulting from the same initial anisotropy function used in figs. 3.5 and 3.11, and charge densities of either 0 or 80% of extremality, but now with the energy density in either case suitably adjusted to fix the equilibrium temperature, $\pi T = 1/L$. One again sees a significant change in the amplitude of the response with increasing charge density, but now with the temperature held fixed, increasing charge density decreases the amplitude of the response. Nevertheless, with time now plotted in units of $(\pi T)^{-1}$, one again sees negligible ($\approx 0.01\%$) change in the time course of the equilibration dynamics as the charge density varies from zero and 80% of $\rho_{\max}$.

Performing the same constant temperature response comparison using the deep pulse initial anisotropy function (whose radial profile is shown in fig. 3.9), we find a larger — but still quite small — variation in the time course, approximately 2%, as the charge density varies from zero to 80% of $\rho_{\max}$.

We have also examined the degree of nonlinearity in the above examples of equilibrating charged plasmas. The results for the relative size of the nonlinearity are quite similar to our earlier results for equilibrating uncharged plasmas. Because of this, we will refrain from presenting explicit nonlinearity plots for charged plasmas.

Finally, as noted earlier, at sufficiently late times the relaxation must be accurately described by a superposition of quasinormal modes (eigenfunctions of the linearized dynamics about the equilibrium solution). Extracting the leading quasinormal mode frequency by fitting the late time ($4 \lesssim v\varepsilon^{1/4} \lesssim 20$) behavior of our calculated pressure anisotropy to

Charged ($\rho \neq 0$, $\mathcal{B} = 0$)				
$\rho/\rho_{\max}$	$\mathrm{Re}\,\lambda/\varepsilon^{1/4}$	$\mathrm{Im}\,\lambda/\varepsilon^{1/4}$	$\lambda/\pi T$	Linearized $\lambda/\varepsilon^{1/4}$
0.0	3.35208 ± 0.00004	-2.95144 ± 0.00013	$3.11946 - 2.74663\,i$	$3.35207 - 2.95150\,i$
0.1	3.34564 ± 0.00016	-2.95468 ± 0.00019	$3.11948 - 2.75763\,i$	$3.34568 - 2.95460\,i$
0.2	3.32624 ± 0.00020	-2.96429 ± 0.00019	$3.13222 - 2.79139\,i$	$3.32630 - 2.96444\,i$
0.3	3.29319 ± 0.00028	-2.98266 ± 0.00036	$3.14987 - 2.85285\,i$	$3.29327 - 2.98287\,i$
0.4	3.24572 ± 0.00007	-3.01376 ± 0.00008	$3.17857 - 2.95141\,i$	$3.24574 - 3.01377\,i$
0.5	3.18366 ± 0.00016	-3.06498 ± 0.00007	$3.22529 - 3.10506\,i$	$3.18370 - 3.06491\,i$
0.6	3.11311 ± 0.00002	-3.15177 ± 0.00002	$3.31032 - 3.35142\,i$	$3.11311 - 3.15176\,i$
0.7	3.07021 ± 0.00006	-3.29402 ± 0.00006	$3.50617 - 3.76176\,i$	$3.07022 - 3.29399\,i$
0.8	3.11863 ± 0.00265	-3.41376 ± 0.00295	$3.99199 - 4.36977\,i$	$3.11848 - 3.42004\,i$

Table 3.1: Lowest quasinormal mode frequency for charge densities ranging from 0 up to 80% of extremality. The second and third columns show results (with estimated uncertainties) for the real and imaginary part of the QNM frequency in units of $\varepsilon^{1/4}$, obtained from fitting the late time behavior of our full nonlinear evolution. The fourth column shows these same results converted to units of πT. (Fractional uncertainties are the same as in the preceding columns.) The rightmost column shows results from an independent analysis of the linearized small fluctuation equations by Janiszewski and Kaminski [85].

a decaying, oscillating exponential, as described in the previous section, yields the results shown in table 3.1. The second and third columns (with uncertainties) show our estimates for the real and imaginary parts of the leading QNM frequency in units of $\varepsilon^{1/4}$, while the fourth column (without uncertainties) shows our estimates converted to units of πT. The rightmost column shows independent results of Janiszewski and Kaminski [85] obtained by analyzing the linearized small fluctuation equations about the RN black brane solution. The agreement is a satisfying confirmation of our numerical accuracy. Interestingly, the imaginary part of the lowest QNM frequency varies by over 15% between $\rho = 0$ and $\rho = 0.8\,\rho_{\max}$. This is enormously larger than the part in 10^4 sensitivity seen in fig. 3.11, and substantially bigger than the largest ($\approx 5\%$) sensitivity we found in the evolution time course with deep pulses, fig. 3.12. The implications of these very differing sensitivities will be discussed further in section 4.7.

3.4.3 Magnetized plasma

We now present results of an analogous investigation of equilibration in plasmas (with vanishing charge density) in a homogeneous magnetic field $\mathcal{B}$. Our discussion will parallel, as much as possible, the previous treatment of charged plasmas. But the breaking of scale invariance by the magnetic field, discussed in section 3.2.1, produces some notable differences. One change, seen in section 3.2.4, is that the anisotropy function $B(v, r)$ must now contain logarithmic terms in its near boundary behavior. We choose our initial anisotropy function to have the form (3.76) in which an adjustable Gaussian is added to the required leading logarithmic term. As in the previous discussion of charged plasmas, we will keep fixed the parameters of the Gaussian part of the initial anisotropy function $B(v_0, r)$ as we dial up the external magnetic field. We will also hold fixed the energy density ε_L defined at a renormalization point $\mu = 1/L$. As shown by the holographic relation (3.42), this is the same as holding fixed the asymptotic coefficient a_4. In the following plots, axis labels involving energy density ε, without any explicit indication of scale, will denote the energy density evaluated at the curvature scale, $\varepsilon(1/L) = \varepsilon_L$. Similarly, the pressure anisotropy $\Delta\mathcal{P}$

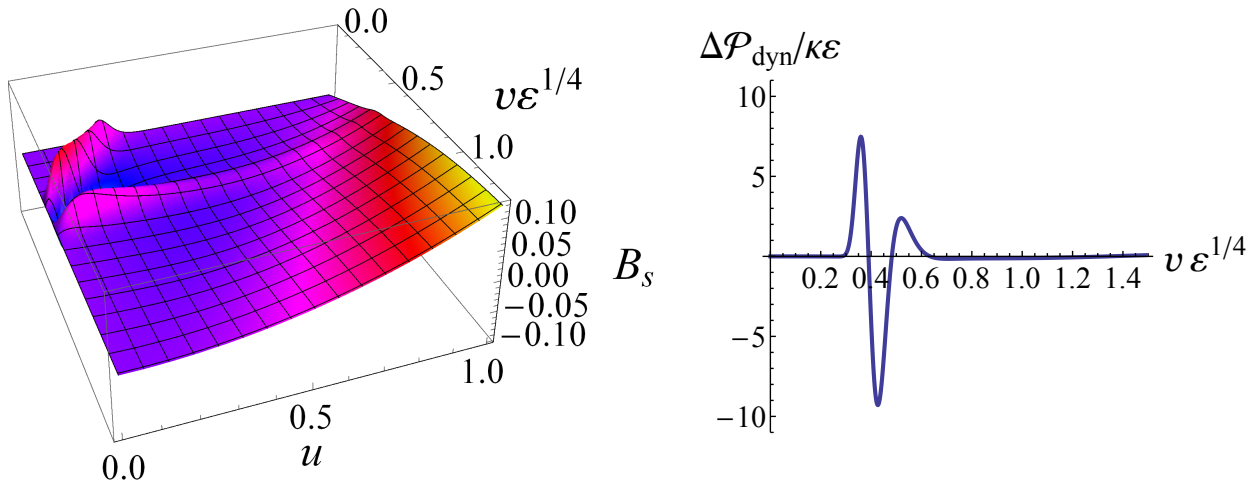

Figure 3.14: Left: The subtracted/rescaled anisotropy function, $B_s(v,u)$, as a function of time v (in units of $\varepsilon_L^{-1/4}$) and inverse radial depth u, for the case of $\mathcal{B}L^2 = 1.0$, with initial Gaussian parameters chosen to match the initial pulse which generated fig. 3.5 ($\mathcal{A} = 5\times 10^{-4}$, $r_0 = 4$, $\sigma = \frac{1}{2}$), and energy density $\varepsilon_L = \frac{3}{4}L^{-4}$. At late times the anisotropy function approaches the non-trivial profile of the equilibrium magnetic brane solution discussed in section 3.2.7. Right: Corresponding evolution of the dynamical contribution to the relative pressure anisotropy , $\Delta\mathcal{P}_{\rm dyn}/\kappa\varepsilon_L$, with both $\Delta\mathcal{P}$ and ε_L evaluated at the scale $1/L$. The late time limit of the pressure anisotropy is non-zero, but too small to be easily visible, $\lim_{v\to\infty}\Delta\mathcal{P}_{\rm dyn}(1/L)/\kappa\varepsilon_L = 0.22$.

should be understood as $\Delta\mathcal{P}(1/L)$ unless otherwise indicated explicitly.

Instead of keeping ε_L fixed as the magnetic field $\mathcal{B}$ is varied, one could choose to hold fixed the energy density $\varepsilon_{\mathcal{B}}$ defined at the scale set by the magnetic field, $\mu = |\mathcal{B}|^{1/2}$. Since the AdS curvature radius L is not a physical scale present in the dual QFT, fixing $\varepsilon_{\mathcal{B}}$ instead of ε_L is arguably more natural. However, for computational reasons it is easier to hold fixed ε_L as the magnetic field is increased. The issue is that accurate numerical calculations become progressively more difficult the deeper one penetrates into the high-field/low-temperature regime, $T^2/|\mathcal{B}| \ll 1$. (This is analogous to the difficulty of approaching extremality in the charged case, where the horizon temperature also vanishes.) By holding fixed ε_L instead of $\varepsilon_{\mathcal{B}}$, we are able to perform scans in $\mathcal{B}$ which avoid dipping too deeply into the very low

temperature region.

Another difference concerns the definition of pressure (or stress) anisotropy. With our choice (3.27) for fixing the scheme dependent ambiguity in the stress-energy tensor, the resulting holographic relation (3.42), when evaluated at $\mu = 1/L$, puts the trace anomaly solely in the transverse components of the stress, T^{11} and T^{22}. So the pressure anisotropy (3.77), defined as the difference between transverse and longitudinal stress, when evaluated at $\mu = 1/L$ has a "kinematic" contribution of $-\frac{1}{4}\kappa\mathcal{B}^2$ plus a "dynamic" contribution of $3\kappa\, b_4(v)$. In presenting results below, we will omit the uninteresting static kinematic contribution, and just plot the dynamic contribution

$$\Delta\mathcal{P}_{\rm dyn} \equiv \tfrac{1}{2}(T^{11} + T^{22}) - T^{33} + \tfrac{1}{4}\kappa\,\mathcal{B}^2\,, \tag{3.79}$$

(relative to the energy density), evaluated at the renormalization point $\mu = 1/L$.[25]

A further difference comes from the fact that equilibrium magnetic brane solutions are intrinsically anisotropic. The anisotropy function B does not vanish at late times, but rather settles down to the profile of the equilibrium magnetic brane solution discussed in section 3.2.7. This is illustrated in figure 3.14, which shows the (subtracted/rescaled) anisotropy function B_s as a function of time v and inverse radial depth u. One sees similar features as in fig. 3.5: the initial pulse propagates outward, reflects off the boundary, and largely disappears into the horizon. But in addition one also sees that the anisotropy function is approaching the non-trivial profile of a static magnetic brane solution.

Correspondingly, the pressure anisotropy in the dual field theory asymptotically approaches a non-zero constant. To examine equilibration, it is the difference between the pressure anisotropy and its asymptotic value which is of interest. As a measure of (near)

[25]Examining the holographic relation (3.42), one sees that simply shifting the renormalization point to $\mu = e^{1/4}/L$ would accomplish the same removal of this uninteresting kinematic contribution to the pressure anisotropy.

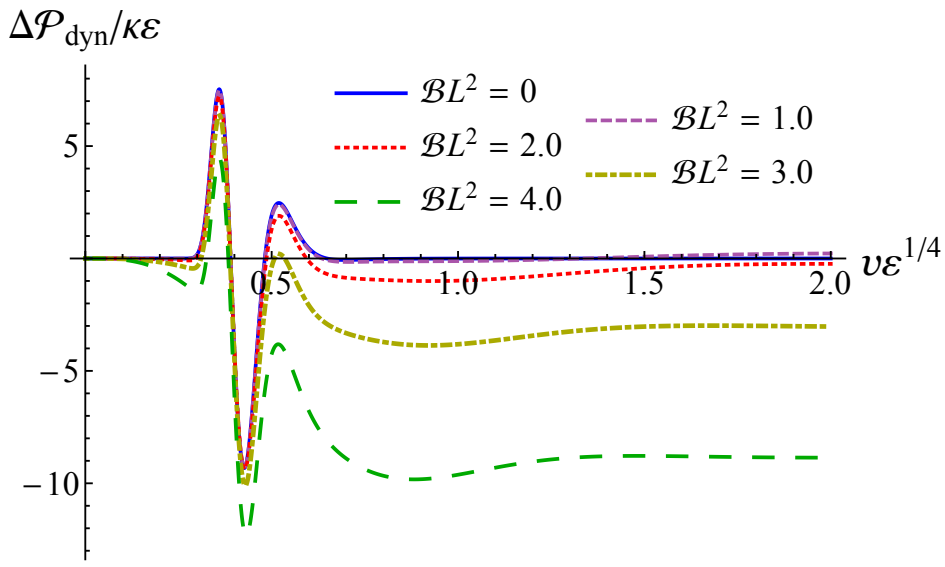

Figure 3.15: Time dependence (in units of $\varepsilon_L^{-1/4}$) of the dynamical pressure anisotropy, at the scale of $1/L$, for values of background magnetic field ranging from 0 to $4/L^2$. The energy density (at the curvature scale) is held fixed, $\varepsilon_L = \frac{3}{4}L^{-4}$, and the parameters of the initial Gaussian pulse in the anisotropy are the same as in fig. 3.14.

equilibration, the condition (3.78) is naturally replaced by

$$\left[\Delta\mathcal{P}(t) - \Delta\mathcal{P}(\infty)\right]/(\kappa\varepsilon_L) \leq 0.1\,, \tag{3.80}$$

for all times $t > t_{\rm eq}$.

The time dependence of the resulting (dynamical contribution to the) pressure anisotropy is shown in fig. 3.15 for a series of magnetic fields, $\mathcal{B}L^2 = 0$, 1, 2, 3, and 4. The energy density is held fixed at $\varepsilon_L = \frac{3}{4}L^{-4}$ and the parameters of the Gaussian pulse in the initial anisotropy function are those of the pulse which generated fig. 3.5 ($\mathcal{A} = 5\times10^{-4}$, $r_0 = 4$, $\sigma = \frac{1}{2}$). For the five cases shown, the ratios of magnetic field to the equilibrium temperature (squared) are given by $\mathcal{B}/T^2 = 0$, 13.0, 30.2, 30.5, and 26.3 for $\mathcal{B}L^2 = 0$, 1, 2, 3 and 4, respectively. Note that, at this fixed value of $\varepsilon_L L^4$, $\mathcal{B}/T^2$ is not monotonic as a function of $\mathcal{B}L^2$. The energy densities at the intrinsic scale set by the magnetic field for this series of solutions are

given by $\varepsilon_{\mathcal{B}}/\mathcal{B}^2 = \infty$, 0.75, 0.36, 0.36, and 0.39, respectively.

Differences in the late time values of the pressure anisotropy are obvious in fig. 3.15.[26] Small temporal variations are also evident after $v \approx 1.3$. These are produced by the relaxation of the initial non-Gaussian background profile of the anisotropy function to the correct equilibrium form. These small variations at relatively late times would be absent if we had constructed our initial anisotropy function by adding a Gaussian perturbation to the equilibrium solution (instead of merely adding a Gaussian to the leading asymptotic term). Given our choice of initial data, there are two distinct time scales in the equilibration shown in figs. 3.14 and 3.15, the first associated with the boundary reflection and subsequent infall of the Gaussian pulse, and the second with the time it takes for the background anisotropy profile to reach its equilibrium form. It is the latter which is responsible for the late time variations; fortunately, there is relatively little ambiguity in separating the two contributions to the dynamics.

Once again, a notable feature of in the comparison of fig. 3.15 is the similarity in the time dependence of the pressure anisotropy during the pulse-driven period of significant departure from equilibrium ($0.2 \lesssim v\varepsilon_L^{1/4} \lesssim 1.0$), when the initial perturbation is reflecting from the boundary. Any reasonably defined measure of equilibration time $t_{\rm eq}$ clearly does not vary much with magnetic field, and neither does $t_{\rm peak}$ for these relatively near boundary pulses. This insensitivity result relies, of course, on the constancy of the initial Gaussian perturbation in the anisotropy function, and also on our choice to hold fixed the energy density at the scale $1/L$.

Fig. 3.16 compares the response, for different values of magnetic field, when one holds fixed the equilibrium temperature T (as well as the initial Gaussian perturbation), instead of fixing the energy density ε_L. With time now plotted in units of $(\pi T)^{-1}$, one also sees remarkable similarity in the time dependence of the response, with the times of the first,

[26]The tiny positive late time pressure anisotropy barely visible in the $\mathcal{B}L^2 = 1$ curve is a consequence of our removal of the static kinematic part of the anisotropy; the final value of the total pressure anisotropy, at the scale $1/L$, monotonically decreases with increasing $\mathcal{B}L^2$ in this series of solutions.

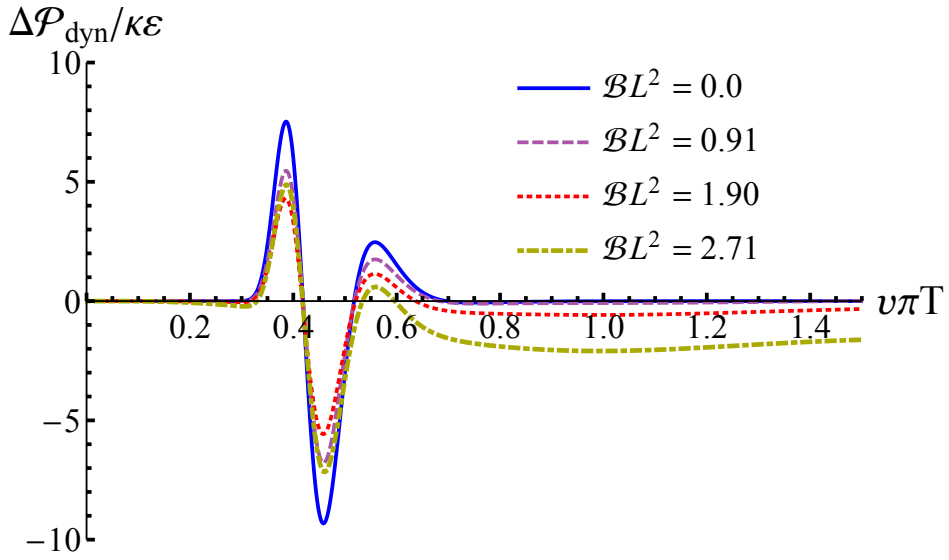

Figure 3.16: Time dependence (in units of $(\pi T)^{-1}$) of the dynamical pressure anisotropy for values of background magnetic field ranging from 0 to $2.71/L^2$. The temperature is held fixed, $\pi TL = 1$, and the parameters of the initial Gaussian pulse in the anisotropy are the same as in fig. 3.14. The values of $\varepsilon_{\mathcal{B}}/\mathcal{B}^2$ for these solutions, in order of increasing field, are ∞, 1.2, 0.51, and 0.39, respectively. One sees very little sensitivity to the magnetic field in the time course of the response.

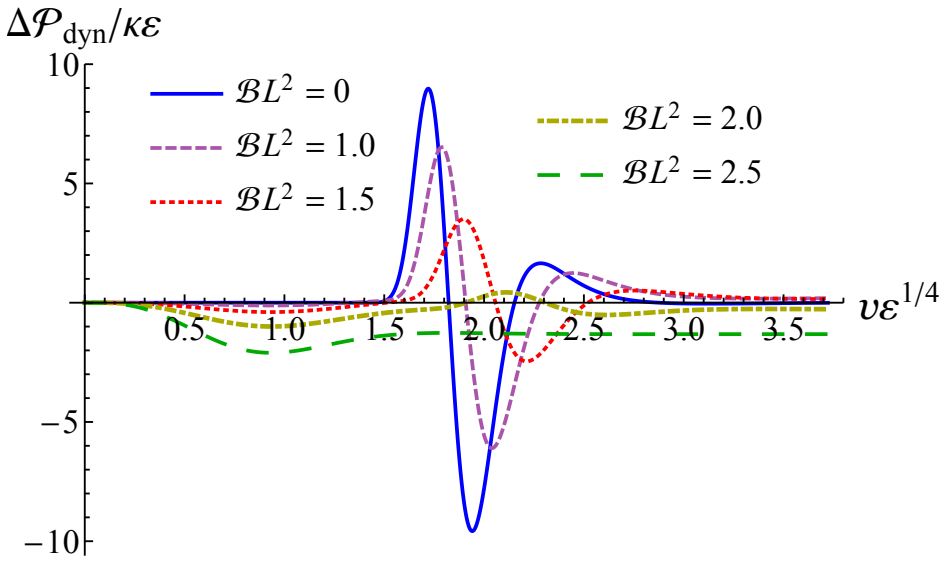

Figure 3.17: Time dependence (in units of $\varepsilon_L^{-1/4}$) of the relative pressure anisotropy for values of background magnetic field ranging from 0 to $2.5/L^2$, for the same deep pulse ($\mathcal{A} = \frac{1}{10}$, $r_0 = \frac{10}{11}$, $\sigma = \frac{1}{20}$) used in fig. 3.9 and fig. 3.12. The energy density $\varepsilon_L = \frac{3}{4}L^{-4}$ is held fixed.

second, or third peaks in the pressure anisotropy varying by less than 0.3% as $\mathcal{B}/T^2$ varies from 0 to 26.7.

Sensitivity to the magnetic field is significantly larger when the initial pulse is placed very close to the horizon. This is shown in fig. 3.17, which plots the time dependence of the dynamical pressure anisotropy for magnetic field values $\mathcal{B}L^2 = 0$, 1, 1.5, 2, and 2.5, using the same "deep pulse" Gaussian parameters ($\mathcal{A} = \frac{1}{10}$, $r_0 = \frac{10}{11}$, $\sigma = \frac{1}{20}$), and fixed energy density $\varepsilon_L = \frac{3}{4}\,L^{-4}$, which generated fig. 3.9. For this series of solutions we have $|\mathcal{B}|/T^2 = 0$, 13.0, 22.85, 30.16, and 31.95, and $\varepsilon_{\mathcal{B}}/\mathcal{B}^2 = \infty$, 0.75, 0.43, 0.36, and 0.35, respectively.

With this deep initial pulse, differences in the time course of the response are much more pronounced. Larger magnetic fields greatly suppress the size of the pulse-driven peaks in the pressure anisotropy (for a fixed amplitude of the initial Gaussian), and lead to increasingly large and negative final values for the anisotropy. For the lowest curve with $\mathcal{B}L^2 = 2.5$, the contribution of the Gaussian pulse is completely swamped by the contribution from the

Magnetic ($\mathcal{B} \neq 0$, $\rho = 0$)						
$\mathcal{B}/T^2$	$\varepsilon_{\mathcal{B}}/T^4$	$\overline{\mathcal{P}}/\kappa T^4$	$\Delta\mathcal{P}/\kappa T^4$	$\mathrm{Re}\,\lambda/\varepsilon_{\mathcal{B}}^{1/4}$	$\mathrm{Im}\,\lambda/\varepsilon_{\mathcal{B}}^{1/4}$	$\lambda/(\pi T)$
0	73.06	24.35	0	3.3521 ± 0.0001	-2.9514 ± 0.0001	$3.1195 - 2.7466\,i$
0.990	72.98	24.16	−1.13	3.357 ± 0.001	-2.93 ± 0.06	$3.124 - 2.73\,i$
5.344	80.74	22.15	−10.60	3.372 ± 0.002	-2.92 ± 0.06	$3.217 - 2.79\,i$
12.953	125.85	13.98	−15.76	3.264 ± 0.007	-2.78 ± 0.01	$3.480 - 2.96\,i$
17.821	170.16	3.79	−9.36	3.161 ± 0.002	-2.69 ± 0.04	$3.634 - 3.09\,i$
22.836	226.69	−11.35	5.00	3.061 ± 0.008	-2.60 ± 0.03	$3.780 - 3.21\,i$
30.161	328.21	−42.21	39.97	2.94 ± 0.01	-2.49 ± 0.03	$3.98 - 3.38\,i$

Table 3.2: Equilibrium energy density, average pressure, and pressure anisotropy, plus lowest quasinormal mode frequency, for various values of the external magnetic field. Reported values of energy densities and pressures are evaluated at a renormalization point $\mu = |\mathcal{B}|^{1/2}$, not at the (physically irrelevant) curvature scale. The pressure anisotropy is the complete value, including the $-\frac{1}{4}\mathcal{B}^2$ kinematic contribution which was removed in figs. 3.15 – 3.17. Results for the lowest quasinormal mode frequency are reported both in units of $\varepsilon_{\mathcal{B}}^{1/4}$ (middle column, with uncertainties), and as well as in units of πT (final column).

relaxation of the background profile of the anisotropy function to the correct equilibrium form. Excluding this curve, the time t_{peak} of the first peak, as well the rough equilibration time t_{eq}, characterizing the portion of the evolution arising from the Gaussian pulse, vary at most by 20% as the magnetic field ranges from 0 to $2/L^2$. This is the largest difference in the relaxation time course we have seen in our exploration of magnetized plasmas with Gaussian initial perturbations.

A constant temperature comparison (not plotted), analogous to fig. 3.16 but using the same deep pulse as in figs. 3.9 and 3.17, shows variations in the time course of up to 15% as $|\mathcal{B}|/T^2$ ranges from 0 to 22 — beyond which the response of the pulse cannot be clearly distinguished from the background evolution.

To conclude this section, we report in table 3.2 equilibrium properties, plus our estimates for the lowest quasinormal mode frequency, for values of magnetic field which extend from

small fields well into the strong field regime. The ratio $\mathcal{B}/T^2$ ranges from zero to just over 30. The equilibrium energy density, pressure, and pressure anisotropy are given in units of T^4, and have been converted from the $\mu = 1/L$ renormalization point used in our calculations (and above presentation) to the intrinsic scale $\mu = |\mathcal{B}|^{1/2}$. Results for the lowest quasinormal mode frequency are given both in units of $\varepsilon_{\mathcal{B}}^{1/4}$ and in units of πT. These estimates are the result of fitting the late time ($4 \lesssim v\, \varepsilon_L^{1/4} \lesssim 9$) behavior of the pressure anisotropy to a decaying, oscillating exponential plus a constant equilibrium offset. To our knowledge, independent results from a linearized analysis of small fluctuations about the (numerically determined) magnetic brane solutions are not currently available. The leading quasinormal mode frequency varies by about 20% as $\mathcal{B}/T^2$ ranges from zero up to 30, monotonically increasing with increasing field when measured in units of πT, but slightly increasing and then decreasing when measured in units of $\varepsilon_{\mathcal{B}}^{1/4}$.

3.5 Discussion

The above results show that to a good (often extremely good) level of accuracy:

1. the pressure anisotropy response is a linear functional of the initial anisotropy pulse profile;

2. the time course of the response, measured in units set by the energy density,[27] is insensitive to the charge density or background magnetic field when the pulse profile and the energy density are held fixed;

3. the time course of the response, measured in units set by the equilibrium temperature, is insensitive to the charge density or background magnetic field when the pulse profile and equilibrium temperature are held fixed.

How can one synthesize these observations? Consider some feature in the time course of the response, such as the time of the first (or second) peak in the pressure anisotropy, or

[27] Specifically, ε_L in the magnetic case.

the approximate equilibration time discussed above. For simplicity, we will focus on the time $t_{\rm peak}$ of the first pressure anisotropy peak. This time must be some function of the equilibrium state parameters (energy density plus charge density or magnetic field), as well as the Gaussian pulse parameters (depth, width, and amplitude).

Consider first the charged case. The response time $t_{\rm peak}$ is a function of the energy density ε, the fraction x of the extremal charge density, and the Gaussian pulse parameters r_0, σ, and $\mathcal{A}$. But since the temperature decreases monotonically with increasing charge density (for fixed energy density) one may equally well regard the equilibrium state as labeled by the energy density ε and temperature T, and write

$$t_{\rm peak}/L = f(\varepsilon L^4, TL, r_0/L, \sigma/L, \mathcal{A})\,, \tag{3.81}$$

for some function f of the indicated arguments. We have written all quantities in dimensionless form using, in effect, our computational units. Our results on the degree of nonlinearity imply that the function f is nearly independent of the last argument, the Gaussian amplitude $\mathcal{A}$. Only for our narrowest pulse, located right at the horizon, did the relative nonlinearity reach 10%. Away from this corner of parameter space, the nonlinearity was substantially smaller, rapidly falling to much less than a percent as the initial pulse becomes less localized at the horizon. So, to a good approximation, one can regard the function f as being independent of $\mathcal{A}$.

For narrow pulses, $\sigma \ll r_0$, the dependence of the response time $t_{\rm peak}$ on the pulse width is negligible; there is a smooth $\sigma \to 0$ limit. To the extent that linearity is a good approximation, one may regard the response from wider pulses as superpositions of the response from narrower pulses (suitably arranged so that their sum reconstructs the wider pulse). As noted in the discussion of fig. 3.7, the first peak in the response is clearly associated with the propagation of the leading edge of the anisotropy pulse — the region of near-maximal slope on the side of the pulse closest to the boundary. Therefore, for pulses of non-negligible width σ centered at some depth r_0, one should expect that the time of the first peak in the

response will be most similar to the corresponding response time for a narrower pulse located not at the depth r_0, but rather at a depth of $r_0 + n\sigma$ for some positive $O(1)$ multiplier n. At the same level of accuracy determined by the degree of nonlinearity, one should be able to merge the dependence of the response time $t_{\rm peak}$ on the depth r_0 and width σ of the initial pulse into a single effective depth $r_{\rm eff}$ given by $r_0 + n\sigma$. (The accuracy of this simplification will be discussed below.) Hence, the above functional dependence for $t_{\rm peak}$ can be replaced by a simpler form,

$$t_{\rm peak}/L \approx g(\varepsilon L^4, TL, r_{\rm eff}/L)\,, \tag{3.82}$$

for some function g. Now, the results of section 3.4.2 (including figs. 3.11 and 3.12 and associated discussion) show that the time course of the pressure anisotropy response has remarkably little dependence on the charge density when comparisons are made holding fixed the initial pulse parameters and the energy density. Since varying the charge density at fixed energy density is, as noted above, equivalent to varying the equilibrium temperature, this implies that the function g describing the response time (3.82) is nearly independent of the second argument, TL. At the same time, the comparisons at fixed temperature also discussed in section 3.4.2 (fig. 3.13 and associated discussion) show that the time course of the pressure anisotropy response *also* has remarkably little dependence on the charge density when the initial pulse parameters and the equilibrium temperature are held fixed. This implies that the function g describing the response time (3.82) is nearly independent of the first argument, εL^4. Hence, at a level of accuracy determined by the minimal level of nonlinearity, and the minimal dependence on charge density in comparisons at both constant energy density and constant temperature, the response time $t_{\rm peak}$ must be a function of *only* the effective depth of the initial pulse,

$$t_{\rm peak}/L \approx h(r_{\rm eff}/L)\,, \tag{3.83}$$

for some function h. Finally, this function must be consistent with the scaling relations discussed in section 3.2.5, which imply that L^2/r scales in the same fashion as a distance

(or time) in the boundary theory. Consequently, the dependence of the response time on the effective depth must have the form

$$t_{\text{peak}} \approx CL^2/r_{\text{eff}}\,, \tag{3.84}$$

for some dimensionless constant C.

A similar line of reasoning is applicable to the magnetic case. Since we used $\varepsilon_L \equiv \varepsilon(L)$ and $\mathcal{B}L^2$ as parameters labeling the equilibrium magnetic brane geometry in our comparisons of magnetic plasma response, it is convenient to view the response time t_{peak} as depending on these parameters plus the Gaussian pulse parameters,

$$t_{\text{peak}}/L = f(\varepsilon_L L^4, \mathcal{B}L^2, r_0/L, \sigma/L, \mathcal{A})\,, \tag{3.85}$$

for some function f. Once again, the observed near-linearity of the response allows us to simplify this to the form

$$t_{\text{peak}}/L \approx g(\varepsilon_L L^4, \mathcal{B}L^2, r_{\text{eff}}/L)\,, \tag{3.86}$$

for some function g. The near-independence of the time course of the response on the magnetic field $\mathcal{B}$, for fixed ε_L and a fixed initial pulse, implies that the function g is nearly independent of its second argument. Because ε_L does not transform homogeneously under the scaling relations (3.43)-(3.45) (due to the use of the curvature scale L instead of a physical scale in the dual QFT for setting the renormalization point) consistency with the scaling relations requires that the function g be independent of its first argument and depend inversely on the third. So, just as for the charged case,

$$t_{\text{peak}} \approx CL^2/r_{\text{eff}}\,, \tag{3.87}$$

for some dimensionless constant C.

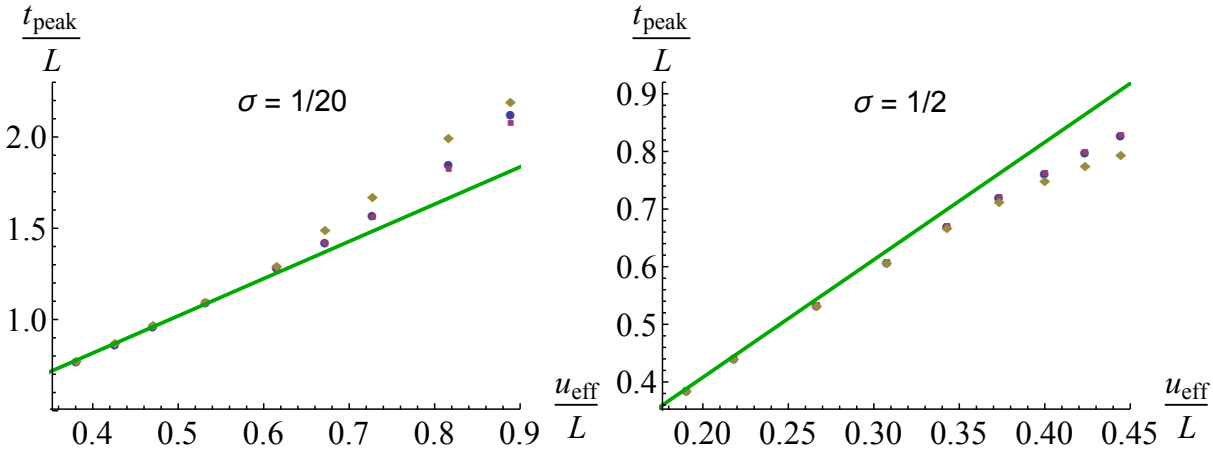

Figure 3.18: Time of the first peak in the pressure anisotropy response as a function of the inverse effective depth of the pulse, $u_{\text{eff}} \equiv 1/r_{\text{eff}}$. The left panel shows results for narrow pulses with $\sigma = 1/20$, while the right panel shows results from wide pulses with $\sigma = 1/2$. Blue circles represent data points from neutral (uncharged, unmagnetized) plasmas, maroon squares represent data points from charged plasmas at 80% of extremality, and gold diamonds represent data points from magnetized plasmas with $\mathcal{B}L^2 = 1.5$. The green straight line shows the prediction of our simple model (3.87) with $n = 2.5$ and $C = 2.04$.

Figure 3.18 compares this simple model with a sample of our data for neutral, charged, and magnetized plasmas. The left panel shows data for relatively narrow pulses of width $\sigma = 1/20$, while the right panel shows data from rather wide pulses with width $\sigma = 1/2$. The abscissa for both panels is the inverse effective depth $u_{\text{eff}} \equiv 1/r_{\text{eff}}$. (Data points at the largest values of u_{eff} shown in these plots come from pulses centered very near the horizon.) In both panels, rather good agreement with the simple model is found when the multiplier n in the effective depth $r_{\text{eff}} \equiv r_0 + n\sigma$ is chosen to be 2.5, and the coefficient

$$C \approx 2.04\,. \tag{3.88}$$

For both sets of data, the model is least accurate for pulses located very close to the horizon. Accuracy for the case of magnetized plasma is a bit worse than for charged or neutral plasma. But for all cases, even in the near-horizon regime, this simple model works at about the 20%

level or better. As pulses move away from the horizon, the accuracy rapidly improves.

3.6 Conclusion

In weakly coupled plasmas, adding a conserved charge density to the system (e.g., flavor charge in a QCD plasma) significantly changes screening lengths. When the associated chemical potential is of order πT, the relative change in the Debye screening length is $O(1)$ [86]. Such changes in screening lengths significantly affect transport coefficients like the viscosity [87]. Lattice studies [88] of the effect of a baryon chemical potential in the deconfined phase, when the system is not asymptotically weakly coupled, claim to find measurable sensitivity in the Debye screening length, comparable to perturbative estimates, but with quite large error bars. Lattice QCD studies of magnetoresponse [69, 70, 71, 72] also find substantial changes in thermodynamics when the magnetic field energy density becomes large compared to T^4.

Consequently, when this work on strongly coupled $\mathcal{N}=4$ SYM plasma was initiated, we expected to find significant changes in equilibration dynamics when a conserved charge density is added to the plasma, or when the system is placed in a background magnetic field. The most notable result we have found is that this expectation was wrong. At least within the range of charge densities we studied, up to 80% of extremality, the equilibration dynamics is remarkably insensitive to the presence of a conserved charge density. Additionally, magnetic fields which are well into the strong field region, $\mathcal{B}/T^2 \gg 1$, induce almost no change in the equilibration time course.

Efforts to use results of holographic calculations in strongly coupled $\mathcal{N}=4$ SYM as the basis for predictions about real heavy ion collisions [5] are inevitably hampered by our limited understanding of the effect on the relevant dynamics of changing the theory from real QCD to a supersymmetric Yang-Mills model theory. From this perspective, the insensitivity of the equilibration dynamics to the charge density is reassuring, as this provides an example where changes in the plasma constituents have very little impact on the overall dynamics.

A further notable feature in our results is the remarkably small degree of nonlinearity

in the dynamics governing the pressure anisotropy. Despite the fact that one is solving the highly nonlinear Einstein equations, the dependence of the induced pressure anisotropy on the initial anisotropy function is surprisingly close to linear. We find deviations from linearity of at most $\approx 30\%$, and this only for initial disturbances which are crafted to reside very deep in the bulk. (This is consistent with earlier work in ref. [53].) For disturbances localized even modestly above the horizon, the degree of nonlinearity quickly drops to sub-percent levels. This near-linearity holds even when the system is far from equilibrium, with pressure anisotropies which are large compared to the energy density.

In the charged case, the sensitivity of the lowest quasinormal mode frequency to the charge density is significantly larger than the sensitivity we find in, and shortly after, the far-from-equilibrium period of the equilibration dynamics. The lowest quasinormal mode dominates the equilibration process at sufficiently late times when all higher modes have decayed away and become negligible relative to the lowest mode.

The near-linearity which we find in the dynamics implies that the deviation from equilibrium, even during the far-from-equilibrium portion of the process, can be represented quite accurately as a sum of quasinormal modes obeying linearized small fluctuation equations. The minimal sensitivity of the equilibration dynamics to the charge density, substantially less than the sensitivity of the lowest quasinormal mode frequency, suggests that during most of the equilibration process many quasinormal modes above the lowest one are contributing, with the sensitivity to the charge density quickly falling with increasing mode number. This is something which could be tested directly in a linearized analysis but, to our knowledge, has not yet been done.

In the magnetic case, we find only modest (few percent) changes induced by the magnetic field in the time course to equilibration, and in the lowest quasinormal mode frequency characterizing very late time behavior. It would be nice to have independent calculations of quasinormal mode frequencies for magnetic branes, including studies of the field dependence of higher mode frequencies.

Although we no longer have reason to expect large effects, it would be natural to generalize

the study of homogeneous equilibration to the case of plasmas with both non-zero charge density and a background magnetic field. Extensions to more complicated inhomogeneous settings, such as colliding shock waves, are also of interest. It would be desirable to gain a clearer understanding of the connection between our choices of gravitational initial data on null slices and boundary observables such as multi-point stress-energy correlators. Can more operational procedures, such as time-dependent background fields [26], produce far-from-equilibrium states which resemble those produced by our "deep pulse" initial data? We hope future work can shed light on some of these topics.

Chapter 4

SPINOR FIELDS IN GENERAL NEWTON-CARTAN BACKGROUNDS

This chapter is based on a publication in collaboration with Andreas Karch and Christoph Uhlemann [89]. Andreas was responsible for bulk of the motivation for this project. Initial exploratory calculations were performed by JF. Final calculations present in the manuscript were independently calculated by both Christoph and JF. The bulk of interpretation, organization, and direction was performed by Christoph. The manuscript was written and edited by all.

4.1 Introduction

In recent years, Galilean invariant (quantum) field theories have found application in prominent condensed matter systems like the unitary Fermi gas and (fractional) quantum hall states [90, 91, 92, 93]. It is desirable to have a formulation of the theories on generic and possibly torsionful curved backgrounds, both to incorporate the effects of e.g. non-trivial lattice backgrounds for condensed matter applications [94], and to couple to gravity. Newton-Cartan spacetimes are the non-relativistic analog of generic (pseudo-)Riemann manifolds. They consist of a topological manifold $\mathcal{M}$ equipped with a nowhere vanishing one-form n singling out a time direction and a co-rank 1 symmetric tensor field h^{-1}, which gives an (inverse) spatial metric on constant-time slices. We use h^{-1} to indicate that it maps from the cotangent space to the tangent space, the opposite direction compared to the metric in a pseudo-Riemannian structure, but note that h^{-1} is not defined as the inverse of some h. The investigation of Newton-Cartan structures and field theories coupled to said structures has a long history in the context of gravitational physics [95, 96, 97], and has more recently

also found its way into holographic studies [98, 99].

In this work we focus on spinor fields, which have been considered previously on Newtonian spacetimes [100]. Newtonian spacetimes are a special class of Newton-Cartan spacetimes where the clock form n is required to be closed, $dn = 0$. To our knowledge, an action for non-relativistic spinor fields in generic Newton-Cartan backgrounds has not been constructed yet. Considering the prevalence of spinor particles in condensed matter systems, we find the pursuit of such a construction to be a worthwhile endeavor. In addition to the motivations mentioned above, n also needs to be left unconstrained in order to understand it as source for the energy current, as emphasized in [93, 101]. The starting point for our construction is the relativistic Dirac Lagrangian, from which we construct a non-relativistic Lévy-Leblond type action [102] by a limiting procedure, which amounts to sending the speed of light to infinity and compensating the rest energy by a fine-tuned chemical potential. This allows us to obtain completely general and even acausal Newton-Cartan backgrounds from relativistic parents.

Insisting on the existence of a non-trivial limit even in spacetimes with no standard notion of causality turns out to be remarkably fruitful. We find that a non-minimal coupling to the background gauge field is needed, and that this non-minimal coupling is indeed crucial even in the most benign backgrounds, to ensure invariance of the final Lagrangian under Milne boosts. The final non-relativistic Lagrangian has all desired symmetries: in addition to the symmetries of the Newton-Cartan structure, it has local Galilean invariance reflecting the gauge redundancy in choosing a local frame as well as invariance under Milne boosts, which reflects the gauge redundancy in choosing a dual vector field v corresponding to the one-form n.[1] The non-minimal coupling that is required to guarantee a non-trivial limit and the presence of these symmetries results in a special value for the gyromagnetic ratio of the non-relativistic spinor field, even on flat space. This special value is $g = 1$, half of

[1]These invariances may be looked at either as spurionic symmetries, or, if the theory is coupled to gravity, as gauge symmetries. Either way, the actual global symmetries of the theory in a given background arise as the subset which leaves that background invariant. For our purposes the two points of view are equivalent.

the relativistic value. Three-dimensional spacetimes are an exception and we discuss these separately, generalizing previous work in [103].

The paper is organized as follows. In sec. 4.2 we set up notation for the relativistic parent geometry and introduce the data that feeds into the non-relativistic limit. We then turn to the actual limiting procedure in sec. 4.3, which contains as main result the non-relativistic Dirac or generalized Lévy-Leblond operator and Lagrangian in eqns. (4.32) and (4.33), respectively. In sec. 4.4 we discuss in detail the invariances that the relativistic symmetries induce in the non-relativistic limit. In particular, we show that the generalized Lévy-Leblond operator defined in eqn. (4.32) transforms covariantly under Milne boosts and local Galilean transformations. To have all mentioned symmetries manifest, we need the non-relativistic spinor to have as many components as the relativistic Dirac spinor has. However, in the non-relativistic limit half of these components are downgraded to auxiliary fields. In sec. 4.5 we solve for these auxiliary fields in causal spacetimes and give a Lagrangian purely in terms of the dynamical fields. We also discuss explicitly the implications for flat space. In sec. 4.6 we specialize to three-dimensional spacetimes, before closing with a discussion in sec. 4.7.

4.2 Relativistic geometry and Newton-Cartan data

We start from a pseudo-Riemann manifold $(\mathcal{M}, g)$, and for the non-relativistic limit we pick a nowhere-vanishing one-form n. For each $p \in \mathcal{M}$, n gives a preferred subspace of $T_p\mathcal{M}$: the "spacelike" vectors which are annihilated by n. If $n \wedge dn = 0$, the Frobenius theorem guarantees that there is a foliation of $\mathcal{M}$ by codimension-1 surfaces, for which the tangent spaces consist exactly of said spacelike vectors (see e.g. the formulation in [104]). This gives a foliation by spacelike hypersurfaces and a notion of causality. However, we will not assume that $n \wedge dn = 0$, but only that n is timelike everywhere. This ensures that the resulting $h^{\mu\nu}$ is positive definite, as required for the Newton-Cartan structure.

With the clock form n in hand, we can define an inverse spatial metric $h^{\mu\nu}$ from the inverse metric $g^{\mu\nu}$. Any one-form λ can be decomposed into spatial and timelike parts as

$\lambda = \lambda_s + n g^{-1}(\lambda, n)/g^{-1}(n,n)$, such that λ_s is spatial, $g^{-1}(\lambda_s, n) = 0$.[2] The inverse spatial metric is then defined by $h^{-1}(\lambda, \tau) = g^{-1}(\lambda_s, \tau_s)$. The rank of $h^{\mu\nu}$ is $d-1$ and it satisfies $h^{\mu\nu} n_\nu = 0$. The triple $(\mathcal{M}, n, h^{-1})$ is called a Galilean structure in [105] and a Leibnizian structure in [106].

Since we start from a relativistic theory on a manifold with a pseudo-Riemannian structure, we can immediately define a vector field v to get a similar split of the tangent space, along with a spatial metric. Since g provides us with an isomorphism of $T_p\mathcal{M}$ and $T_p^\star M$, we can simply define v by $v^\mu = g^{\mu\nu} n_\nu / g^{-1}(n,n)$, s.t. $n_\mu v^\mu = 1$. We can then define projectors on the spatial part for tensors as

$$P_\mu{}^\nu = g_\mu{}^\nu - n_\mu v^\nu \ . \tag{4.1}$$

For the (inverse) spatial metrics we use the symbols $h^{-1} = h^{\mu\nu}\partial_\mu \otimes \partial_\nu$ and $h = h_{\mu\nu} dx^\mu \otimes dx^\nu$, with the understanding that $h^{\mu\nu}$ and $h_{\mu\nu}$ as matrices are not inverse to each other. They are inverse as maps only when restricted to the spatial subspace singled out by $P_\mu{}^\nu$. With the projectors (4.1) we then have

$$h_{\mu\nu} = P_\mu{}^\rho P_\nu{}^\sigma g_{\rho\sigma} \ , \qquad\qquad h^{\mu\nu} = P_\rho{}^\mu P_\sigma{}^\nu g^{\rho\sigma} \ . \tag{4.2}$$

For such a generic choice of n, the metric can then be decomposed in an ADM-like fashion as

$$g_{\mu\nu} = \frac{n_\mu n_\nu}{g^{-1}(n,n)} + h_{\mu\nu} \ , \qquad\qquad g^{\mu\nu} = g^{-1}(n,n) v^\mu v^\nu + h^{\mu\nu} \ . \tag{4.3}$$

We fix $g^{-1}(n,n) = -c^{-2}$ in the following, such that the split of the (inverse) metric reduces to the choices made in [107], namely $g_{\mu\nu} = -c^2 n_\mu n_\nu + h_{\mu\nu}$ and $g^{\mu\nu} = -c^{-2} v^\mu v^\nu + h^{\mu\nu}$. This does not restrict the class of Newton-Cartan geometries that can be obtained from the reduction

[2] Spelling out the notation more explicitly, $g^{-1}(a,b)$ and $g(a,b)$ mean $g^{\mu\nu} a_\mu b_\nu$ and $g_{\mu\nu} a^\mu b^\nu$, respectively. The one-forms are understood as $n = n_\mu dx^\mu$ and analogously for λ, λ_s.

– for given Newton-Cartan data one can always choose a suitable pseudo-Riemann metric such that our conditions are met.

From the Newton-Cartan perspective, the logic is quite disparate. Without a pseudo-Riemann metric, n and h^{-1} alone do not determine a unique v or h. The conditions $n_\mu v^\mu = 1$ and $v^\mu h_{\mu\nu}$ are invariant under Milne boosts, which change v and h but leave n and h^{-1} invariant. In the non-relativistic limit, this freedom in the choice of v and h arises as follows [107]. In the $c \to \infty$ limit, n and h^{-1} are the dominant structures in g and g^{-1}, respectively. That is,

$$c^{-2} g_{\mu\nu}|_{c\to\infty} = -n_\mu n_\nu \ , \qquad\qquad g^{\mu\nu}|_{c\to\infty} = h^{\mu\nu} \ . \tag{4.4}$$

We can then extract n from $c^{-2}g|_{c\to\infty}$ – up to a sign ambiguity in "taking the square root" – and h^{-1} from $g^{-1}|_{c\to\infty}$. The pseudo-Riemannian structure thus reduces to a Newton-Cartan structure when $c \to \infty$. The derived quantities v and h, on the other hand, only enter as subleading terms in g^{-1} and g, respectively. Redefining n and h^{-1} by subleading terms gives the same Newton-Cartan structure but changes v and h, and we indeed recover the Milne transformations. We will see this more explicitly in sec. 4.4.1.

4.2.1 Frames and spinors

Now that we have discussed how the metric data is decomposed for a given n, we turn to the objects associated with the frame bundle: the vielbein (solder form), spin connection and spinors. From the decomposition of $g_{\mu\nu}$ in terms of n_μ, $h_{\mu\nu}$, we immediately get an induced decomposition of the Minkowski metric in terms of $n_a = e^\mu_a n_\mu$, namely

$$\eta_{ab} = -c^2 n_a n_b + h_{ab} \ , \qquad h_{ab} = P_a{}^c P_b{}^d \eta_{cd} \ , \qquad P^a{}_b = \eta^a{}_b - v^a n_b \ . \tag{4.5}$$

The decomposition of $g^{\mu\nu}$ in terms of v^μ and $h^{\mu\nu}$ likewise induces a decomposition of η^{ab}. We also have $h_{\mu\nu} = e^a_\mu e^b_\nu h_{ab}$ and analogously for $h^{\mu\nu}$. The (inverse) vielbein can correspondingly

be decomposed as

$$e^a_\mu = n_\mu v^a + \widetilde{e}^a_\mu \ , \qquad\qquad e^\mu_a = v^\mu n_a + \widetilde{e}^\mu_a \ , \tag{4.6}$$

where the tilde denotes a spatial projection on the Lorentz index, $\widetilde{e}^a_\mu = P_b{}^a e^b_\mu$ and $\widetilde{e}^\mu_a = P_a{}^b e^\mu_b$. Occasionally we will find it useful to explicitly split Lorentz indices as $a = (\underline{0}, i)$, and we generally use an underline to distinguish Lorentz from coordinate indices whenever explicit values are used. With the Minkowski metric $\eta = -c^2 dt^2 + d\vec{x}^2$ and the two decompositions of g as

$$g_{\mu\nu} = -c^2 n_\mu n_\nu + h_{\mu\nu} \ , \qquad\qquad g_{\mu\nu} = -c^2 e^{\underline{0}}_\mu e^{\underline{0}}_\nu + e^i_\mu e^j_\nu \delta_{ij} \ , \tag{4.7}$$

we immediately find

$$e^{\underline{0}} = n + \frac{1}{c^2} a \ , \tag{4.8}$$

where a is $\mathcal{O}(1)$. To keep the notation clean we will partly use index-free notation to suppress coordinate indices, e.g. for the above $e^{\underline{0}} = e^{\underline{0}}_\mu dx^\mu$, $n = n_\mu dx^\mu$ and $a = a_\mu dx^\mu$ are understood – they are all one-forms. We also note that $n_b = \delta_{b\underline{0}} - c^{-2} a_b$, which will be useful below. We then have $e^{\underline{0}}|_{c\to\infty} = n$, which makes $e^a|_{c\to\infty}$ into a Galilei frame as defined in [95]. The subleading part of the vielbein, a, plays the role of the mass gauge field in [108]. Note that, since $e^{\underline{0}}$ transforms under local Lorentz transformations while n does not, a transforms non-trivially under local Lorentz boosts, in spite of not having a Lorentz index. We will see in sec. 4.4 that the orders in c work out.

We now turn to the spin connection. In the relativistic theory we start with a torsion-free

background[3], so the spin connection can be expressed entirely in terms of the vielbein as

$$\omega_{\mu\nu\rho} = 3\Omega_{[\mu\nu\rho]} - 2\Omega_{\nu\rho\mu} \ , \qquad\qquad \Omega_{\mu\nu\rho} = e_{\rho a}\partial_{[\mu}e^{a}_{\nu]} \ . \tag{4.9}$$

Converting all indices to coordinate indices obscures the structure of ω as an $\mathfrak{so}(1, d-1)$-valued one form, but we find it useful for explicit computations. Despite the absence of Lorentz indices, this expression for the spin connection still transforms non-trivially under local Lorentz transformations, as appropriate for a connection. We isolate the divergent pieces in ω as follows. With the vielbein as discussed above, we have $\Omega_{\mu\nu\rho} = -c^2 e^0_\rho \partial_{[\mu}e^0_{\nu]} + \delta_{ij}e^i_\rho\partial_{[\mu}e^j_{\nu]}$. Using eqn. (4.8) we then find

$$\omega_{\mu\nu\rho} = c^2\left(2n_\mu\partial_{[\nu}n_{\rho]} - 3n_{[\mu}\partial_\nu n_{\rho]}\right) + \dot{\omega}_{\mu\nu\rho} \ , \tag{4.10}$$

where $\dot{\omega}_{\mu\nu\rho}$ is $\mathcal{O}(1)$. Explicitly, we have

$$\dot{\omega}_{\mu\nu\rho} = 3\dot{\Omega}_{[\mu\nu\rho]} - 2\dot{\Omega}_{\nu\rho\mu} \ , \qquad \dot{\Omega}_{\mu\nu\rho} = e_{\rho i}\partial_{[\mu}e^i_{\nu]} - a_\rho\partial_{[\mu}n_{\nu]} - n_\rho\partial_{[\mu}a_{\nu]} - c^{-2}a_\rho\partial_{[\mu}a_{\nu]} \ . \tag{4.11}$$

Finally, we come to the spinors themselves and to the Clifford algebra. We decompose the generators as

$$\gamma^\mu = \not{v}v^\mu + \widetilde{\gamma}^\mu \ , \qquad\qquad \not{n} = n_\mu\gamma^\mu \ , \qquad\qquad \widetilde{\gamma}^\mu = P_\nu{}^\mu\gamma^\nu \ , \tag{4.12}$$

and analogously for lowered spacetime and Lorentz indices. With n as additional geometric data, we can define a new "chirality" operator for the spinors, similarly to the tensor projectors in (4.1). This is regardless of whether the relativistic spin group admits chiral

[3]When coupled to gravity in a 1st-order formalism, spinor fields produce torsion when the spin connection is determined from its equation of motion. That torsion is quadratic in the Dirac field and would show up in the Lagrangian. However, it drops out once the gravitational coupling is sent to zero. One can nevertheless study torsionful backgrounds as a starting point, which we leave for the future.

representations. Namely,

$$P_\pm = \frac{1}{2}(\mathbb{1} \pm ic\not{n}) \ . \tag{4.13}$$

In the non-relativistic limit we expect a pair of spinors with half as many components as the relativistic Dirac spinor, which differ in their dynamics [102]. It is thus natural to expect projectors to be relevant for the reduction. With $P_\pm$ we decompose the Dirac field ψ as

$$\psi = \psi_+ + \psi_- \ , \qquad\qquad \psi_\pm = P_\pm \psi \ . \tag{4.14}$$

With $\gamma^{\underline{0}}\gamma_\mu^\dagger\gamma_{\underline{0}} = -\gamma_\mu$ we have $\overline{P_\pm} = \gamma^{\underline{0}}(P_\pm)^\dagger\gamma_{\underline{0}} = P_\pm$ and thus $\overline{P_\pm\psi} = \overline{\psi}P_\pm$.

4.3 Non-relativistic limits in generic backgrounds

We now set up and perform the non-relativistic limit for a Dirac field in generic backgrounds. We start with a free Dirac field coupled non-minimally to a background gauge field C, which sources the U(1) particle number current. The Lagrangian is

$$L = i\overline{\psi}\not{D}\psi - i\left(D_\mu\overline{\psi}\right)\gamma^\mu\psi - 2imc\overline{\psi}\psi + \frac{\alpha}{mc}F_{\mu\nu}\overline{\psi}\gamma^{\mu\nu}\psi \ , \tag{4.15}$$

where $F = dC$ or $F_{\mu\nu} = \partial_\mu C_\nu - \partial_\nu C_\mu$. The reason for including the non-minimal coupling will become apparent below. The covariant derivative reads

$$D_\mu\psi = \partial_\mu\psi + \frac{1}{4}\omega_{\mu ab}\gamma^{ab} - iC_\mu \ . \tag{4.16}$$

Our convention for the Clifford algebra generators is $\{\gamma^a, \gamma^b\} = 2\eta^{ab}\mathbb{1}$ with $\gamma^{\underline{0}}\gamma_a^\dagger\gamma_{\underline{0}} = -\gamma_a$, and we use $\overline{\psi} = \psi^\dagger c\gamma^{\underline{0}}$ to have $\overline{\psi}$ of the same order in c as ψ. The action of D_μ on $\overline{\psi}$ is determined from $\overline{\psi}\psi$ being a scalar and the Leibniz rule. Moreover, we have ω and C real and iD_μ is formally self-adjoint with respect to the usual inner product for spinors. To set the stage, we determine the scaling weights of $\psi_\pm$ as $c \to \infty$ from a flat-space analysis.

Our guideline will be to obtain non-trivial dynamics at $c \to \infty$. The reduction in generic backgrounds will be done afterwards.

4.3.1 Scaling weights from flat space

We take Minkowski space with $g = -c^2 dt^2 + d\vec{x}^2$ and fix $e^a_\mu = \delta^a_\mu$. For the non-relativistic limit we choose $n = dt$. We note that fixing an expression for n to all orders in c also fixes a Milne frame, and we have $v = \partial_t$. The Lagrangian given by eqn. (4.15) becomes

$$\begin{aligned} L = i\overline{\psi}_\pm \widetilde{\gamma}^\mu \left(\partial_\mu - iC_\mu\right)\psi_\mp \pm \frac{1}{c}\overline{\psi}_\pm\big(\partial_0 - iC_0\big)\psi_\pm - imc\overline{\psi}_\pm\psi_\pm \\ + \frac{\alpha}{2mc}F_{\mu\nu}\overline{\psi}_\pm\widetilde{\gamma}^{\mu\nu}\psi_\pm \pm \frac{i\alpha}{mc^2}F_{\mu\nu}v^\nu\overline{\psi}_\pm\widetilde{\gamma}^\mu\psi_\mp + \text{c.c.}\ , \end{aligned} \tag{4.17}$$

where a sum over the upper and lower choices for the subscripts is implicit. The dominant part of the mass term will dominate all derivative terms at $c \to \infty$, and it therefore needs to be canceled in order to get a non-trivial non-relativistic theory. The lesson from [107] is to turn on an $\mathcal{O}(c^2)$ background gauge field giving a chemical potential as

$$C_\mu = -mc^2 n_\mu + mA_\mu\ , \tag{4.18}$$

where the $\mathcal{O}(1)$ part, A, becomes the non-relativistic gauge field. We will see below that this is also the correct choice for curved spaces, unless the number of spacetime dimensions is three, a case we will discuss separately. For the scaling analysis we set $A = 0$, and noting that $dn = 0$ the Lagrangian (4.17) with the gauge field (4.18) then becomes

$$L = i\overline{\psi}_\pm\widetilde{\gamma}^\mu\partial_\mu\psi_\mp \pm \frac{1}{c}\overline{\psi}_\pm\partial_0\psi_\pm \pm imc\overline{\psi}_\pm\psi_\pm - imc\overline{\psi}_\pm\psi_\pm + \text{c.c.}\ , \tag{4.19}$$

The mass-like term resulting from the leading piece of eqn. (4.18) has opposite signs for the two chiralities, allowing for a cancellation of only one of the actual mass terms. With our choice of C this is the one for ψ_+. For ψ_-, the mass term dominates its time-derivative piece, and we get a non-dynamical auxiliary field, as expected from [102, 100].

For generic scaling of $\psi_\pm$, the equations of motion for $\psi_\pm$ decouple at $c \to \infty$. Depending on which of the terms is dominant, the equation resulting from varying ψ_- then is either $\psi_- = 0$ or $\widetilde{\gamma}^\mu \partial_\mu \psi_+ = 0$. Neither of those yields non-trivial dynamics for ψ_+ when combined with the equation resulting from variation of ψ_+. To get a non-trivial limit, the mixed term in (4.19) has to contribute at the same order as the mass term for ψ_-. That is, $\psi_+ = \mathcal{O}(c\psi_-)$. The overall scaling of the Lagrangian can be absorbed by a rescaling at the end, so we simply fix $\psi_\pm = \mathcal{O}(c^{\pm 1/2})$.

4.3.2 Non-relativistic limit in generic backgrounds

We now perform the non-relativistic limit for generic curved backgrounds and generic choice of n. From [102] we expect that we need to keep all components of the relativistic Dirac spinor. With the scaling determined from the flat case, we define our non-relativistic spinor, Ψ, as

$$\Psi = \mathcal{P}\psi\big|_{c\to\infty} , \qquad\qquad \mathcal{P} = c^{-\frac{1}{2}} P_+ + c^{\frac{1}{2}} P_- . \tag{4.20}$$

Note that Ψ is $\mathcal{O}(1)$ and indeed keeps as many non-trivial components as the Dirac spinor we started with. We will justify calling it a non-relativistic spinor in sec. 4.4.

We will disassemble the Lagrangian into its building blocks as far as possible. To perform the non-relativistic limit we write the Lagrangian of eqn. (4.15) as

$$L = i\overline{\psi}\left(\not{D} - mc - \frac{i\alpha}{2mc}\not{F}\right)\psi + \text{c.c.} , \qquad\qquad \not{F} = F_{\mu\nu}\gamma^{\mu\nu} . \tag{4.21}$$

The operator $\mathcal{P}$ is invertible, and we define $\widetilde{\mathcal{P}}$ such that $\widetilde{\mathcal{P}}\mathcal{P} = \mathcal{P}\widetilde{\mathcal{P}} = \mathbb{1}$. This allows us to conveniently insert identities in the Lagrangian (4.21), and with the definition of Ψ in eqn. (4.20) we see

$$L = i\overline{\Psi}\,\widetilde{\mathcal{P}}\left(\not{D} - mc - \frac{i\alpha}{2mc}\not{F}\right)\widetilde{\mathcal{P}}\,\Psi + \text{c.c.} , \qquad\qquad \widetilde{\mathcal{P}} = c^{\frac{1}{2}} P_+ + c^{-\frac{1}{2}} P_- . \tag{4.22}$$

We want to define the non-relativistic Lagrangian as $L_{\rm nr} = L|_{c\to\infty}$, and to obtain a non-trivial limit we will have to fix α. Since Ψ is $\mathcal{O}(1)$ by definition, it just remains to evaluate what will become the definition of our non-relativistic Dirac operator. Namely,

$$\not{\mathcal{D}}_\alpha := \widetilde{\mathcal{P}}\left(\not{D} - mc - \frac{i\alpha}{2mc}\not{F}\right)\widetilde{\mathcal{P}}\Big|_{c\to\infty} . \tag{4.23}$$

The covariant derivative was defined in eqn. (4.16), and we choose C in accordance with eqn. (4.18). We will also need the spin connection as evaluated in eqn. (4.10). With these results, we find for the partial derivative and gauge field parts of $\not{\mathcal{D}}_\alpha$

$$\widetilde{\mathcal{P}}\gamma^\mu(\partial_\mu - iC_\mu)\widetilde{\mathcal{P}}\Big|_{c\to\infty} = (-iP_+ v^\mu + \widetilde{\gamma}^\mu)\left(\partial_\mu - \frac{i}{2}(\partial_\mu a_b)e^b_\nu\widetilde{\gamma}^\nu P_+ - imA_\mu\right) + mc^2P_+ - mP_- . \tag{4.24}$$

For quantities which are $\mathcal{O}(1)$ at $c\to\infty$, like e^a and A, we use the same symbol to denote the non-relativistic object, with the understanding that the latter is the leading part only. This applies to the right hand side of the above equation and to avoid unnecessarily complicated notation we will use that convention in the following when $c\to\infty$ is clear from the context. The mass term is simply $\widetilde{\mathcal{P}}mc\widetilde{\mathcal{P}} = mc^2P_+ + mP_-$, and we see the divergent piece here cancel against that of eqn. (4.24). The remaining terms of $\not{\mathcal{D}}_\alpha$ contain the spin connection as well as the non-minimal coupling. As seen from eqn. (4.10), the spin connection has an $\mathcal{O}(c^2)$ piece. Looking, then, at the divergent part of the spin connection and non-minimal coupling pieces of $\not{\mathcal{D}}_\alpha$, we find

$$\widetilde{\mathcal{P}}\left(\Omega - \frac{i\alpha}{2mc}\not{F}\right)\widetilde{\mathcal{P}}\Big|_{\mathcal{O}(c^2)} = \frac{c^2}{8}\partial_{[\mu}n_{\nu]}P_+\left(c\not{n}\gamma^{\mu\nu} - 3\gamma^{\mu\nu}c\not{n} + 8i\alpha\gamma^{\mu\nu}\right)P_+ \tag{4.25a}$$

$$= ic^2\left(\frac{1}{4} + \alpha\right)P_+\partial_{[\mu}n_{\nu]}\gamma^{\mu\nu}P_+ , \tag{4.25b}$$

where $\Omega = \frac{1}{4}\gamma^\mu\omega_{\mu ab}\gamma^{ab}$. If $\alpha \neq -\frac{1}{4}$, this term dominates the Lagrangian at large c. One could imagine modifying the leading behavior of C to cancel this divergence, e.g. by adding a term

proportional to dn to eqn. (4.18). This will indeed work for three-dimensional spacetimes, which we discuss in sec. 4.6. Generically, however, the divergence can not be canceled this way due to the different Clifford algebra structures of Ω and $\not{C}$. A possible workaround one may think of is modifying the projectors $P_\pm$ by adding terms like $(n \wedge dn)_{\mu\nu\rho}\gamma^{\mu\nu\rho}$, but ensuring that the projectors square to themselves then is problematic and we did not find a reasonable solution from this route. A different variant of the non-minimal coupling term to cancel the divergence would be $\overline{\psi}(C \wedge dC)_{\mu\nu\rho}\gamma^{\mu\nu\rho}\psi$, but this is not gauge invariant. We are thus lead to conclude that in order to find non-trivial dynamics, we must fix

$$\alpha = -\frac{1}{4} \ . \tag{4.26}$$

Before moving on, we want to elaborate a bit on the divergent terms in eqn. (4.25). If $n \wedge dn = 0$, we can use $\{\gamma^\mu, \gamma^{\nu\rho}\} = 2\gamma^{\mu\nu\rho}$ to see that

$$P_\pm \gamma^{\nu\rho}\partial_{[\nu}n_{\rho]}P_\pm = \pm icP_\pm n_\mu \{\gamma^\mu, \gamma^{\nu\rho}\}P_\pm \partial_{[\nu}n_{\rho]} = \pm 2icP_\pm \gamma^{\mu\nu\rho}P_\pm n_{[\mu}\partial_\nu n_{\rho]} = 0 \ . \tag{4.27}$$

That means as long as $n \wedge dn = 0$, the divergent terms in eqn. (4.25) actually vanish by themselves, and one might hope to get away without fixing $\alpha = -\frac{1}{4}$. We will see below that symmetry considerations nevertheless call for the choice of α in eqn. (4.26), even on flat space. The reason is simple: while the divergent terms themselves vanish for $n \wedge dn = 0$, their Milne variations for generic α propagate into the $\mathcal{O}(1)$ part, such that the final expression for $\not{\mathcal{D}}$ in eqn. (4.32) does not transform covariantly. We come back to Milne variations more explicitly in sec. 4.4.1. With the choice of $\alpha = -\frac{1}{4}$, $\widetilde{\mathcal{P}}\left(\Omega - \frac{i\alpha}{2mc}\not{F}\right)\widetilde{\mathcal{P}}$ is indeed finite for generic Newton-Cartan backgrounds, and we find

$$\begin{aligned}\widetilde{\mathcal{P}}\left(\Omega + \frac{i}{8mc}\not{F}\right)\widetilde{\mathcal{P}}\Big|_{c\to\infty} = (-iP_+ v^\mu + \widetilde{\gamma}^\mu)\,\frac{1}{4}\dot{\omega}_{\mu\nu\rho}\,(\widetilde{\gamma}^{\nu\rho} - 2i\widetilde{\gamma}^\nu v^\rho P_+) + \frac{i}{8}F^{(A)}_{\mu\nu}\widetilde{\gamma}^{\mu\nu}P_+ \\ + \frac{1}{2}T^{\mathrm{c}}_{\mu\nu}v^\nu P_+\widetilde{\gamma}^\mu - \frac{i}{4}T^{\mathrm{c}}_{\mu\nu}\widetilde{\gamma}^{\mu\nu}P_- + \frac{1}{4}T^{\mathrm{c}}_{\mu\nu}\widetilde{\gamma}^\mu v^\nu \ ,\end{aligned} \tag{4.28}$$

where $F^{(A)} = dA$ and $T^{\mathrm{c}} = dn$. For $\not{\mathcal{D}}_{-1/4}$ we then find from eqns. (4.24), (4.28) and the mass term that

$$\not{\mathcal{D}}_{-\frac{1}{4}} = \left(-iP_+ v^\mu + \widetilde{\gamma}^\mu\right) \mathcal{D}_\mu - 2mP_- + \frac{i}{8} F^{(A)}_{\mu\nu} \widetilde{\gamma}^{\mu\nu} P_+ - \frac{i}{4} T^{\mathrm{c}}_{\mu\nu} \left(\widetilde{\gamma}^{\mu\nu} P_- - 2iv^\mu P_+ \widetilde{\gamma}^\nu + i\widetilde{\gamma}^\mu v^\nu\right) \ . \tag{4.29}$$

Note that the $P_\pm$ projectors when acting on Ψ are $\mathcal{O}(1)$. The covariant derivative $\mathcal{D}_\mu$ is defined as

$$\mathcal{D}_\mu := \partial_\mu + \frac{1}{4} \hat{\omega}_{\mu\nu\rho} \left(\widetilde{\gamma}^{\nu\rho} - 2i\widetilde{\gamma}^\nu v^\rho P_+\right) - imA_\mu \ . \tag{4.30}$$

The final non-relativistic spin connection $\hat{\omega}$ used in (4.30) is given by $\hat{\omega}_{\mu\nu\rho} = \dot{\omega}_{\mu\nu\rho} + e^b_\nu n_\rho \partial_\mu a_b|_{c\to\infty}$. More explicitly, with $f = da$ it is given by

$$\hat{\omega}_{\mu\nu\rho} = 3\hat{\Omega}_{[\mu\nu\rho]} - 2\hat{\Omega}_{\nu\rho\mu} + e^b_\nu n_\rho \partial_\mu a_b \ , \qquad \hat{\Omega}_{\mu\nu\rho} = e_{\rho i} \partial_{[\mu} e^i_{\nu]} - \frac{1}{2} a_\rho T^{\mathrm{c}}_{\mu\nu} - \frac{1}{2} n_\rho f_{\mu\nu} \ . \tag{4.31}$$

The conversion to frame indices proceeds via $\hat{\omega}_\mu{}^a{}_b = \eta^{ac} \hat{\omega}_{\mu\nu\rho} e^\nu_c e^\rho_b|_{c\to\infty} = h^{ac} \hat{\omega}_{\mu\nu\rho} e^\nu_c e^\rho_b$. We take the expression for $\not{\mathcal{D}}_{-1/4}$ in eqn. (4.29), which is given purely in terms of Newton-Cartan data and has the divergent pieces canceled, to define $\not{\mathcal{D}}$ without a subscript, which finally is our non-relativistic Dirac or Lévy-Leblond operator. With $\dot{\gamma}^\mu = -iv^\mu P_+$ it reads

$$\not{\mathcal{D}} := \left(\dot{\gamma}^\mu + \widetilde{\gamma}^\mu\right) \mathcal{D}_\mu - 2mP_- + \frac{i}{8} F^{(A)}_{\mu\nu} \widetilde{\gamma}^{\mu\nu} P_+ - \frac{i}{4} T^{\mathrm{c}}_{\mu\nu} \left(\widetilde{\gamma}^{\mu\nu} P_- + 2\dot{\gamma}^\mu \widetilde{\gamma}^\nu + i\widetilde{\gamma}^\mu v^\nu\right) \ , \tag{4.32a}$$

$$\mathcal{D}_\mu = \partial_\mu + \frac{1}{4} \hat{\omega}_{\mu\nu\rho} \left(\widetilde{\gamma}^{\nu\rho} + 2\widetilde{\gamma}^\nu \dot{\gamma}^\rho\right) - imA_\mu \ . \tag{4.32b}$$

The operator $\mathcal{D}_\mu$ looks strikingly similar to the definition of the covariant derivative in [100]. It is different in that our Clifford algebra is not directly the one associated to the degenerate bilinear form given by $h^{\mu\nu}$: our $\dot{\gamma}^a n_a$, which corresponds to γ^0 in [109, 100], squares to itself rather than to zero. We will see below that the spin group constructed from our Clifford algebra nevertheless agrees with [109, 100]. With the manifestly finite

(massive) non-relativistic Dirac operator (4.32), we then find the general non-relativistic spinor Lagrangian

$$L_{\rm nr} = i\overline{\Psi}\not{\mathcal{D}}\Psi + \text{c.c.} \ . \tag{4.33}$$

This expression for the Lagrangian itself hides all the details, like couplings to the clock torsion on spacetimes with $dn \neq 0$ etc. These are manifest in the non-relativistic Dirac operator $\not{\mathcal{D}}$ in (4.32). We will see below that $\not{\mathcal{D}}$, i.e. the complete operator, is the preferred one from the symmetry perspective. Finally, we note that the volume form needed to construct an action from this Lagrangian is just the standard Newton-Cartan volume form discussed e.g. in [105]. Namely, vol $= \sqrt{\det \boldsymbol{\gamma}}\, dx^0 \wedge \cdots \wedge dx^{d-1}$, where $\boldsymbol{\gamma}_{\mu\nu} = n_\mu n_\nu + h_{\mu\nu}$.

4.4 Symmetries

Our main focus will be on Milne and local Galilean transformations, which we discuss in detail in the next two subsections. Under diffeomorphisms the vielbein and spin connection transform covariantly. The spinor field transforms as a spinor under local Galilean transformations, but as a scalar under diffeomorphisms. The Lagrangian (4.33) thus transforms as a scalar and the fact that we are considering spinor fields does not interfere with the symmetries of the Newton-Cartan structure. The U(1) gauge symmetry also only needs a brief discussion. The gauge field A inherits the gauge transformations from those of C via eqn. (4.18), since n is invariant. The projector $\mathcal{P}$ is gauge invariant, so the transformation of Ψ is the same as for ψ, and since and the derivative in eqn. (4.32b) is gauge covariant, $\not{\mathcal{D}}$ transforms correctly. As a result, the Lagrangian in eqn. (4.33) is invariant, as desired.

4.4.1 Milne boosts

As discussed in [107], shifting the clock form, n, by certain one-forms which are subleading in c does not alter the Newton-Cartan structure obtained in the $c \to \infty$ limit. We discuss this systematically, adding some details to the analysis of [107], before turning to the invariance

of our non-relativistic Lagrangian.

Milne transformations

Since $g_{\mu\nu}$ does not depend on the decomposition into n and h, we can immediately infer how $h_{\mu\nu}$ transforms under shifts in n. Namely, we let

$$n_\mu \to n'_\mu = n_\mu - c^{-2}\xi_\mu \ , \qquad h_{\mu\nu} \to h'_{\mu\nu} = h_{\mu\nu} - \xi_\mu n_\nu - \xi_\nu n_\mu + c^{-2}\xi_\mu\xi_\nu \ . \tag{4.34}$$

In the relativistic theory we have $v^\mu = g^{\mu\nu}n_\nu/g^{-1}(n,n)$, as explained in sec. 4.2. Using that $v'^\mu = g^{\mu\nu}n'_\nu/g^{-1}(n',n')$ and that g^{-1} is invariant, we find

$$v^\mu \to v'^\mu = \frac{v^\mu + h^{\mu\nu}\xi_\nu - c^{-2}v^\mu\,\xi(v)}{-c^2 g^{-1}(n',n')} \ . \tag{4.35}$$

Demanding that $h_{\mu\nu}$ remains of rank $d-1$ with null eigenvector v', i.e. $h'_{\mu\nu}v'^\nu = 0$, implies

$$\xi_\mu h^{\mu\nu}\xi_\nu + 2\xi_\mu v^\mu = c^{-2}(\xi_\mu v^\mu)^2 \ . \tag{4.36}$$

This same constraint also ensures that the norm of n is invariant, $g^{-1}(n',n') = -c^{-2}$. The constraint in eqn. (4.36) is quadratic in ξ, and we expect two branches of solutions. To understand these solutions, we split ξ into timelike and spatial parts

$$\xi_\mu = n_\mu\lambda + \zeta_\mu \ , \qquad v^\mu\zeta_\mu = 0 \ , \qquad \zeta_\mu\zeta^\mu = (c^{-2}\lambda - 2)\lambda \ . \tag{4.37}$$

The last equation fixing λ in terms of ζ implements the constraint (4.36), and the indices of the purely spatial ζ_μ can be freely raised and lowered with the spatial metric, i.e. $\zeta^\mu = h^{\mu\nu}\zeta_\nu$. Note that $\lambda \to 2c^2 - \lambda$ leaves the right hand side of the last equation in (4.37) invariant. We find two solutions for λ,

$$\lambda(\zeta) = c^2 - c\sqrt{c^2 + \zeta_\mu\zeta^\mu} \ , \qquad \widetilde{\lambda}(\zeta) = 2c^2 - \lambda(\zeta) \ . \tag{4.38}$$

The first solution is $\mathcal{O}(1)$ in the large-c limit, and choosing it gives a family of transformations which are connected to the identity: as $\zeta^\mu\zeta_\mu \to 0$ also $\lambda(\zeta) \to 0$, and thus $\xi \to 0$. These are what we will call Milne boosts. The transformations with the second choice are not connected to the identity: for $\zeta^\mu\zeta_\mu \to 0$ we get $\widetilde{\lambda}(\zeta) \to 2c^2$. In contrast to the other choice, this does change the Newton-Cartan data. It corresponds to $n \to -n$ while $h_{\mu\nu}$ stays the same, so this is similar to a time reflection. This transformation is compatible with the condition on the norm of n, and with h^{-1} remaining corank 1. The pseudo-Riemann metric g does not need to have any discrete or continuous isometries for this second branch to exist. Note, however, that this is different from the notion of time reflection symmetry in the relativistic theory, and this ambiguity in "taking the square root" has been well appreciated in, e.g., [95, 100, 97]. The entire second branch can be obtained by combining the "time reflection" with the Milne boosts connected to the identity.

With the constraint (4.36) and either choice of solution for λ, the expression for v' in eqn. (4.35) simply evaluates to

$$v'^\mu = v^\mu \left(1 - c^{-2}\lambda\right) + \zeta^\mu \ . \tag{4.39}$$

This turns into $v \to -v$ for the time reflection, as expected. For the inverse spatial metric we find

$$h'^{\mu\nu} = h^{\mu\nu} + c^{-2}\left(\zeta^\mu\zeta^\nu + 2(1 - c^{-2}\lambda)v^{(\mu}\zeta^{\nu)}\right) + c^{-4}v^\mu v^\nu\zeta^\rho\zeta_\rho \ . \tag{4.40}$$

It satisfies $n'_\mu h^{\mu\nu}$ and is invariant under time reflection, again as expected. The vielbein does not change under Milne boosts, but the decomposition of $e^{\underline{0}}$ which we set up in eqn. (4.8) does. Similarly, the relativistic gauge field C is also invariant, but since the non-relativistic gauge field A arises from the decomposition of C, via (4.18), A transforms as well. We find

$$a \to a + \xi \ , \qquad\qquad A \to A - \xi \ . \tag{4.41}$$

To complete the discussion, we give the Milne transformations of the non-relativistic quantities. That is, the leading order in c of the above discussion. The quantities n, $h^{\mu\nu}$, e^a_μ and e^μ_a are invariant, while

$$v^\mu \to v^\mu + \zeta^\mu \ , \qquad\qquad h_{\mu\nu} \to h_{\mu\nu} - 2\zeta_{(\mu} n_{\nu)} + n_\mu n_\nu \zeta^2 \ , \tag{4.42}$$

along with $a \to a + \xi$ and $A \to A - \xi$, where $\xi|_{c\to\infty} = \zeta - \frac{1}{2} n \zeta^2$. Note that this transforms only objects associated directly with the (co)tangent bundle. The vielbein, which solders the frame bundle to the tangent bundle, is invariant.

Milne invariance of the non-relativistic Lagrangian

We want to verify that the non-relativistic Lagrangian, eqn. (4.33), is invariant under Milne boosts. One might expect that any Lagrangian resulting from a non-relativistic limit should be Milne invariant automatically, since the relativistic theory is. That was part of the motivation to study non-relativistic limits in [107]. However, our Lagrangian arises as the $\mathcal{O}(1)$ part in the $c \to \infty$ limit of the relativistic Lagrangian *after* divergences of $\mathcal{O}(c^2)$ canceled between the spin connection and the non-minimal coupling term. More precisely, the non-relativistic Dirac operator $\not{\mathcal{D}}$ in (4.32) was derived from $\not{\mathcal{D}}_{-1/4}$ in (4.23) following this procedure. As such, two additional criteria must be met to obtain a Milne covariant operator and an invariant Lagrangian. The first is that the divergences need to cancel for generic n, without restricting it to satisfy e.g. $n \wedge dn = 0$. The reason is that this condition is preserved by the transformation (4.34) only to leading order. So if the divergences canceled for $n \wedge dn = 0$ only, performing a shift of n as in (4.34) would produce $\mathcal{O}(1)$ pieces from the $O(c^2)$ divergences. Since the full relativistic Lagrangian is invariant, these $\mathcal{O}(1)$ pieces would have to be canceled by what we defined as non-relativistic Lagrangian and $L_{\rm nr}$ could not be invariant. We carefully avoided using such restrictions in sec. 4.3, where we explicitly included acausal spacetimes with $n\wedge dn \neq 0$. The second condition is that the identities which were used to show that the divergent parts cancel must be preserved by the transformation

(4.34), again also at subleading order in c. This condition is independent from the first one, and we will see an example of how the non-relativistic Lagrangian fails to be invariant if it is not met in sec. 4.5. The mechanism is the same as before: if the identities are not preserved exactly, the $\mathcal{O}(c^2)$ divergent terms produce $\mathcal{O}(1)$ pieces when shifting n, and these have to be compensated by the transformation of $L_{\rm nr}$. When these two criteria are met, our procedure gives an invariant Lagrangian. For our construction, meeting the second condition just amounts to $ic\not{n}P_\pm = \pm P_\pm$ being preserved under (4.34), which is certainly the case. Thus, we indeed expect $L_{\rm nr}$ to be Milne invariant. However, a complete discussion of the symmetries certainly has to include the transformations of the individual building blocks of the Lagrangian, and to derive these we go through the above arguments more explicitly now.

We start with the non-relativistic spinor $\Psi = \mathcal{P}\psi$. Since ψ does not transform under Milne boosts, the only transformation is that resulting from $\mathcal{P}$. We find

$$\Psi \to \Psi + \frac{i}{2}\not{\zeta} P_+ \Psi \ , \qquad\qquad \overline{\Psi} \to \overline{\Psi} + \frac{i}{2}\overline{\Psi} P_+ \not{\zeta} \ . \tag{4.43}$$

To derive the transformation of $\not{\mathcal{D}}$ in (4.32), which defines the operator in terms of non-relativistic objects, we start from $\not{\mathcal{D}}_\alpha$ in (4.23). Namely,

$$\not{\mathcal{D}}_\alpha = \widetilde{\mathcal{P}} \left(\not{D} - mc - \frac{i\alpha}{2mc} \not{F} \right) \widetilde{\mathcal{P}} \Big|_{c\to\infty} \ . \tag{4.44}$$

Once again, the only objects transforming non-trivially under Milne boosts are the projectors $\widetilde{P}$. We find

$$\not{\mathcal{D}}_\alpha \to \Big(\mathbb{1} - \frac{i}{2}\not{\zeta} P_- \Big) \not{\mathcal{D}}_\alpha \Big(\mathbb{1} - \frac{i}{2} P_- \not{\zeta} \Big) \ , \tag{4.45}$$

and $\not{\mathcal{D}}_\alpha$ thus transforms covariantly for any α. To infer whether $\not{\mathcal{D}}$ in (4.32) transforms covariantly, we note that between $\not{\mathcal{D}}_\alpha$ and $\not{\mathcal{D}}$ we have canceled the divergences in (4.25), along with the mass term and the leading part of C. We then need to check whether or

not these divergent pieces contribute a non-trivial Milne variation at $\mathcal{O}(1)$. We define a shorthand for the divergent pieces with general α as

$$\not{\mathcal{D}}_{\alpha,\mathrm{div}} := \widetilde{\mathcal{P}} \left(\not{D} - mc - \frac{i\alpha}{2mc} \not{F} \right) \widetilde{\mathcal{P}} \Big|_{\mathcal{O}(c^2)} \tag{4.46a}$$

$$= c^2 P_+ \left[\frac{1}{8} \partial_{[\mu} n_{\nu]} \left(c\not{n} \gamma^{\mu\nu} - 3\gamma^{\mu\nu} c\not{n} + 8i\alpha\gamma^{\mu\nu} \right) + imc\not{n} - m \right] P_+ \ . \tag{4.46b}$$

The first term in square brackets combines the divergent pieces coming from the spin connection and the non-minimal coupling, as given in eqn. (4.25). The second term is the divergent piece coming from the relativistic background gauge field C, and the last one is the mass term. We start with the terms containing m. After the Milne transformation they become

$$P'_+ \left(imc\not{n}' - m \right) P'_+ \ . \tag{4.47}$$

The projectors shift in the same way as $\not{n}$ does, so the identity $ic\not{n} P_\pm = \pm P_\pm$ which made them cancel in the first place also makes their Milne transformed versions cancel. They thus do not contribute a Milne variation to the $\mathcal{O}(1)$ part.

For the spin connection part and the non-minimal coupling term we use exactly the same argument, and absorb $\not{n}'$ into P'_+. This yields

$$\not{\mathcal{D}}'_{\alpha,\mathrm{div}} = ic^2 \left(\frac{1}{4} + \alpha \right) P'_+ \partial_{[\mu} n'_{\nu]} \gamma^{\mu\nu} P'_+ \tag{4.48a}$$

$$= \not{\mathcal{D}}_{\alpha,\mathrm{div}} - i \left(\frac{1}{4} + \alpha \right) P_+ \partial_{[\mu} \xi_{\nu]} \gamma^{\mu\nu} P_+ + \dots \ , \tag{4.48b}$$

where the dots in the second line denote terms without derivatives of ξ. From eqn. (4.48a) we find that for $\alpha = -\frac{1}{4}$ the variations cancel exactly, in addition to $\not{\mathcal{D}}_{\alpha,\mathrm{div}}$ itself vanishing. We also see now what the implications of that choice of α are when $n \wedge dn = 0$. In that case, $\not{\mathcal{D}}_{\alpha,\mathrm{div}} = 0$ for any choice of α, as can be seen by using (4.27). However, the Milne variation in (4.48b) does *not* vanish: recall that the dots denote terms without derivatives of ξ and can thus not cancel the first term. Since the entire $\not{\mathcal{D}}_\alpha$ still is Milne covariant, this means that $\not{\mathcal{D}}$

transforms with the opposite non-covariant $d\xi$-term. That is, for $\alpha \neq -\frac{1}{4}$ the non-relativistic Dirac operator $\not{\mathcal{D}}$ defined in (4.32) transforms non-covariantly even for $n \wedge dn = 0$, e.g. on flat space with $n = dt$.

Coming back to $\alpha = -\frac{1}{4}$, eqn. (4.48a) shows that the divergent pieces which we canceled on the way from $\not{\mathcal{D}}_\alpha$ to $\not{\mathcal{D}}$ do not contribute a Milne variation. With the analogous statement for the mass-like terms as shown above, this completes the argument that $\not{\mathcal{D}}$ indeed transforms as

$$\not{\mathcal{D}} \to \Big(\mathbb{1} - \frac{i}{2}\not{\xi} P_-\Big)\not{\mathcal{D}}\Big(\mathbb{1} - \frac{i}{2} P_- \not{\xi}\Big) \ . \tag{4.49}$$

We see that the non-relativistic Dirac/Lévy-Leblond operator transforms covariantly, and together with eqn. (4.43) that our non-relativistic Lagrangian (4.33) is thus Milne invariant. As a final remark on Milne invariance, note that we needed a in the non-relativistic Lagrangian and its Milne transformation. This allowed us to separate the spin connection into leading pieces having only n in eqn. (4.10), as opposed to the full $e^{\underline{0}}$, which is crucial for the cancellation of the Milne variations.

4.4.2 Local Galilean transformations

We now come to local Galilean invariance. We will need the induced transformations for the spinor and vielbein, i.e. for spinor and vector representations. The latter are straightforward, while the spinor transformations are a bit more subtle. In the relativistic theory we want to look at a combination of local Lorentz transformations and Milne boosts which leave $\not{n}$ and thus the projectors $P_\pm$ invariant. This particular combination will turn out to induce local Galilean transformations on the non-relativistic objects. Under a local Lorentz transformation we have $\not{n} \to \Lambda_s \not{n} \Lambda_s^{-1}$, and to keep $\not{n}$ invariant, we will compensate with a Milne boost.[4] We start with a Lorentz transformation parametrized by τ as $\Lambda_s = \exp(\tau_{ab}\Sigma^{ab})$, where Σ^{ab}

[4]Milne and local Lorentz transformations leave the norm of n_a invariant and, as we shall see shortly, transform it by subleading terms only, so they can indeed compensate each other.

is a basis of the Lie algebra $\mathfrak{so}(1, d-1)$. We have

$$\not{n} \to e^{\tau_{ab}\Sigma^{ab}} \not{n} e^{-\tau_{ab}\Sigma^{ab}} = \not{n} + [\tau_{ab}\Sigma^{ab}, \not{n}] + \dots \ , \qquad \Sigma^{ab} = \frac{1}{2}\gamma^{ab} \ . \tag{4.50}$$

We start with the infinitesimal transformation, the exponentiated version then works analogously. The antisymmetric parameter matrix τ can be decomposed into

$$\widetilde{\tau}_{ab} = P_a{}^c P_b{}^d \tau_{cd} \ , \qquad \tau_a = 2\tau_{ab} v^b \ , \tag{4.51}$$

such that $\tau_{ab}\Sigma^{ab} = \widetilde{\tau}_{ab}\Sigma^{ab} + \tau_a n_b \Sigma^{ab}$. Note that $\tau_a v^a = 0$. Since $\widetilde{\tau}_{ab}\Sigma^{ab}$ commutes with $\not{n}$, we have

$$\delta_{\mathrm{L}} \not{n} = [\tau_{ab}\Sigma^{ab}, \not{n}] = [\tau_a \Sigma^{ab} n_b, \not{n}] = \frac{1}{2}[\tau_a \widetilde{\gamma}^a \not{n}, \not{n}] = -\frac{1}{c^2}\tau_a \widetilde{\gamma}^a \ . \tag{4.52}$$

To compensate for the change in $\not{n}$ due to the local Lorentz transformation δ_L, we combine it with a Milne boost under which $\delta_{\mathrm{M}} n_\mu = c^{-2}\tau_\mu$, where $\tau_\mu = 2e^a_\mu \tau_{ab} v^b$ is spatial. This works out just as well for the finite transformations. For the Lorentz transformation we simply exponentiate $\tau_{ab}\Sigma^{ab}$. For the Milne boost we use the notation of (4.34) and set $\xi_\mu = \lambda n_\mu + \tau_\mu$ with $\lambda = c^2 - c\sqrt{c^2 + \tau^\mu \tau_\mu}$. We note that only a subset of the quantities transforms under Milne boosts. In particular, the vielbein is invariant and is thus only affected by the local Lorentz transformation. But it is the particular combination of Milne and Lorentz transformations that leaves $\mathcal{P}$ and $\widetilde{\mathcal{P}}$ invariant.

Vector representation and spin connection

We start by recapitulating how a local Lorentz transformation contracts to a local Galilean transformation for the vector representation. We take a Lorentz transformation parametrized

by an orthogonal matrix Λ satisfying $\Lambda^T \eta \Lambda = \eta$, or with explicit indices

$$\Lambda^b{}_a \eta_{bc} \Lambda^c{}_d = \eta_{ad} \ . \tag{4.53}$$

Projecting this on the spatial components shows $n_a \Lambda^a{}_c P_b{}^c \big|_{c\to\infty} = 0$, and we find

$$\Lambda^a{}_b \big|_{c\to\infty} = \widetilde{\Lambda}^a{}_b + \Lambda^a n_b \ , \qquad \widetilde{\Lambda}^a{}_b = P^a{}_c \Lambda^c{}_d P^d{}_b \ , \qquad \Lambda^a = \Lambda^a{}_b v^b \ . \tag{4.54}$$

To make the structure more apparent, we can fix e^a_μ such that $n_a = \delta_{a\underline{0}}$, and then write $\Lambda^a{}_b \big|_{c\to\infty}$ in matrix form as

$$\Lambda^a{}_b \big|_{c\to\infty} = \begin{pmatrix} 1 & 0 \\ \Lambda^i & \widetilde{\Lambda}^i{}_j \end{pmatrix} \ . \tag{4.55}$$

This is the fundamental linear representation of the Galilean group. We can sharpen the fall-off behavior of $\Lambda^{\underline{0}}{}_b$ as follows. From $g = e^{\underline{0}}_\mu e^{\underline{0}}_\nu + e_{\mu i} e^i_\nu = e'^{\underline{0}}_\mu e'^{\underline{0}}_\nu + e'_{\mu i} e'^i_\nu$, we see that boosts only transform the $\mathcal{O}(c^{-2})$ part of $e^{\underline{0}}$, i.e. a in the notation of eqn. (4.8). Note, however, that under the particular linear combination of local Lorentz and Milne transformations we are looking at here (which will give local Galilean transformations), n_μ and $e^{\underline{0}}$ transform in the same way, and thus a is invariant. This is different from [108] – without gauge fixing $e^\mu_{\underline{0}} = v^\mu$, we have the Milne and local Galilean transformations disentangled.

We now come to the spin connection $\hat{\omega}$ defined in eqn. (4.31). To make its structure as a Lie-algebra-valued one-form explicit, we look at

$$\hat{\omega}_\mu{}^a{}_b = \eta^{ac} e^\nu_c \hat{\omega}_{\mu\nu\rho} e^\rho_b \big|_{c\to\infty} \ . \tag{4.56}$$

The only explicit c-dependence on the right hand side of eqn. (4.56) is in η. Due to $n_a \eta^{ac} =$

$\mathcal{O}(c^{-2})$, only $P^a{}_c\hat{\omega}_\mu{}^c{}_b$ has non-vanishing components at $c \to \infty$. More explicitly,

$$\hat{\omega}_\mu{}^a{}_b = \hat{\omega}_{\mu\nu\rho}\,\widetilde{e}^{\nu a}\widetilde{e}^\rho_b + \hat{\omega}_{\mu\nu\rho}\,\widetilde{e}^{\nu a}v^\rho n_b =: \widetilde{\omega}_\mu{}^a{}_b + \varpi_\mu{}^a n_b \ . \tag{4.57}$$

This defines a spin connection for spatial rotations $\widetilde{\omega}$, and ϖ is the boost connection. We note that $n_a\varpi_\mu{}^a = 0$. To make the structure more apparent, we can write eqn. (4.57) for $n_a = \delta_{a\underline{0}}$ as

$$\hat{\omega}_\mu{}^a{}_b = \begin{pmatrix} 0 & 0 \\ \varpi_\mu{}^i & \widetilde{\omega}_\mu{}^i{}_j \end{pmatrix} \ . \tag{4.58}$$

This structure is exactly what we expect for a one-form with values in the Lie algebra of the Galilei group. It immediately implies $D_\mu n_a = \partial_\mu n_a + \hat{\omega}_\mu{}^b{}_a n_b = 0$. We also have $D_\mu h^{ab} = 0$, which makes our connection satisfy the analog of metric compatibility spelled out in [108]. The non-relativistic Christoffel symbols $\dot{\Gamma}^\rho_{\mu\nu}$ can then be defined from $D_\mu e^a_\nu = 0$.

The spinor

To justify calling Ψ defined in (4.20) a non-relativistic spinor, we have to show that it indeed carries a spin representation of the Galilean group. We restrict the discussion to infinitesimal transformations, the exponentiated ones again follow a similar logic. As explained above, we take a local Lorentz transformation accompanied by a Milne boost such that the projectors $P_\pm$ are invariant. The relativistic spinor ψ is Milne invariant, so the transformation $\psi \to \psi + \delta\psi$ is solely due to the Lorentz part

$$\delta\psi = \tau_{ab}\Sigma^{ab} \ , \qquad\qquad \Sigma^{ab} = \frac{1}{2}\gamma^{ab} \ . \tag{4.59}$$

The transformation of Ψ can be derived using (4.20). Separating the time and spatial components using (4.51), we find

$$\delta\Psi = \widetilde{\tau}_{ab}\widetilde{\Sigma}^{ab}\Psi - i\tau_a\widetilde{\gamma}^a\left(c^{-\frac{1}{2}}P_+ - c^{-\frac{3}{2}}P_-\right)\psi\big|_{c\to\infty} , \qquad \widetilde{\Sigma}^{ab} = P_c{}^a P_d{}^b\Sigma^{cd} . \tag{4.60}$$

To get the second term, we have used that $P_\pm\Sigma^{ab}n_b = \Sigma^{ab}n_bP_\mp$, along with $i\not{n}P_\pm = \pm c^{-1}P_\pm$. Note how this mixes the orders in c, and exchanges the projectors for the boosts.[5] Evaluating eqn. (4.60) in the $c\to\infty$ limit leaves only the first term in the parentheses, and we find

$$\delta\Psi = \left[\widetilde{\tau}_{ab}\widetilde{\Sigma}^{ab} - \tau_a\Sigma^a\right]\Psi , \qquad \Sigma^a = \frac{i}{2}\widetilde{\gamma}^aP_+ . \tag{4.61}$$

The $\widetilde{\Sigma}^{ab}$ generate the Lie algebra of $\mathrm{SO}(d-1)$. Furthermore, due to $P_\pm\widetilde{\gamma}^a = \widetilde{\gamma}^aP_\mp$, the Σ^a's commute with each other. The remaining commutator evaluates to

$$\left[\widetilde{\Sigma}^{ab},\Sigma^c\right] = h^{bc}\Sigma^a - h^{ac}\Sigma^b . \tag{4.62}$$

That is precisely the Galilean Lie algebra, and we have thus obtained the Galiliean spin representation, induced by the local Lorentz transformations of ψ on our spinor Ψ as defined in (4.20). This indeed justifies calling it a non-relativistic spinor.

Note that for the construction of that spin representation we did not go through constructing a Clifford algebra for a degenerate space (the tangent space with the inverse spatial metric $h^{\mu\nu}$). This is different from the approach of [109, 100]. What we called $\dot{\gamma}^\mu$ or $v^\mu P_+$ does not square to zero but to itself. The crucial point, however, is that Σ^a still squares to zero and satisfies the commutator relations that the Galilean boost generator satisfies in [109, 100].

---

[5]Note also how it was important to keep the projectors invariant. Otherwise we would get $\Psi \to \Lambda_s\mathcal{P}\Lambda_s^{-1}\Lambda_s\psi = \Lambda_s\Psi$. This would give *only* the spatial rotations at $c\to\infty$, as $\tau_a\widetilde{\gamma}^a$ looses one power in c without exchanging projectors.

Dirac operator

The remaining task is to show that the non-relativistic Dirac operator $\not{\mathcal{D}}$ transforms covariantly under local Galilean transformations. To that end, $\not{\mathcal{D}}_\alpha$ in (4.23) again is a good starting point. We introduce a shorthand X and write

$$\not{\mathcal{D}}_\alpha = \widetilde{\mathcal{P}} X \widetilde{\mathcal{P}}\Big|_{c\to\infty} , \qquad\qquad X = \not{D} - mc - \frac{i\alpha}{2mc}\not{F} . \tag{4.63}$$

X is invariant under Milne boosts, and since the relativistic covariant derivative transforms covariantly under local Lorentz transformations, $\delta\not{D} = [\tau_{ab}\Sigma^{ab}, \not{D}]$, we have $\delta X = [\tau_{ab}\Sigma^{ab}, X]$. We thus find

$$\delta\not{\mathcal{D}}_\alpha = \widetilde{\mathcal{P}}[\tau_{ab}\Sigma^{ab}, X]\widetilde{\mathcal{P}}\Big|_{c\to\infty} = [\widetilde{\tau}_{ab}\widetilde{\Sigma}^{ab}, \not{\mathcal{D}}_\alpha] + \tau_a\overline{\Sigma}^a\not{\mathcal{D}}_\alpha + \not{\mathcal{D}}_\alpha\tau_a\Sigma^a , \tag{4.64}$$

where $\overline{\Sigma}^a = \gamma^{\underline{0}}(\Sigma^a)^\dagger\gamma_{\underline{0}}$. The transformation (4.64) is precisely how a non-relativistic Dirac operator should change under local Galilean transformations to get an invariant Lagrangian, noting that $\delta\overline{\Psi} = -\overline{\Psi}(\tau_a\overline{\Sigma}^a + \widetilde{\tau}_{ab}\widetilde{\Sigma}^{ab})$.

To show that $\not{\mathcal{D}}$ transforms correctly we once again have to check that the transformations of the divergent pieces canceled on the way from $\not{\mathcal{D}}_\alpha$ to $\not{\mathcal{D}}$ do not pollute the $\mathcal{O}(1)$ part. This boils down to almost the same argument as given in sec. 4.4.1 for the Milne boosts. This time, however, $\not{n}$ and P_+ are both invariant. The analog of (4.48a), i.e. the transformation of the divergent parts in $\not{\mathcal{D}}_\alpha$, but now under the particular combination of Milne boost and local Lorentz transformation, reads

$$\not{\mathcal{D}}'_{\alpha,\mathrm{div}} = ic^2\left(\frac{1}{4} + \alpha\right) P_+\partial_{[\mu}n'_{\nu]}\gamma'^{\mu\nu}P_+ . \tag{4.65}$$

Note that P_+ and $\not{n}$ do not transform, but n_μ and the inverse vielbeine in $\gamma^{\mu\nu}$ do. We see that the variations cancel just in the same way as they did for Milne boosts when $\alpha = -\frac{1}{4}$ – the point is that $P_\pm$ and $\not{n}$ still transform the same way. For $\alpha \neq -\frac{1}{4}$, $\partial_{[\mu}n'_{\nu]}$ again produces

a $d\xi$ term at $\mathcal{O}(1)$, even if $n \wedge dn = 0$. So we once again need $\alpha = -\frac{1}{4}$, and then find

$$\delta \not{\mathcal{D}} = [\widetilde{\tau}_{ab}\widetilde{\Sigma}^{ab}, \not{\mathcal{D}}] + \tau_a \overline{\Sigma}^a \not{\mathcal{D}} + \not{\mathcal{D}} \tau_a \Sigma^a \ , \tag{4.66}$$

as needed to have the non-relativistic Lagrangian (4.33) invariant.

We note that $(\dot{\gamma}^\mu + \widetilde{\gamma}^\mu)\mathcal{D}_\mu$ alone transforms covariantly under spatial rotations. This is because the additional pieces in $\not{\mathcal{D}}$ transform covariantly by themselves, and spatial rotations do not alter the cancellation of the $n \wedge dn$ divergent pieces. However, for the local Galilean boosts which arise as combination of local Lorentz and Milne transformations, we do require the non-minimal coupling term to get covariant transformation of the $\mathcal{O}(1)$ part alone.

In summary, we have shown that each of the pieces in the non-relativistic Lagrangian (4.33) transforms covariantly under local Galilean transformations, and we thus have an invariant Lagrangian. The local Galilean transformations arise from the relativistic theory as combination of Milne boosts and local Lorentz transformations such that $\not{n}$ and thus the projectors $P_\pm$ are invariant. This combination is different from Milne boosts alone: the latter act on the "metric data" and leave the vielbein invariant, while the former act on the vielbein and "frame data". We note that these statements depart from those in [108], where Milne transformations were identified with Galilean boosts. Having Milne and Galilean transformations as separate invariances seems to make sense from a general perspective: Milne boosts reflect the gauge redundancy in splitting the cotangent space into time and spatial directions, via v, while the local Galilean symmetries reflect the gauge redundancy in choosing a section in the frame bundle, which is a different geometric object. Technically, the reason we can see the two invariances separately is that we did not gauge fix $e^\mu_{\underline{0}} = v^\mu$. Upon imposing that choice, our constructions for the frame data agree with [108].

4.5 Causal spacetimes

We now specialize to causal spacetimes and derive a Lagrangian for the dynamical fields alone from the general non-relativistic Lagrangian (4.33). By causal spacetimes we mean

Newton-Cartan backgrounds with $n \wedge dn = 0$, ensuring that a foliation in terms of constant-time hypersurfaces exists. As seen in eqn. (4.32), the equation of motion for $\Psi_- := P_-\Psi$ does not have a time derivative and is a constraint equation. One can then integrate Ψ_- out and write a Lagrangian purely in terms of $\Psi_+ := P_+\Psi$. This obscures the structure and part of the symmetries but allows for easier comparison to some of the existing literature.

To facilitate the computations, we split the derivative part of $\not{\mathcal{D}}$ as

$$(\dot{\gamma}^\mu + \widetilde{\gamma}^\mu)\,\mathcal{D}_\mu =: \not{D}_s + \not{D}_t \ , \tag{4.67}$$

such that $[\not{D}_t, \not{n}] = 0$ and $\{\not{D}_s, \not{n}\} = 0$, and thus $[\not{D}_t, P_\pm] = 0$ and $\not{D}_s P_\pm = P_\mp \not{D}_s$. The explicit expressions are

$$\not{D}_{\rm s} = \widetilde{\gamma}^\mu \left[\partial_\mu + \frac{1}{4}\hat{\omega}_{\mu\nu\rho}\widetilde{\gamma}^{\nu\rho} - imA_\mu\right] \ , \quad \not{D}_{\rm t} = \dot{\gamma}^\mu \left[\partial_\mu + \frac{1}{4}(\hat{\omega}_{\mu\nu\rho} + 2\hat{\omega}_{\nu\rho\mu})\widetilde{\gamma}^\nu\widetilde{\gamma}^\rho - imA_\mu\right] \ . \tag{4.68}$$

These are defined out of convenience for the split into "chiral" components, and we leave a check of their transformation properties for the future. So far with no extra assumptions, we then find for the non-relativistic Lagrangian (4.33)

$$\begin{aligned} L_{\rm nr} = {} & i\overline{\Psi}_+\left[\not{D}_{\rm t} + \frac{i}{8}\not{F}^{(A)}\right]\Psi_+ + i\overline{\Psi}_-\left[\not{D}_{\rm s} + \frac{1}{4}T^{\rm c}_\mu\widetilde{\gamma}^\mu\right]\Psi_+ \\ & + i\overline{\Psi}_+\left[\not{D}_{\rm s} + \frac{3}{4}T^{\rm c}_\mu\widetilde{\gamma}^\mu\right]\Psi_- - i\overline{\Psi}_-\left[2m + \frac{i}{4}\not{T}^{\rm c}\right]\Psi_- + \text{c.c.} \ , \end{aligned} \tag{4.69}$$

where $\not{F}^{(A)} = F^{(A)}_{\mu\nu}\widetilde{\gamma}^{\mu\nu}$, analogously $\not{T}^{\rm c} = T^{\rm c}_{\mu\nu}\widetilde{\gamma}^{\mu\nu}$, and $T^{\rm c}_\mu = T^{\rm c}_{\mu\nu}v^\nu$. We now exploit the simplifications that are specific to causal spacetimes. From eqn. (4.27), we see that the torsion coupling $\overline{\Psi}_-\not{T}^{\rm c}\Psi_-$ in (4.69) drops out in causal spacetimes. We can then solve the Ψ_- equation of motion for Ψ_-, which yields

$$\Psi_- = \frac{1}{2m}\left[\not{D}_{\rm s} + \frac{1}{4}T^{\rm c}_\mu\widetilde{\gamma}^\mu\right]\Psi_+ \ . \tag{4.70}$$

Substituting this back into the Lagrangian (4.69), we find an expression purely in terms of Ψ_+. Namely,

$$L_{\rm nr} = i\overline{\Psi}_+\Big[\not{D}_{\rm t} + \frac{i}{8}\not{F}^{(A)}\Big]\Psi_+ + \frac{i}{2m}\overline{\Psi}_+\Big[\not{D}_{\rm s} + \frac{3}{4}T^{\rm c}_\mu\widetilde{\gamma}^\mu\Big]\Big[\not{D}_{\rm s} + \frac{1}{4}T^{\rm c}_\mu\widetilde{\gamma}^\mu\Big]\Psi_+ + \text{c.c.}\ . \tag{4.71}$$

We note that the "chirality" of Ψ_+ is not preserved by local Galilean boosts or Milne boosts. This can be seen explicitly from eqns. (4.43) and (4.61), which show that either of the boosts produces a negative chirality piece from a positive chirality spinor. Thus, the split into chiralities depends on the chosen frame, which makes the full non-relativistic Lagrangian (4.33) more appealing. What remains a symmetry of (4.71) is a combination of local Galilean transformations and Milne boosts, where ζ_μ, parametrizing the Milne boost, is related to τ_a parametrizing a local Galilean boost, such that ψ is invariant.[6]

4.5.1 Implications for flat space

As an illustrative example, we spell out the non-relativistic Lagrangian and Dirac operator explicitly for a flat Newton-Cartan spacetime, by which we mean $n = dt$ and $h^{-1} = \delta^{ij}\partial_i \otimes \partial_j$. To get this structure from a non-relativistic limit we choose $g = -c^2dt^2 + d\vec{x}^2$ and $n = dt$. We also fix the vielbein to $e^a_\mu = \delta^a_\mu$, which completely fixes the local Lorentz symmetry in the relativistic theory and correspondingly the local Galilean symmetry in the non-relativistic limit. The global symmetries are those combinations of diffeomorphisms and Galilean transformations which leave the Newton-Cartan structure and the chosen frame invariant. These choices also fix $a = 0$ from (4.8). The non-relativistic Lagrangian (4.33)

[6] In the language of sec. 4.4.1, the reason for not having all symmetries realized is that the second criterion is not met: disposing of Ψ_-, to have a Lagrangian in terms of Ψ_+ only, leaves Ψ_+ as just a spinor with half as many components, as opposed to being defined from Ψ with an explicit projector P_+ as before. With the projector implicit, the identity $ic\not{n}\Psi_+ = \Psi_+$, which we need to show that the divergences cancel, is not preserved by (4.34).

becomes

$$L_{\rm nr} = i\overline{\Psi}\left[(\dot{\gamma}^\mu + \widetilde{\gamma}^\mu)\,(\partial_\mu - imA_\mu) - 2mP_- + \frac{i}{8}F^{(A)}_{\mu\nu}\widetilde{\gamma}^{\mu\nu}P_+\right]\Psi + \text{c.c.}\ . \tag{4.72}$$

We see that, not quite surprisingly, all the extra torsion couplings have dropped out. The non-minimal coupling to the background gauge field, however, is still present. Solving for Ψ_- once again yields eqn. (4.71), which for the flat case reads

$$L_{\rm nr} = \overline{\Psi}_+\Big[v^\mu\,(\partial_\mu - imA_\mu) - \frac{1}{8}\not{F}^{(A)}\Big]\Psi_+ + \frac{i}{2m}\overline{\Psi}_+\Big[\widetilde{\gamma}^\mu\,(\partial_\mu - imA_\mu)\Big]^2\Psi_+ + \text{c.c.}\ . \tag{4.73}$$

Note that the coupling to $\not{F}^{(A)}$ in the first term is the result of the non-minimal coupling term in (4.15) with $\alpha = -\frac{1}{4}$. Evaluating the squared spatial Dirac operator in the second term yields, as usual, a Laplace operator (the spatial one in this case) and a coupling to the gauge field strength

$$[\widetilde{\gamma}^\mu\,(\partial_\mu - imA_\mu)]^2 = \triangle_{\rm s} - \frac{im}{2}\widetilde{\gamma}^{\mu\nu}F^{(A)}_{\mu\nu}\ , \qquad \triangle_{\rm s} = h^{\mu\nu}(\partial_\mu - imA_\mu)(\partial_\nu - imA_\nu)\ . \tag{4.74}$$

The analog in curved backgrounds would have additional curvature and torsion couplings.[7] In flat space the non-relativistic Lagrangian simply becomes

$$L_{\rm nr} = \overline{\Psi}_+ v^\mu\,(\partial_\mu - imA_\mu)\,\Psi_+ + \frac{i}{2m}\overline{\Psi}_+\,\triangle_{\rm s}\,\Psi_+ + \frac{1}{8}\overline{\Psi}_+\widetilde{\gamma}^{\mu\nu}F^{(A)}_{\mu\nu}\Psi_+ + \text{c.c.}\ . \tag{4.75}$$

The crucial feature of this Lagrangian is the magnetic coupling to $\widetilde{\gamma}^{\mu\nu}F^{(A)}_{\mu\nu}$. Had we started with just a free Dirac field, without the non-minimal coupling term in eqn. (4.15), the coefficient of $\overline{\Psi}_+\widetilde{\gamma}^{\mu\nu}F^{(A)}_{\mu\nu}\Psi_+$ would be $\frac{1}{4}$, which is just the contribution from eqn. (4.74) corresponding to the familiar relativistic gyromagnetic ratio $g=2$. The effect of the non-minimal coupling with $\alpha = -\frac{1}{4}$ in the non-relativistic theory is to reduce this coupling to $\frac{1}{8}$,

[7] In fact, one would conveniently define the curvatures from this sort of relation. That is, write $\not{\mathcal{D}} =: (\dot{\gamma}^\mu + \widetilde{\gamma}^\mu)\hat{\mathcal{D}}_\mu$ and then define spatial and boost curvature and torsion along the lines of $[\hat{\mathcal{D}}_\mu, \hat{\mathcal{D}}_\nu] =: R^{ab}_{\mu\nu}\widetilde{\Sigma}_{ab} + R^a_{\mu\nu}\Sigma_a + T^a_{\mu\nu}(\widetilde{\gamma}_a + \dot{\gamma}_a)$.

corresponding to $g=1$. We thus explicitly see how demanding either consistency in generic backgrounds or Milne invariance in any background has striking implications even for flat space. We note that the preferred value of g for which we find the full symmetry realized is precisely $g = 2s$, where $s = \frac{1}{2}$ is the spin.

4.6 Three-dimensional spacetimes

In sec. 4.3 we saw that the divergences in the spin connection part can not in general be canceled by a modification of the gauge field (4.18), and we thus needed the non-minimal coupling term with $\alpha = -\frac{1}{4}$. This was because the divergences in $\not{C}$ and Ω have different Clifford algebra structures. The antisymmetric product of k γ-matrices is generically related to an antisymmetric product of $d-k$ ones in d dimensions, by a form of Hodge duality. This turns out to make a difference precisely for $d=3$. In our conventions we have

$$\gamma_{\mu\nu\rho} = \pm c\epsilon_{\mu\nu\rho}\mathbb{1} \ , \tag{4.76}$$

where $\epsilon_{\mu\nu\rho} = \det(e)\,\varepsilon_{\mu\nu\rho}$ and $\varepsilon_{\mu\nu\rho} = \pm 1, 0$. Note that $\det(e) = \sqrt{\det \boldsymbol{\gamma}}$, where $\boldsymbol{\gamma}_{\mu\nu} = n_\mu n_\nu + h_{\mu\nu}$ was used to define the volume form in sec. 4.3. Therefore, $\epsilon_{\mu\nu\rho}$ is $\mathcal{O}(1)$ at $c\to\infty$ and we have an explicit factor of c on the right hand side of eqn. (4.76). The sign is a matter of convention and we pick the positive one. We then immediately get $\gamma^{\mu\nu} = c\epsilon^{\mu\nu\rho}\gamma_\rho$. With this identity we can further evaluate the divergence in the spin connection part included in eqn. (4.25), which in $d=3$ becomes

$$\widetilde{\mathcal{P}}\Omega\widetilde{\mathcal{P}}\Big|_{\mathcal{O}(c^2)} = \frac{ic^2}{4}(\star dn)_\mu\, P_+ c\gamma^\mu P_+ \ , \qquad\qquad (\star dn)_\mu = \epsilon_\mu{}^{\nu\rho}\partial_\nu n_\rho \ . \tag{4.77}$$

The indices of $\epsilon_\mu{}^{\nu\rho}$ in the definition of $\star dn$ are raised with the relativistic metric. This divergence has the same Clifford algebra structure as the terms resulting from the $\not{C}$ term in the relativistic Lagrangian, and modifying C thus is an additional option now to cancel

the divergences. There are two candidate terms, and our ansatz for the gauge field is

$$C_\mu = -mc^2\left(n_\mu + f_1(\star dn)_\mu + f_2\mathcal{B}n_\mu\right) + mA_\mu \ , \qquad \mathcal{B} = \frac{1}{\det e}\varepsilon^{\alpha\beta\gamma}n_\alpha\partial_\beta n_\gamma \ , \tag{4.78}$$

where f_1 and f_2 are functions of n and its derivatives. Note that both extra terms agree at leading order in c, due to $v^\mu(\star dn)_\mu = -c^2\epsilon^{\alpha\beta\gamma}n_\alpha\partial_\beta n_\gamma = \mathcal{B}$. As far as canceling the divergent piece is concerned, they are thus equally useful. However, they are different in the subleading orders. The form of the non-relativistic Lagrangian will depend on the relative strength of f_1 and f_2, but the difference merely corresponds to a redefinition of the non-relativistic gauge field. This can be seen by noting that, with $f_+ := f_1 + f_2$ and $\mathcal{T}_\mu := \epsilon_{\mu\nu\rho}v^\rho h^{\nu\sigma}T^{\mathrm{c}}_\sigma$,

$$C_\mu = -mc^2 n_\mu\left(1 + f_+\mathcal{B}\right) + m\mathcal{A}_\mu \ , \qquad \mathcal{A}_\mu = A_\mu + f_1\mathcal{T}_\mu \ . \tag{4.79}$$

Note that $v^\mu\mathcal{T}_\mu = 0$. We will include the non-minimal coupling term with generic α and determine f_+ from the requirement that $\widetilde{\mathcal{P}}(\not{D} - mc - \frac{i\alpha}{2mc}\not{F})\widetilde{\mathcal{P}}$ be finite. To find the non-relativistic Dirac operator with these extra parameters, we need to calculate the individual pieces again. For the spin connection part we find, using $\widetilde{\gamma}^{\mu\nu}T^c_{\mu\nu} = 2\mathcal{B}c\not{n}$,

$$\widetilde{\mathcal{P}}\Omega\widetilde{\mathcal{P}} = \frac{1}{4}\mathcal{B}(c^2P_+ + P_-) + (\dot{\gamma}^\mu + \widetilde{\gamma}^\mu)\frac{1}{4}\dot{\omega}_{\mu\nu\rho}\left(\widetilde{\gamma}^{\nu\rho} + 2\widetilde{\gamma}^\nu\dot{\gamma}^\rho\right) + \frac{1}{2}\widetilde{\gamma}^\mu T^{\mathrm{c}}_\mu \ , \tag{4.80}$$

Here and in the next two equations, contributions which vanish when $c \to \infty$ have been dropped. For the remaining parts of the derivative we find

$$\begin{aligned}\widetilde{\mathcal{P}}\left[\gamma^\mu\left(\partial_\mu - iC_\mu\right)\right]\widetilde{\mathcal{P}} = (\dot{\gamma}^\mu + \widetilde{\gamma}^\mu)\left(\partial_\mu + \frac{1}{2}(\partial_\mu a_b)e^b_\nu n_\rho\widetilde{\gamma}^\nu\dot{\gamma}^\rho - imA_\mu\right) \\ + m(1 + f_+\mathcal{B})\left(c^2P_+ - P_-\right) \ .\end{aligned} \tag{4.81}$$

Evaluating the mass term is straightforward, and the only non-trivial information we still need is the non-minimal coupling term, which evaluates to

$$\begin{aligned}\widetilde{\mathcal{P}}\Big(-\frac{i\alpha}{2mc}\not{F}\Big)\widetilde{\mathcal{P}} = \alpha\mathcal{B}\,(1+f_+\mathcal{B})\left(c^2P_+ - P_-\right) + i\alpha\,(1+f_+\mathcal{B})\,T^c_{\mu\nu}\,(\dot\gamma^\mu\widetilde\gamma^\nu + \widetilde\gamma^\mu\dot\gamma^\nu) \\ -\frac{i\alpha}{2}\not{F}^{(\mathcal{A})}P_+ + \alpha\widetilde\gamma^\mu(P_+ - P_-)\partial_\mu(f_+\mathcal{B})\ .\end{aligned} \tag{4.82}$$

Note that $F^{(\mathcal{A})} = d\mathcal{A}$ is the field strength of the modified gauge field $\mathcal{A}$. Demanding the divergent pieces in $\widetilde{\mathcal{P}}(\not{D} - mc - \frac{i\alpha}{2mc}\not{F})\widetilde{\mathcal{P}}$ to cancel can now be seen to imply

$$f_+ = -\frac{\alpha+\frac{1}{4}}{m+\alpha\mathcal{B}}\ . \tag{4.83}$$

With that relation we see that the divergences cancel and that there are no $\mathcal{O}(c)$ subleading divergences. Using eqn. (4.83) we can assemble the non-relativistic Dirac operator $\not{\mathcal{D}}$, which now is $\not{\mathcal{D}}_\alpha$ with generic α, expressed in terms of Newton-Cartan data. This yields

$$\begin{aligned}\not{\mathcal{D}} = (\dot\gamma^\mu + \widetilde\gamma^\mu)\,\mathcal{D}^{(\mathcal{A})}_\mu - 2mP_- - \frac{i\alpha}{2}\not{F}^{(\mathcal{A})}P_+ + \frac{1}{2}\widetilde\gamma^\mu T^{\rm c}_\mu + \frac{1}{2}\mathcal{B}P_- \\ + i\alpha(1+f_+\mathcal{B})T^c_{\mu\nu}\,(\dot\gamma^\mu\widetilde\gamma^\nu + \widetilde\gamma^\mu\dot\gamma^\nu) + \alpha\widetilde\gamma^\mu(P_+ - P_-)\partial_\mu(f_+\mathcal{B})\ ,\end{aligned} \tag{4.84}$$

where the superscripts on $\mathcal{D}_\mu$ and F indicate that we have replaced A_μ by $\mathcal{A}_\mu$. The derivative $\mathcal{D}_\mu$ was defined in eqn. (4.32b), and the slashed quantities below eqn. (4.69). On causal spacetimes, where $\mathcal{B} = 0$, we have $-mf_+ = \alpha + \frac{1}{4} =: \alpha_+$. The non-relativistic Lagrangian once again is

$$L_{\rm nr} = i\overline\Psi\not{\mathcal{D}}\Psi + \text{c.c.}\ . \tag{4.85}$$

The arguments for invariance under local Galilean transformations and Milne boosts proceed along the lines given in sec. 4.4. The divergent pieces cancel again exactly, leaving the symmetry transformations induced from the relativistic ones as symmetries of the non-relativistic Lagrangian. We will see below, however, that the transformations are altered. We have thus

obtained the fully covariant version of the Lagrangian studied in [103], where e.g. a Milne frame was fixed and local Galilean invariance was not obvious. To complete the discussion, we note that α_+ is related to the gyromagnetic ratio g by $4\alpha_+ = g - 1$. On spacetimes with $n \wedge dn = 0$ we can integrate out the Ψ_- part of the two-component spinor Ψ, as shown in the previous section, to obtain a Lagrangian for the one-component field Ψ_+ only. This is the language used in [103].

We now come to the transformation properties under Milne boosts and local Galilean transformations. The only quantity for which the transformation changes is the non-relativistic gauge field A. Due to the difference in the leading term in eqn. (4.78) as compared to eqn. (4.18), the shifts of n by a subleading part according to eqn. (4.34) result in a different behavior. To match the transformations to [107], we set $\mathcal{B} = 0$ *after* the variations are performed. We then find

$$A_\mu \to A_\mu - \xi_\mu - f_2 n_\mu \epsilon^{\nu\rho\sigma} \partial_\nu (n_\rho \xi_\sigma) - (f_1 + 2f_2) n_\mu \epsilon^{\nu\rho\sigma} n_\nu \partial_\rho \xi_\sigma \ . \tag{4.86}$$

This reduces to $A \to A - \xi$ as given in eqn. (4.41) for $\alpha_+ = f_1 = f_2 = 0$, or $g = 1$. Upon identifying g_1 with $f_1 + 2f_2$ and g_2 with f_2, (4.86) are the modified Milne variations corresponding to the two different non-relativistic magnetic moment terms discussed in [107]. For $\mathcal{B} \neq 0$ the expressions are more bulky, but the structure is the same. We thus find that both transformations can be realized as symmetries in a non-relativistic limit, and we are not restricted to the linear combination with $g_1 = -2g_2$ discussed in [107]. The fields were assigned trivial transformation under Milne boosts in [107], and we can understand this from our perspective as follows: when eliminating Ψ_- by its equation of motion, as done in sec. 4.5, we found that the remaining symmetry is a combination of Milne boosts and local Galilean transformations, precisely such that Ψ is invariant.

The magnetic moment term proportional to g_2 was shown in sec. 2.7 of [105] to reproduce the anomalous diffeomorphisms found for $g \neq 1$ in [103] as follows. The analysis of [103] should be understood as working in a fixed Milne frame. Splitting coordinates into (x^0,

x^i) as in [103], it is fixed to $v = e^{\Phi}\partial_0$ and we have $h = g_{ij}dx^i \otimes dx^j$. Now the combined transformation of v under a diffeomorphism generated by a vector field X and a Milne boost is $\delta v = \mathcal{L}_X v + \zeta$, or

$$\delta v^\mu = X^\nu \partial_\nu v^\mu - v^\nu \partial_\nu X^\mu + \zeta^\mu \ . \tag{4.87}$$

To compensate the change in Milne frame brought about by a diffeomorphism, i.e. to keep $v^i = 0$, it has to be accompanied by a Milne boost with $\zeta_\mu = h_{\mu\nu} v^\rho \partial_\rho X^\nu$. The combined diffeomorphism and Milne transformations with $\zeta_\mu = h_{\mu\nu} v^\rho \partial_\rho X^\nu$ are then the symmetries discussed in [103].

As a last remark we note that, since local Galilean transformations were induced from the relativistic theory as a combination of Milne boosts and local Lorentz transformations, having $g \neq 1$ also changes the behavior under local Galilean transformations.

4.7 Discussion

We have given a procedure to construct covariant non-relativistic Lagrangians for spinor fields in general Newton-Cartan backgrounds from relativistic parents. As emphasized already in [102], spin is tied intrinsically to the spacetime symmetries also in the non-relativistic setting, as opposed to factoring off as internal symmetry. For a given Newton-Cartan structure (n, h^{-1}), one constructs a pseudo-Riemann metric (4.3) and our limiting procedure gives the non-relativistic Lagrangian (4.33) with the non-relativistic Dirac/Lévy-Leblond operator (4.32). This Lagrangian has all desired invariances – invariance under local Galilean transformations, Milne boosts, U(1) transformations and the symmetries of the Newton-Cartan structure – and the individual objects transform covariantly. For that result it was crucial to insist on having a non-trivial limit also for acausal Newton-Cartan spacetimes with non-vanishing $n \wedge dn$. There is no need to identify local Galilean with Milne boosts in our construction, and under diffeomorphisms all quantities transform covariantly. Upon gauge fixing, this setting can be specialized to recover previous results: fixing the timelike part of

the inverse vielbein to v links local Galilean to Milne boosts, as done in [108], and fixing a Milne frame reproduces the diffeomorphisms of [103]. The non-relativistic spinor fields have as many components as a relativistic Dirac spinor, in accordance with [102, 109, 100]. Half of the components are auxiliary fields and substituting them by their on-shell values retains half of the degrees of freedom as dynamical fields, but obscures some of the symmetries. This connects our results to the language used in part of the more recent literature.

In order to have the entire set of symmetries realized without restricting the number of spacetime dimensions, we needed to include a non-minimal coupling term in the relativistic parent with a specific strength. This results in the non-relativistic spinor coupling with gyromagnetic ratio $g = 1$. An exception occurs for three-dimensional spacetimes. In three dimensions, generic g is possible, but $g \neq 1$ results in modified Milne transformations, which upon gauge fixing reproduces the anomalous diffeomorphisms found in earlier approaches. We did not specifically study the two-dimensional case, but expect that generic g will be possible then without anomalous transformations. For dimensions greater than three, our construction requires $g = 1$, unless part of the symmetries are sacrificed along with the existence of a non-trivial limit when $n \wedge dn \neq 0$. These results suggest a dependence on the chosen Milne frame when $g \neq 1$.

An immediate generalization of the constructions laid out in this work is to include torsion in the relativistic parent theory. The Newton-Cartan structure (n, h^{-1}) can be and has been equipped with a connection as extra structure, although somewhat implicitly. Our construction started in the relativistic theory with the Levi-Civita connection, which gave a non-relativistic connection without spatial torsion in the $c \to \infty$ limit. Including torsion in the parent theory would generalize this. Another forward direction is to take our theory as starting point for an investigation of anomalies in an intrinsically non-relativistic setting, without resorting to a relativistic parent and null reduction [110, 111]. Finally, we mention the construction of supermultiplets for Newton-Cartan supergravity theories in [112, 113]. Our limiting procedure may help to implement a non-relativistic limit for the fermionic fields directly in relativistic supergravities, to obtain the transformation laws and dynamics

for Newton-Cartan supergravities in a very direct way from known relativistic theories.

BIBLIOGRAPHY

[1] J. M. Maldacena, *The Large N limit of superconformal field theories and supergravity*, *Int. J. Theor. Phys.* **38** (1999) 1113–1133, [hep-th/9711200].

[2] O. Aharony, S. S. Gubser, J. M. Maldacena, H. Ooguri and Y. Oz, *Large N field theories, string theory and gravity*, *Phys.Rept.* **323** (2000) 183–386, [hep-th/9905111].

[3] E. D'Hoker and D. Z. Freedman, *Supersymmetric gauge theories and the AdS/CFT correspondence*, hep-th/0201253.

[4] E. Witten, *Anti-de Sitter space and holography*, *Adv. Theor. Math. Phys.* **2** (1998) 253–291, [hep-th/9802150].

[5] J. Casalderrey-Solana, H. Liu, D. Mateos, K. Rajagopal and U. A. Wiedemann, *Gauge/string duality, hot QCD and heavy ion collisions*, 1101.0618.

[6] M. Ammon and J. Erdmenger, *Gauge/Gravity Duality: Foundations and Applications*. Cambridge University Press, 2015.

[7] H. Nastase, *Introduction to AdS-CFT*, 0712.0689.

[8] A. V. Ramallo, *Introduction to the AdS/CFT correspondence*, *Springer Proc. Phys.* **161** (2015) 411–474, [1310.4319].

[9] R. C. Myers, *Dielectric branes*, *JHEP* **12** (1999) 022, [hep-th/9910053].

[10] S. Lee, S. Minwalla, M. Rangamani and N. Seiberg, *Three point functions of chiral operators in D = 4, N=4 SYM at large N*, *Adv. Theor. Math. Phys.* **2** (1998) 697–718, [hep-th/9806074].

[11] D. Z. Freedman, S. D. Mathur, A. Matusis and L. Rastelli, *Correlation functions in the CFT(d) / AdS(d+1) correspondence*, *Nucl. Phys.* **B546** (1999) 96–118, [hep-th/9804058].

[12] D. T. Son and A. O. Starinets, *Minkowski space correlators in AdS / CFT correspondence: Recipe and applications*, *JHEP* **09** (2002) 042, [hep-th/0205051].

[13] S. de Haro, S. N. Solodukhin and K. Skenderis, *Holographic reconstruction of spacetime and renormalization in the AdS/CFT correspondence*, *Commun. Math. Phys.* **217** (2001) 595–622, [hep-th/0002230].

[14] K. Skenderis, *Lecture notes on holographic renormalization*, *Class. Quant. Grav.* **19** (2002) 5849–5876, [hep-th/0209067].

[15] J. I. Kapusta and C. Gale, *Finite-Temperature Field Theory*. Cambridge University Press, second ed., 2006.

[16] E. Witten, *Anti-de Sitter space, thermal phase transition, and confinement in gauge theories*, *Adv. Theor. Math. Phys.* **2** (1998) 505–532, [hep-th/9803131].

[17] S. S. Gubser, I. R. Klebanov and A. W. Peet, *Entropy and temperature of black 3-branes*, *Phys. Rev.* **D54** (1996) 3915–3919, [hep-th/9602135].

[18] C. P. Burgess, N. R. Constable and R. C. Myers, *The Free energy of N=4 superYang-Mills and the AdS / CFT correspondence*, *JHEP* **08** (1999) 017, [hep-th/9907188].

[19] E. Shuryak, *Why does the quark gluon plasma at RHIC behave as a nearly ideal fluid?*, *Prog. Part. Nucl. Phys.* **53** (2004) 273–303, [hep-ph/0312227].

[20] E. V. Shuryak, *What RHIC experiments and theory tell us about properties of quark-gluon plasma?*, *Nucl. Phys.* **A750** (2005) 64–83, [hep-ph/0405066].

[21] D. Bak, A. Karch and L. G. Yaffe, *Debye screening in strongly coupled $\mathcal{N} = 4$ supersymmetric Yang-Mills plasma*, *JHEP* **0708** (2007) 049, [0705.0994].

[22] S. S. Gubser and A. Karch, *From gauge-string duality to strong interactions: a pedestrian's guide*, *Ann.Rev.Nucl.Part.Sci.* **59** (2009) 145–168, [0901.0935].

[23] A. Karch, *Recent Progress in Applying Gauge/Gravity Duality to Quark-Gluon Plasma Physics*, 1108.4014.

[24] C. P. Herzog, A. Karch, P. Kovtun, C. Kozcaz and L. G. Yaffe, *Energy loss of a heavy quark moving through N=4 supersymmetric Yang-Mills plasma*, *JHEP* **07** (2006) 013, [hep-th/0605158].

[25] A. O. Starinets, *Quasinormal modes of near extremal black branes*, *Phys. Rev.* **D66** (2002) 124013, [hep-th/0207133].

[26] P. M. Chesler and L. G. Yaffe, *Horizon formation and far-from-equilibrium isotropization in supersymmetric Yang-Mills plasma*, *Phys.Rev.Lett.* **102** (2009) 211601, [0812.2053].

[27] P. M. Chesler and L. G. Yaffe, *Numerical solution of gravitational dynamics in asymptotically anti-de Sitter spacetimes*, *JHEP* **07** (2014) 086, [1309.1439].

[28] P. M. Chesler and L. G. Yaffe, *Holography and colliding gravitational shock waves in asymptotically AdS_5 spacetime*, *Phys.Rev.Lett.* **106** (2011) 021601, [1011.3562].

[29] P. M. Chesler and W. van der Schee, *Early thermalization, hydrodynamics and energy loss in AdS/CFT*, *Int. J. Mod. Phys.* **E24** (2015) 1530011, [1501.04952].

[30] S. A. Hartnoll, *Lectures on holographic methods for condensed matter physics*, *Class. Quant. Grav.* **26** (2009) 224002, [0903.3246].

[31] J. McGreevy, *Holographic duality with a view toward many-body physics*, *Adv. High Energy Phys.* **2010** (2010) 723105, [0909.0518].

[32] J. F. Fuini, III and A. Karch, *Energy Loss Calculations of Moving Defects for General Holographic Metrics*, *Phys. Rev.* **D85** (2012) 066006, [1112.2747].

[33] S. Gubser, I. R. Klebanov and A. M. Polyakov, *Gauge theory correlators from noncritical string theory*, *Phys.Lett.* **B428** (1998) 105–114, [hep-th/9802109].

[34] S. Janiszewski and A. Karch, *Moving Defects in AdS/CFT*, *JHEP* **1111** (2011) 044, [1106.4010].

[35] C. P. Herzog, A. Karch, P. Kovtun, C. Kozcaz and L. G. Yaffe, *Energy loss of a heavy quark moving through $N = 4$ supersymmetric Yang-Mills plasma*, *JHEP* **07** (2006) 013, [hep-th/0605158].

[36] C. P. Herzog, *Energy loss of heavy quarks from asymptotically AdS geometries*, *JHEP* **09** (2006) 032, [hep-th/0605191].

[37] S. Janiszewski, *Perturbations of moving membranes in AdS_7*, 1112.0085.

[38] A. Karch and E. Katz, *Adding flavor to AdS / CFT*, *JHEP* **0206** (2002) 043, [hep-th/0205236].

[39] P. Breitenlohner and D. Z. Freedman, *Positive Energy in anti-De Sitter Backgrounds and Gauged Extended Supergravity*, *Phys.Lett.* **B115** (1982) 197.

[40] J. Camino, A. Paredes and A. Ramallo, *Stable wrapped branes*, *JHEP* **0105** (2001) 011, [hep-th/0104082].

[41] N. Itzhaki, J. M. Maldacena, J. Sonnenschein and S. Yankielowicz, *Supergravity and the large N limit of theories with sixteen supercharges*, *Phys.Rev.* **D58** (1998) 046004, [hep-th/9802042].

[42] I. Kanitscheider and K. Skenderis, *Universal hydrodynamics of non-conformal branes*, *JHEP* **0904** (2009) 062, [0901.1487].

[43] A. Karch, M. Kulaxizi and A. Parnachev, *Notes on Properties of Holographic Matter*, *JHEP* **0911** (2009) 017, [0908.3493].

[44] S. S. Gubser, *Breaking an Abelian gauge symmetry near a black hole horizon*, *Phys.Rev.* **D78** (2008) 065034, [0801.2977].

[45] S. A. Hartnoll, C. P. Herzog and G. T. Horowitz, *Building a Holographic Superconductor*, *Phys.Rev.Lett.* **101** (2008) 031601, [0803.3295].

[46] S. S. Gubser and A. Yarom, *Pointlike probes of superstring-theoretic superfluids*, *JHEP* **1003** (2010) 041, [0908.1392].

[47] S. S. Gubser, C. P. Herzog, S. S. Pufu and T. Tesileanu, *Superconductors from Superstrings*, *Phys. Rev. Lett.* **103** (2009) 141601, [0907.3510].

[48] C. Herzog and A. Vuorinen, *Spinning Dragging Strings*, *JHEP* **0710** (2007) 087, [0708.0609].

[49] J. F. Fuini and L. G. Yaffe, *Far-from-equilibrium dynamics of a strongly coupled non-Abelian plasma with non-zero charge density or external magnetic field*, *JHEP* **07** (2015) 116, [1503.07148].

[50] D. T. Son and A. O. Starinets, *Viscosity, black holes, and quantum field theory*, *Ann.Rev.Nucl.Part.Sci.* **57** (2007) 95–118, [0704.0240].

[51] S. S. Gubser, I. R. Klebanov and A. M. Polyakov, *Gauge theory correlators from non-critical string theory*, *Phys. Lett.* **B428** (1998) 105–114, [hep-th/9802109].

[52] M. P. Heller, D. Mateos, W. van der Schee and D. Trancanelli, *Strong coupling isotropization of non-Abelian plasmas simplified*, *Phys.Rev.Lett.* **108** (2012) 191601, [1202.0981].

[53] M. P. Heller, D. Mateos, W. van der Schee and M. Triana, *Holographic isotropization linearized*, *JHEP* **1309** (2013) 026, [1304.5172].

[54] J. Casalderrey-Solana, M. P. Heller, D. Mateos and W. van der Schee, *From full stopping to transparency in a holographic model of heavy ion collisions*, *Phys.Rev.Lett.* **111** (2013) 181601, [1305.4919].

[55] J. Casalderrey-Solana, M. P. Heller, D. Mateos and W. van der Schee, *Longitudinal coherence in a holographic model of p-Pb collisions*, *Phys.Rev.Lett.* **112** (2014) 221602, [1312.2956].

[56] W. van der Schee, P. Romatschke and S. Pratt, *Fully dynamical simulation of central nuclear collisions*, *Phys.Rev.Lett.* **111** (2013) 222302, [1307.2539].

[57] H. Bantilan and P. Romatschke, *Simulation of black hole collisions in asymptotically AdS spacetimes*, 1410.4799.

[58] P. M. Chesler and L. G. Yaffe, *Holography and off-center collisions of localized shock waves*, 1501.04644.

[59] A. Adams, P. M. Chesler and H. Liu, *Holographic turbulence*, *Phys.Rev.Lett.* **112** (2014) 151602, [1307.7267].

[60] A. Adams, P. M. Chesler and H. Liu, *Holographic vortex liquids and superfluid turbulence*, *Science* **341** (2013) 368–372, [1212.0281].

[61] E. Shuryak, *Why does the quark gluon plasma at RHIC behave as a nearly ideal fluid?*, *Prog. Part. Nucl. Phys.* **53** (2004) 273–303, [hep-ph/0312227].

[62] J. Stachel, A. Andronic, P. Braun-Munzinger and K. Redlich, *Confronting LHC data with the statistical hadronization model*, *J.Phys.Conf.Ser.* **509** (2014) 012019, [1311.4662].

[63] A. Andronic, P. Braun-Munzinger, K. Redlich and J. Stachel, *The statistical model in Pb-Pb collisions at the LHC*, *Nucl.Phys.* **A904-905** (2013) 535c–538c, [1210.7724].

[64] V. Skokov, A. Y. Illarionov and V. Toneev, *Estimate of the magnetic field strength in heavy-ion collisions*, *Int.J.Mod.Phys.* **A24** (2009) 5925–5932, [0907.1396].

[65] U. Gursoy, D. Kharzeev and K. Rajagopal, *Magnetohydrodynamics, charged currents and directed flow in heavy ion collisions*, *Phys.Rev.* **C89** (2014) 054905, [1401.3805].

[66] N. Agasian and S. Fedorov, *Quark-hadron phase transition in a magnetic field*, *Phys.Lett.* **B663** (2008) 445–449, [0803.3156].

[67] K. Fukushima, D. E. Kharzeev and H. J. Warringa, *Real-time dynamics of the chiral magnetic effect*, *Phys.Rev.Lett.* **104** (2010) 212001, [1002.2495].

[68] D. E. Kharzeev, L. D. McLerran and H. J. Warringa, *The effects of topological charge change in heavy ion collisions: 'event by event P and CP violation'*, *Nucl.Phys.* **A803** (2008) 227–253, [0711.0950].

[69] G. Bali, F. Bruckmann, G. Endrodi, S. Katz and A. Schafer, *The QCD equation of state in background magnetic fields*, 1406.0269.

[70] M. D'Elia, S. Mukherjee and F. Sanfilippo, *QCD phase transition in a strong magnetic background*, *Phys.Rev.* **D82** (2010) 051501, [1005.5365].

[71] P. Buividovich, M. Chernodub, E. Luschevskaya and M. Polikarpov, *Numerical evidence of chiral magnetic effect in lattice gauge theory*, *Phys.Rev.* **D80** (2009) 054503, [0907.0494].

[72] M. Abramczyk, T. Blum, G. Petropoulos and R. Zhou, *Chiral magnetic effect in 2+1 flavor QCD+QED*, *PoS* **LAT2009** (2009) 181, [0911.1348].

[73] D. Galante and M. Schvellinger, *Thermalization with a chemical potential from AdS spaces*, *JHEP* **1207** (2012) 096, [1205.1548].

[74] E. Caceres and A. Kundu, *Holographic thermalization with chemical potential*, *JHEP* **1209** (2012) 055, [1205.2354].

[75] A. Giordano, N. E. Grandi and G. A. Silva, *Holographic thermalization of charged operators*, 1412.7953.

[76] E. Caceres, A. Kundu, J. F. Pedraza and D.-L. Yang, *Weak field collapse in AdS: introducing a charge density*, 1411.1744.

[77] A. Buchel, M. P. Heller and R. C. Myers, *Equilibration rates in a strongly coupled nonconformal quark-gluon plasma*, 1503.07114.

[78] E. D'Hoker and P. Kraus, *Magnetic brane solutions in AdS*, *JHEP* **0910** (2009) 088, [0908.3875].

[79] A. Chamblin, R. Emparan, C. V. Johnson and R. C. Myers, *Charged AdS black holes and catastrophic holography*, *Phys.Rev.* **D60** (1999) 064018, [hep-th/9902170].

[80] E. D'Hoker and P. Kraus, *Charged magnetic brane solutions in AdS_5 and the fate of the third law of thermodynamics*, *JHEP* **1003** (2010) 095, [0911.4518].

[81] M. Henningson and K. Skenderis, *The holographic Weyl anomaly*, *JHEP* **9807** (1998) 023, [hep-th/9806087].

[82] M. Taylor, *More on counterterms in the gravitational action and anomalies*, hep-th/0002125.

[83] J. P. Boyd, *Chebyshev and Fourier spectral methods*. Dover, 2nd ed., 2001.

[84] H. Bantilan, F. Pretorius and S. S. Gubser, *Simulation of asymptotically AdS_5 spacetimes with a generalized harmonic evolution scheme*, *Phys.Rev.* **D85** (2012) 084038, [1201.2132].

[85] S. Janiszewski and M. Kaminski, *Quasinormal modes of magnetic and electric black branes versus far from equilibrium anisotropic fluids*, *Phys. Rev.* **D93** (2016) 025006, [1508.06993].

[86] J. I. Kapusta and C. Gale, *Finite-Temperature Field Theory Principles and Applications*. Cambridge University Press, 2nd ed., 2006.

[87] P. Arnold, G. D. Moore and L. G. Yaffe, *Transport coefficients in high temperature gauge theories. II: Beyond leading log*, *JHEP* **05** (2003) 051, [hep-ph/0302165].

[88] J. Takahashi, K. Nagata, T. Saito, A. Nakamura, T. Sasaki et al., *Color screening potential at finite density in two-flavor lattice QCD with Wilson fermions*, *Phys.Rev.* **D88** (2013) 114504, [1308.2489].

[89] J. F. Fuini, A. Karch and C. F. Uhlemann, *Spinor fields in general Newton-Cartan backgrounds*, *Phys. Rev.* **D92** (2015) 125036, [1510.03852].

[90] D. T. Son and M. Wingate, *General coordinate invariance and conformal invariance in nonrelativistic physics: Unitary Fermi gas*, *Annals Phys.* **321** (2006) 197–224, [cond-mat/0509786].

[91] C. Hoyos and D. T. Son, *Hall Viscosity and Electromagnetic Response*, *Phys. Rev. Lett.* **108** (2012) 066805, [1109.2651].

[92] D. Thanh Son, *Newton-Cartan Geometry and the Quantum Hall Effect*, 1306.0638.

[93] A. Gromov and A. G. Abanov, *Thermal Hall Effect and Geometry with Torsion*, *Phys. Rev. Lett.* **114** (2015) 016802, [1407.2908].

[94] T. L. Hughes, R. G. Leigh and O. Parrikar, *Torsional Anomalies, Hall Viscosity, and Bulk-boundary Correspondence in Topological States*, *Phys. Rev.* **D88** (2013) 025040, [1211.6442].

[95] H. P. Künzle, *Galilei and lorentz structures on space-time : comparison of the corresponding geometry and physics*, *Annales de l'institut Henri Poincaré (A) Physique théorique* **17** (1972) 337–362.

[96] C. Duval and H. P. Kunzle, *Minimal Gravitational Coupling in the Newtonian Theory and the Covariant Schrodinger Equation*, *Gen. Rel. Grav.* **16** (1984) 333.

[97] C. Duval, G. Burdet, H. P. Kunzle and M. Perrin, *Bargmann Structures and Newton-Cartan Theory*, *Phys. Rev.* **D31** (1985) 1841–1853.

[98] M. H. Christensen, J. Hartong, N. A. Obers and B. Rollier, *Torsional Newton-Cartan Geometry and Lifshitz Holography*, *Phys. Rev.* **D89** (2014) 061901, [1311.4794].

[99] M. H. Christensen, J. Hartong, N. A. Obers and B. Rollier, *Boundary Stress-Energy Tensor and Newton-Cartan Geometry in Lifshitz Holography*, *JHEP* **01** (2014) 057, [1311.6471].

[100] H. P. Kunzle and C. Duval, *Dirac Field On Newtonian Space-Time*, *Annales Poincare Phys. Theor.* **41** (1984) 363–384.

[101] B. Bradlyn and N. Read, *Low-energy effective theory in the bulk for transport in a topological phase*, *Phys. Rev.* **91** (Mar., 2015) 125303, [1407.2911].

[102] J.-M. Levy-Leblond, *Nonrelativistic particles and wave equations*, *Commun. Math. Phys.* **6** (1967) 286–311.

[103] M. Geracie, D. T. Son, C. Wu and S.-F. Wu, *Spacetime symmetries of the quantum Hall effect*, *Phys. Rev.* **91** (Feb., 2015) 045030, [1407.1252].

[104] R. M. Wald, *General Relativity*. 1984.

[105] K. Jensen, *On the coupling of Galilean-invariant field theories to curved spacetime*, 1408.6855.

[106] X. Bekaert and K. Morand, *Connections and dynamical trajectories in generalised Newton-Cartan gravity I. An intrinsic view*, 1412.8212.

[107] K. Jensen and A. Karch, *Revisiting non-relativistic limits*, *JHEP* **1504** (2015) 155, [1412.2738].

[108] M. Geracie, K. Prabhu and M. M. Roberts, *Curved non-relativistic spacetimes, Newtonian gravitation and massive matter*, 1503.02682.

[109] J. A. Brooke, *A Galilean Formulation of Spin. 1. Clifford Algebras and Spin Groups*, *J. Math. Phys.* **19** (1978) 952–959.

[110] K. Jensen, *Anomalies for Galilean fields*, 1412.7750.

[111] A. Jain, *Galilean Anomalies and Their Effect on Hydrodynamics*, 1509.05777.

[112] R. Andringa, E. A. Bergshoeff, J. Rosseel and E. Sezgin, *3D Newton-Cartan supergravity*, *Class. Quant. Grav.* **30** (2013) 205005, [1305.6737].

[113] E. Bergshoeff, J. Rosseel and T. Zojer, *Newton-Cartan (super)gravity as a non-relativistic limit*, *Class. Quant. Grav.* **32** (2015) 205003, [1505.02095].